Physiological roles of histone acetyltransferase p300 in the progression of renal fibrosis

Hyunsik Kim

The Graduate School
Yonsei University
Department of Medical Science

Physiological roles of histone acetyltransferase p300 in the progression of renal fibrosis

A Dissertation Submitted
to the Department of Medical Science
and the Graduate School of Yonsei University
in partial fulfillment of the
requirements for the degree of
Doctor of Philosophy in Medical Science

Hyunsik Kim

June 2024

This certifies that the Dissertation
of Hyunsik Kim is approved.

Thesis Supervisor	Ho-Geun Yoon
Thesis Committee Member	Jae Myun Lee
Thesis Committee Member	Hoon Young Choi
Thesis Committee Member	Beom Seok Kim
Thesis Committee Member	Ho-Shik Kim

The Graduate School
Yonsei University
June 2024

ACKNOWLEDGEMENTS

It's been a long and winding road, and it's almost at the end. Since my first steps of this journey in 2019, a lot has happened to get me to where I am today. I think it was the support and help of so many people that made me grow and mature from a freshly graduated university student who was immature and inexperienced in academics, research, and life. So I'd like to express my gratitude to them here, even if it's not enough.

First and foremost, I would like to thank my advisor and mentor, Professor Ho-Geun Yoon. I remember the first time I came to meet with Prof. Ho-Geun Yoon. I think it was his words that told me that I can do it, even though I had poor scientific background. Always carefully guiding me through my lack of scientific logic and research, and shining a light in front of me when I was lost or wandering, kept me moving forward. And I've learned so much about how to approach life as a grown-up. Thank you again.

I wish to thank Prof. Jae Myun Lee, Prof. Bum-Seok Kim, Prof. Hoon-Young Choi, and Prof. Ho-Shik Kim for their guidance and support during the process of completing my doctoral thesis. I am also very grateful to professors of biochemistry and molecular biology department who have always given me many comments and advice on my research. Many thanks to Prof. Sang-wook Park, Jaewoo Kim, Kyung-hee Chun, Kyung-seop Kim, and Man-wook Heo.

I would also like to thank the members of my lab who have become my family throughout the long course of my degree. First, I would like to thank Prof. Jungyoon Yoo for helping me get started when I was a clumsy researcher. I know that it was not easy to turn me from a clumsy and mistaken person into a single researcher, and not only that, whenever my willpower and confidence was low, he gave me a lot of encouragement and support from a distance, which helped me to have more courage. And, I'd also like to thank Dr. Soo-yeon Park, who has always been a cornerstone of our lab. She helped me so much in experiments and research, and was always the

moral anchor of the lab during my degree journey. Thank you once again.

I also appreciate Dr. Soo-Yeon Lee, the only senior who shared my degree with me. Because of her footsteps, I believe I haven't gotten lost in my journey. I am also very grateful to Jaehwan, who I spent the largest time with and had the most conversations with during my degree. Thanks to him, I was never bored. I would also like to thank Seunghee, who always took on the annoying and difficult duties, so that I could focus on my research a little more. Even though we're not currently together, I would also like to thank Dr. Mi-Jeong Kim and Dr. Seung-Hyun Lee who have taught me many things, big and small, during my degree course. And, I want to also thank the alumni who have already graduated and are living the fulfilling life, Su-bhin, the senior and junior who first came here and helped me adapt, gyeong-eun, who always made us laugh.

Additionally, I want to express my gratitude to the members of my biochemistry and molecular biology department. I especially want to thank my one and only colleague who entered same year and also friend, Kyu-Hye, who has always been with me throughout my degree journey. I would also like to thank Dr. Yo-seop Lee, Dr. Nahee Hwang, Dr. sun-ho Lee, Chan-sik Kim, and Yoon-ji Cha for their help during research.

Also, I want to express my deep gratitude to prof. Sungryul Yoo of the Department of Clinical laboratory science, who guided me to step into the academic career road, and thanks to him, I was able to start all of this and I was proud to identify myself as a clinical medical technologist.

I would also like to thank the people who always stood by my side and cheered me on whenever I was exhausted and tired during my long degree program. First of all, Kihwan and Namgyu, who are always there for me even if I don't say anything, just by being there, thank you, being with you always made my heart feel at ease. And a big thank you to our clinical pathology cheongryong friend gichang, Soo-jae, In-tae, Jin-woo, Jae-yong, Jin-kyu, Larry Lim, I could hold on because you relieved my stress and supported me. And thank you to my Endmatch, the MondayCarlo tennis team, for making me forget everything when we were together. And I’d also like to thank

all my middle and high school friends, juniors and seniors of the Department of Clinical laboratory science for calling me up, drinking, and hanging out whenever you think of it.

I want to express my deep appreciation to my family, who have supported me the closest and most. First of all, I would like to thank my two grandmothers, who have always been very supportive, and because they believed in me, I was able to believe in myself. I'm a bad grandson, but I'll try to be a good grandson now. I would also like to thank my uncle and aunts, for always having my back. I know I've had so much support and encouragement from a young age. Lastly, I am immeasurably grateful to my mom and dad for being by my side from start to finish. I love you

I have received so much help and support from so many people during my degree journey, but looking back, I don't think I've given back to others as much as I've received. I'm late to the party, but I promise to give back what I've received, and I promise to everyone I've mentioned here that I will use this undeserved support and encouragement to become a better researcher in the future.

Once again, I would like to thank everyone who supported me throughout my degree journey

Thank you.

2024.06

Sincerely, Hyunsik Kim

TABLE OF CONTENTS

LIST OF FIGURES

LIST OF TABLES

ABSTRACT

Physiological roles of histone acetyltransferase p300 in the progression of renal fibrosis

Renal fibrosis is a common accompanied event in chronic kidney disease (CKD) patients and it has a high prevalence in the world. However, detailed study of kidney fibrosis is still needed to understand the exact pathogenesis and propose the effective treatment approach. In this study, the elevated expression of the histone-acetyltransferase, E1A-associated protein p300 (p300) was observed in patients with CKD such as Focal segmental glomerulosclerosis (FSGS) and IgA nephropathy (IgAN). In addition, three different mouse models of renal fibrosis were used to verify the expression of p300 in progression of renal fibrosis and an increase of p300 expression was observed in all three renal fibrosis models. Furthermore, p300 protein was specifically upregulated in kidney proximal tubule cells during renal fibrosis progression and the stability of p300 protein is regulated by AKT-mediated phosphorylation of the Serine 1834 site. Moreover, a protein phosphatase, Mg2+/Mn2+ dependent 1K (PPM1K) was identified that specifically de-phosphorylates p300 at Serine 1834 site, which leads to a significant reduction in p300 stability and renal fibrosis. Interestingly, mesenchymal transition and angiogenesis pathway are altered in renal proximal tubule cells-specific p300 knock-out mice during renal fibrosis. In addition, elevation of p300 in renal proximal tubule cells was verified to promote renal fibrosis development by regulating Endothelial-to-Mesenchymal transition (EndoMT) as well as Epithelial-to-Mesenchymal transition (EMT) via upregulating the expression of mesenchymal transition-related secreted proteins Periostin (POSTN), Follistatin-like 1 (FSTL1), and Fascin Actin-Bundling Protein 1 (FSCN1). Finally, using

the well-known p300-specific inhibitors A6 and C646, the anti-fibrotic effects of these p300 selective inhibitors were demonstrated in a mouse model of renal fibrosis. Collectively, the results demonstrate the roles of p300 in the development of renal fibrosis and suggest p300 as a promising target for the treatment of advanced CKD. Furthermore, selective inhibitors of p300 are proposed as promising therapeutic agents for renal fibrosis.

Key words : p300, chronic kidney disease, kidney fibrosis, PPM1K, EndoMT

1. INTRODUCTION

Chronic kidney disease (CKD) is a collective term for chronic conditions that occur due to various causes such as hypertension, diabetes, hyperlipidemia, autoimmune diseases, metabolic acidosis and genetic disorders in kidney including diabetes nephropathy (DN), Focal segmental glomerulosclerosis (FSGS) and IgA nephropathy (IgAN)[1-7]. Recently, CKD has emerged as a significant social problem because of the increasing prevalence of various chronic diseases related to lifestyle, dietary habits, and environmental changes. It affects over 10% of the global population, over the 800 million people, and its prevalence continues to rise annually. Especially, in the End-stage of renal failure with CKD, dialysis and transplantation are necessary[8-11].

Fibrosis, a major consequence of CKD progression, is an irreversible process induced by the chronic deposition of extracellular matrix (ECM) such as collagen and Fibronectin. ECM structures are replacing normal tissue and it lead to structural and functional failure of organs [12,13]. Fibrosis is regulated by various physiological factors such as TGF-β, PDGF-β, interleukins (IL-1, IL-6, IL-10), chemokines (CCL2, CCL5), VEGF, physical stretching, fatty acid oxidation and gut microbiota like *Bacteroides fragilis*[14-24]. Particularly, kidneys fibrosis is accompanied with inflammation, activation of resident fibroblasts, cell death of tubular cells, Epithelial-to-Mesenchymal transition (EMT), or destruction of the peritubular capillary network, leading to malfunction of the nephron system[25-30]. Unfortunately, there is no effective treatment manner that can reverse renal fibrosis currently available.

Fibrosis is driven by ECM deposition secreted from myofibroblasts, thus, tracing the origin of myofibroblasts is important for the studying pathogenesis of fibrosis. According to many reports, myofibroblasts are originated from a variety of cells, including fibroblasts, fibrocytes, macrophage,

pericyte, epithelial cells, and endothelial cells[25,31]. In kidney, although many studies suggest that EMT may play an important role in the development of fibrosis, recent studies have reported that the actual transition proportion of epithelial cells to mesenchymal cells is not larger than expect[32-34]. Therefore, more detail studies are needed to elucidate other pathways of trans-differentiation to myofibroblast during renal fibrosis. Recently, many studies have shown that Endothelial-to-Mesenchymal transition (EndoMT) contributes to the development of fibrosis similar to EMT. According to a recent report, Unilateral ureteral obstruction (UUO), streptozotocin (STZ) and Alport's disease-induced mouse fibrosis models using lineage-tracing transgenic mice were established to determine the origin of myofibroblasts in the kidney, and it was reported that some cells Co-expressed the endothelial cell marker CD31 and the mesenchymal cell marker alpha-SMA in those mouse models[35]. In addition, it was confirmed that the inhibition of EndoMT by blocking TGF-β signaling led to a significant reduction of fibrosis progression in UUO induced mouse fibrosis model[36].

Proximal tubular cells (PTC) is one of the cells that make up the renal nephron and it is the most abundant cell in the renal cortex. PTCs have numerous mitochondria and highly participate in substance exchange during excretory process[37,38]. Histologically, PTCs are located in upper region of nephron and it is structurally near to the capillaries and glomeruli[39-41]. PTCs cells are stimulated by a variety of excreted proteins and molecules due to their role in secreting molecules into urine, but it vulnerable to damage due to lower levels of intrinsic antioxidant and anti-apoptotic proteins, and high oxygen consumption, and reactive oxygen species (ROS) generation[42-47]. PTC damage has been observed in various diseases conditions, including polycystic kidney disease, congenital renal syndromes, diabetic nephropathy and mouse fibrosis model such as unilateral ureteral obstruction (UUO) model[48-54]. Interestingly, in diabetic nephropathy, a major cause of CKD, the primary site of

stress response in the kidney is suggested to be PTCs rather than glomeruli[37,55,56]. Therefore, it was presuming that PTCs are directly or indirectly damaged in acute and chronic diseases of kidney and PTCs are play key roles in various kidney diseases development.

Endothelial cells, forming the inner lining of blood vessels along with pericytes, contribute to vascular structure composition. They regulate proteins and molecules passage, immune cell infiltration, hormone and cellular signaling, blood clotting, and vascular regeneration[57-63]. mesenchymal transition such as Epithelial-to-Mesenchymal transition (EMT) and Endothelial-to-Mesenchymal transition (EndoMT) is a process that cells transform into mesenchymal cells and each processed through similar physiological pathway. Various signaling pathways, including CAV1, WNT, Notch1, TGF-beta, ET-1, and hypoxia condition, induce mesenchymal transition in different type of tissue, ultimately leading to extracellular matrix (ECM) deposition and fibrosis[64-70].

Epigenetic changes mediate physiological regulation in various biological pathway such as embryogenesis, cell differentiation, tissue composition, aging, and tumor formation[71-75]. Epigenetic changes include DNA methylation, histone modification, non-coding RNAs (ncRNAs), and microRNAs, and epigenetic dysregulation causes various diseases, including fibrosis of diverse organ such as liver, kidney, and lung[76-80]. Histone acetylation, regulated by histone acetyltransferases (HAT) and histone de-acetyltransferases (HDAC), is important to regulating normal and disease states[73,81,82]. E1A-associated protein p300 also known as p300 and KAT3B is one of the histone acetyltransferase (HAT) enzymes, which acetylates lysine residues on histones and it induces histone modification to regulate gene transcription. Histone acetyltransferases p300 is involved in cell growth, differentiation, proliferation, survival, and senescence[83-85], and recent studies suggested that p300 protein were related with various diseases including cancer, inflammation, and fibrotic diseases[86-90]. In various organs, including the liver, lungs, uterus and hearts, changes in the

expression of p300 protein have been associated with fibrosis-related diseases. In liver fibrosis, p300 of hepatic endothelial cells regulates fibrosis by mediating C-C motif chemokine ligand 2 and, in hepatic stellate cells, p300 protein stability was increased by mechanical stress, which promotes activation into myofibroblasts, In pulmonary fibrosis, elevation of p300 has been reported in IFP patients, and p300 is specifically upregulated in alveolar type-2 cells, which regulate fibrosis via promoting M2 macrophage proliferation, In cardiac fibrosis, inhibition of p300 attenuated hypertension-induced renal fibrosis[86,91-94]. p300 histone acetyltransferase is activated by various stimuli. In fibroblasts, TGF-beta signal and PDGF-beta signal affect p300 activation[88,95,96], and in human endothelial cells, TNF-alpha signal increases p300 levels[93]. In addition, it is known that the protein level of p300 is increased through stability regulation due to phosphorylation of the Serine 1834 site of p300 in human-derived cell[86,97].

However, it is still unclear what molecular mechanisms regulate p300 expression in renal fibrosis and which p300-mediated physiological pathways is involved in the mesenchymal transition of renal cells and fibrosis development. Therefore, it is necessary to investigate the function and molecular pathways of p300 in the progression of renal fibrosis. In addition, demonstration of changes in the stability and phosphorylation of p300 during renal fibrosis and screening to discover the partner phosphatase of p300 that specifically reduces phosphorylation is necessary.

In this study, increased protein expression levels of p300 were found in the kidneys of renal fibrosis mouse model and kidney samples from patients with CKD. Specifically, a significant elevation of p300 protein was observed in proximal tubular cells during renal fibrosis progression. In addition, the upregulation of stability via the phosphorylation of p300 lead to an increase in the levels of the p300 protein. Moreover, the stability of p300 is regulated by the de-phosphorylation of a specific site mediated by a specific phosphatase. Finally, the increase of p300 levels in proximal

tubular cells induces mesenchymal transition during renal fibrosis progression. Specifically, focused on the mesenchymal transition of endothelial cells, the study demonstrated that p300 in proximal tubular cells regulates the expression of genes mediating EndoMT during progression of renal fibrosis.

2. MATERIALS AND METHODS

2.1. Clinical sample of Chronic kidney disease (CKD) patients

Kidney tissue sample of CKD were obtained from the Severance Hospital tissue bank and this research was approved by the Ethics Committee of the Institutional Review Board (IRB) of Severance Hospital (protocol no.4.2024.0314). Kidney tissues from CKD patients with Minimal Change Disease (MCD), Focal segmental glomerulosclerosis (FSGS), and IgA nephropathy (IgAN) and normal kidney tissue purchased from TissueArray.Com LLC were included in this study. Written informed consent was obtained from all patients. CKD patients were diagnosed by institutional diagnostic criteria including blood BUN, urine protein, creatinine, histopathologic classification, Stanford classification, MEST-C scoring, etc.

2.2. Cell culture

Human proximal tubule cell line (HK2) and human umbilical cord-derived endothelial cell line (HUVEC) were purchased from American Type Culture Collection (Manassas, VA, USA). HK2 were maintained in RPMI1640 (Corning Inc., Corning, NY, USA) supplemented with 10% FBS and 1% antibiotic-antimitotic solution. HUVEC were maintained in Endothelial Cell medium (Sciencell Research Laboratories Carlsbad, CA, USA). Primary proximal tubular cells(PTEC) were isolated from mouse kidney and maintained in RPMI1640 (Corning, NY, USA) supplemented with 10% FBS and 1% antibiotic-antimitotic solution. All cells were incubated at 37˚C and 5% CO2. HK2 and PTEC were starved in no-serum media for 2 hours and then stimulated with 20 ng/ml TGF-β1(Prospec, Rehovot, Israel). Concentration of cell cultured medium were performed using

VIVASPIN 20 (SATOROUS, Göttingen, Germany) following the manufacturer's protocol. Transient transfection was performed using Lipofectamine 3000 and RNAiMAX (Thermo Fisher Scientific, Waltham, MA, USA). HK2 and HUVEC cell co-culture systems were organized using transwell (Corning Inc., Corning, NY, USA). HK2 were treated by 3μM C646 (Selleckchem LLC, TX, USA) or 3 μM A6 and then collected 24 hours after treatment. The plasmid we used for p300 overexpression was cloned into PSG5-HA and the plasmid used for phosphatase overexpression was cloned into PSG5-Flag. The siRNA of PPM1K used to knock-down PPM1K was produced by Genolution (Seoul,Korea). Sequence of siPPM1K #1:5'- GGGAUAACCGCAUUGAUGAUU-3', 5'-UCAUCAAUGCGGUUAUCCCUU-3' siPPM1K #3:5' -CUUCCUAAGGAGAAGAACUUU -3', 5'- AGUUCUUCUCCUUAGGAAGUU-3'

2.3. Animal model

All animal experiments were approved by Yonsei University College of Medicine Institutional Animal Care and Use Committee (IACUC No. 2023-0025) 8-weeks C57BL/6 mice were purchased from ORIENT BIO Inc. (Seongnam, Korea). The mice were maintained in specific pathogen free condtion(SPF) and 12-hour light/dark cycle conditions. Mice with conventionally p300 deficient from kidney proximal tubular cells, were generated by intercrossing γGT-1 Cre mice and p300 Floxed mice. These mice were purchased from The Jackson Laboratory (Bar Harbor, ME, USA). Unilateral Ureteral Obstruction (UUO) surgery was performed under anesthesia with incision in the lateral abdomen and ligation of a single ureter. Folic acid (FA) administration was performed by FA dissolved in Sodium-Bicarbonate, which was injected intraperitoneally once at 250 kg/kg. The streptozotocin-unilateral nephrectomy (STZ-UNx) model was established by first performing open unilateral nephrectomy surgery after anesthesia, and 1 week later, 50 mg/kg STZ was injected intra-peritoneally for 5 days. STZ was dissolved in 0.025M sodium citrate and the mice were validated

by checking fasting blood glucose(>300mg/dL). PPM1K overexpression mice via adenovirus infection were introduced with Ad5-GFP-Flag-PPM1K (1x10^10vp) by direct sub-capsular injection into the kidney, and viral infection was confirmed by detecting GFP in the kidney tissue. Anesthesia was induced by Zoletil (50 mg/ml) and Rumpun (23.32 mg/ml).

2.4. CRSPR-Cas9

The p300 deficient HK2 cells were engineered via the Crispr-cas9 method. The sgRNA (5' GTACGACTAGGTACAGGCGA 3') designed by Chop-Chop was inserted into the px549 plasmid vector. Vectors were introduced into HK2 cells via electroporation and selected by puromycin treatment. And the expression of p300 was confirmed by RT-qPCR and western blot.

2.5. Site direct mutation

The mutant constructs of p300 and PPM1K were created by DNA polymerases master mixes (Thermo Fisher Scientific, Waltham, MA, USA). All constructs were verified by DNA sequencing from Macrogen Co. (Seoul, Korea)

2.6. Histological staining

Histologic staining was performed using de-paraffinized kidney tissue. Masson trichrome staining was performed via Wiegert's Iron Hematoxylin kit (Sigma-Aldrich, Burlington, MA, USA) and MTS Kit (Sigma-Aldrich, Burlington, MA, USA) following the manufacturer's protocol. Picro-sirius red staining was performed via the Picro-Sirius Red Stain Kit (Abcam, Cambridge, UK). Kidney sections were submerged in Picro-Sirius Red solution for 2 hours at room temperature, washed twice with 5% acidified water, and then washed twice with absolute alcohol. After staining, sections were mounted using a hydrophilic mounting solution. To perform the

Immunohistochemisry (IHC) and immunofluorescences staining (IF). The de-paraffinized kidney sections has been treated with antigenic revitalization by Antigen Unmasking solution (Vector Laboratories, Burlingame, CA, USA) in the pressing cooker at 5 minutes. Peroxidase blocking step was performed by Dako REAL Peroxidase-blocking Soltion (Dako, Glostrup, Denmark). Unmasked and peroxidase blocked kidney tissue were incubated with a primary antibody against p300, PPM1K, CD31, AQP1, AQP2, WT1, FSTL1, FSCN1, POSTN, Albumin, KIM-1, Vimentin, Col1A. For IHC, primary antibody staining was followed by HRP-conjugated anti-rabbit secondary antibody using Envision+ system-HRP Labelled Polymer anti-rabbit (Dako, Glostrup, Denmark) and visualized by 3'- diaminobenzidine substrate (Vector Laboratories, CA, USA). For IF, Dylight 488 anti-mouse antibody (1:500, Vector Laboratories, CA, USA) and Dylight 549 anti-rabbit anti-body (1:500, Vector Laboratories, CA, USA) were used for fluorescent labeling. To immunostain with antibodies whose host is mouse, they were initially fluorescently labeled with Zenon kit. To immune-stain with anti-mouse antibody, the antibody was initially fluorescently labeled with Zenon Labeling Kits following the manufacturer's protocol. Detailed antibody information is listed in Table 1. Quantification of IHC were assessed by ImageJ and co-localization were assessed by ZEN application.

2.7. RNA isolation and reverse transcription-quantitative polymerase chain reaction

Total RNA was extracted from kidney tissues and cells using the RNAiso Plus reagent (TaKaRa Bio, Otsu, Japan) following the manufacturer's instructions. The RNA quantity and purity were analysed by a NanoDrop 2000 spectrophotometer (Thermo Fisher Scientific, MA, USA). Extracted

RNA were reverse-transcribed using Cell-script (CellSafe, Yongin, Korea) following the manufacturer's instructions. qRT-PCR analyses were performed using FastStart Universal SYBR Green Master (ROX) reagents (Roche, Basel, Switzerland) and ABI Prism 7700 (Applied Biosystems, CA, USA). Target gene expression levels were normalized by comparison to GAPDH expression levels. All reactions were performed in triplicate. The detailed primer information used for amplification is listed in Table 2.

2.8. Western blot

Kidney tissue and cells were lysed by Lysis Buffer(Triton X100 0.2%, EGTA 1 mM, NaF 1 mM, NaCl 150 mM, Na3VO4 1 mM, EDTA 1 mM, 50 mM Tris HCl pH 7.4, Xpert proteinase inhibitor cocktail (Gene depot, TX, USA)). Protein lysates were separate by centrifugation at 12,000 rpm at 4°C for 15 minutes and then boiled with 5X SDS sample buffer (20% SDS, 50% Glycerol, 0.1% bromophenol blue solution, 0.5% 2-mercaptoethanol) at 95°C for 5 minutes. Boiled protein samples were separated by electrophoresis on a polyacrylamide gel and gel was transferred to NC (GE healthcare, IL, USA) membranes. The following primary antibodies were used: Anti-p300, Anti-PPM1k, Anti-AQP-1, Anti-AKT, Anti-p-AKT, Anti-p-p300, Anti-Col1a, Anti-CTGF, Anti-FSTL1, Anti-FSCN1, Anti-POSTN, Anti-alpha-SMA, Anti-p53, Anti-HA, Anti-Flag and Anti-beta-actin. The secondary antibodies used were: anti-mouse HRP-antibody (1:5000, 31430, Thermo Fisher Scientific, MA, USA) and anti-rabbit HRP- antibody (1:5000, 31460, Thermo Fisher Scientific, MA, USA). Chemiluminescence signals were visualized on the Fusion SOLO S device (Vilber, Marne-la-Vallée, France) and quantified using FIJI-Image-J software. Detailed antibody information is listed in Table 3.

2.9. Immunoprecipitation assay

Cells were were lysed by Lysis BF(Triton X100 0.2%, EGTA 1 mM, NaF 1 mM, NaCl 150 mM, Na3VO4 1 mM, EDTA 1 mM, 50 mM Tris HCl pH 7.4, Xpert proteinase inhibitor cocktail (Gene depot, TX, USA)). Protein lysates were separate by centrifugation at 12,000 rpm at 4°C for 15 minutes. A 10% input sample was remained and the lysates were rotated with HA-magnetic beads (Sigma-Aldrich, MA, USA) for 24 hours at 4˚C. After rotation, the lysate and bead mixture was placed on a magnetic rack and the supernatant was removed. The beads were washed with lysis BF for 20 minutes RT and then placed back on the magnetic rack. Repeat the previous washing process 3 times. Proteins were eluted in 1x sodium dodecyl sulfate buffer (20% SDS, 50% Glycerol, 0.1% bromophenol blue solution, 0.5% 2-mercaptoethanol) after boiling for 10 minutes at 95°C.

2.10. In vitro translation system

in vitro transcription and translations were performed using a TNT T7 quick coupled transcription/translation kit following the manufacturer's protocol (Promega Corporation, Madison, WI, USA).

2.11. Kidney functional test

Blood samples were collected from the heart of anesthetized mice, and the blood was separated to the serum by centrifugation. BUN (Blood Urea Nitrogen) and serum Creatinine were measured with a biochemistry analyzer (Dri-chem NX500, FUJIFILM, Tokyo, Japan).

2.12. Proximity ligation assay (PLA)

PLA was performed using the Duolink® Proximity Ligation Assay kit. The assay was performed according to the manufacturer's protocol and used Anti-p300(SC48343, Santa Cruz Biotechnology, Dallas, TX, USA), Anti-PPM1K antibodies (ab135286, Abcam, Cambridge, UK). Cells were

prepared by fixation in 4% paraformaldehyde and permeabilizing with Triton-X100. Paraffine embedded tissues were de-paraffinized with xylene and hydration with 100%, 90%, 80% EtoH, before permeabilization with Triton-X100. The samples were mounted with Duo-link mounting Sol. and observed by Zeiss LSM 900 microscope

2.13. 3-Dimesional imaging

For 3-Dimensional imaging, a Paraformaldehyde-fixed 1mm^3 section of renal cortex was cleared using SCARF-claer buffer and C-MATCH buffer on a C-Stain device (Crayon tech., Gyeong-gi-Do, Korea). Cleared kidney tissue was immersed in a solution of CD31 (ab28364, Abcam, Cambridge, UK) antibody diluted 1:250 in 3% BSA with sodium azide and shaking at 37'C for 3 days. After washing with BSA three times, kidney tissue was immersed in a solution of Dylgiht-649 Anti-rabbit antibody diluted 1:200 in 3% BSA with sodium azide and shaking at 37'C for 2 days. Stained tissue was mounted using C-MATCH solution in a confocal dish. Images and videos were acquired using a Zeiss LSM 900 instrument (Carl Zeiss, Baden-Württemberg, Germany), and image processing and quantification were performed using Zeiss' ZEN blue program.

2.14. Sircol collagen assay

Fresh kidney with no-capsule digested by 0.1 mg/ml pepsin in acetic acid at room temperature overnight and then centrifuge at 12,000 rpm for 20 minutes. The content of collagen in kidney is measured according to the instructions for a Sircol collagen assay kit (Biocolor, Carrickfergus, U.K.). Briefly, 50 ml of tissue-free supernatant of pepsin-digested kidney and the standards are incubated with 1 ml of Sircol dye reagent for 30 minutes on a rotary table. After centrifugation and washing with 750 ml of ice-cold acid-salt wash reagent, the collagen-dye pellet is suspended with 500 ml of alkali reagent and then samples are read at 555 nm by adding 200 ml of the collagen supernatant in

alkali reagent into 96-well plates. The content of collagen in each sample is calculated according to the standard curve.

2.15. Public data analysis

To determine gene expression levels in the Gene expression omnibus (GEO) dataset (GSE142025, GSE212681), we used GEO2R web-based tool provided by NCBI. The ChIP-sequencing(GSE75948) data and ATAC-sequencing(GSE197815) data were then visualized using the Intergrative Genomics View (https://igv.org/) application to identify promoter enrichment and chromatin accessibility. And Single-cell RNA-sequencing of CKD patients were analyzed by Cellenic® provide by Biomage (https://www.biomage.net/) and UMAPs of single cell RNA-sequencing were visualized using CELLXGENE discover (https://cellxgene.cziscience.com/).

2.16. RNA-sequencing

For bulk RNA-sequencing, RNA extracted with the QIAEN RNeasy® kit from cortex sections of kidneys was used. RNA purity was measured with a Nanodrop2000 (Thermo Fisher Scientific, MA, USA). RNA-sequencing was performed and analyzed on Macrogen Co. (Seoul, Korea) with QuantSeq 3` mRNA-Seq protocol (UCSC, mm10). Pathway analysis was performed using PANTHER-based GO enrichment analysis (MSigDB Hallmark) from the Gene Ontology (GO) Resource (https://geneontology.org/)[98]. The heatmap and pathway dot graph were visualized using SRplot- Science and Research online plot (bioinformatics.com.cn)[99].

2.17. CUT&TAG analysis

To perform CUT&TAG analysis, mouse kidney proximal tubular cells were initially isolated. Using the gentleMACS™ Dissociator (Miltenyi Biotec, Bergisch Gladbach, Germany). The kidneys

were minced by Brain_03, Spleen_04 programs, and RBCs were removed using Red Blood Cell Lysis Solution (Miltenyi Biotec, NRW, Germany) and minced tissue were incubated with 1:500 Fluorescein-Tetragonolobus Lectin (FL-1321-2, Vector laboratories, CA, USA) for 2 hours at room temperature. BD FACS Aria III was used for cell isolation by Flow cytometry. FITC positive cells were isolated using BD FACS Aria III and confirmed as PTC cells by RT-qPCR and IF. Using the isolated PTCs, we generated sequencing-ready libraries by CUT&TAG analysis kit (Active Motif, CA, USA) according to the manufacturer's protocol using an anti-rabbit p300 antibody (CS86377, Cell signaling technology, MA, USA). CUT&TAG products were sequenced and analyzed on a HiSeq2500 instrument (Illumina Inc., CA, USA) at Macrogen Co. (Seoul, Korea) and Gene annotation analysis was performed using the GREAT web based tool(https://great.stanford.edu/great/public/html/, UCSC mm10).

2.18. Statistical analysis

Statistical analyses were performed by one-way ANOVA (comparisons of more than two groups, using Mann Whitney or Kruskal Wallis analyses) and T-test analyses (comparisons of two groups). Correlation analysis was calculate by simple linear regression analyses. Statistical analyses were performed using GraphPad Prism 9 (GraphPad Software Inc, La Jolla, CA, USA). A p-value of < 0.05 was considered a statistically significant difference.

Table 1. The primers used for site-directed mutagenesis

Gene name (Forward: F; Reverse: R)	Sequence 5'-3'
P300 S1834A_F	CGCAGGAGGATGGCCGCCATGCAGCGGACTGG
P300 S1834A_R	CCAGTCCGCTGCATGGCGGCCATCCTCCTGCG
PPM1K N94K_F	ATCAGCTTGGAAAAAGTGGGGTGCG
PPM1K N94K_R	CGCACCCCACTTTTTCCAAGCTGAT

Abbreviations: S, Serine; A, Alanine; N, Asparagine; K, Lysine.

Table 2. The primer used for RT-qPCR

Gene name (Forward: F; Reverse: R)	Sequence 5'-3'
human_COL1A1_F	TCCTGCTGGTGAGAAAGGAT
human_COL1A1_R	TCCAGCAATACCCTGAGGTC
human_COL3A1_F	TGGTCTGCAAGGAATGCCTGGA
human_COL3A1_R	TCTTTCCCTGGGACACCATCAG
human_CTGF_F	CAAGGGCCTCTTCTGTGACT
human_CTGF_R	ACGTGCACTGGTACTTGCAG
human_TNC_F	CAGAAGCCGAACCGAAGTT
human_TNC_R	TTCATCAGCTGTCCAGGACAGA
human_ACTA2(αSMA)	CTGGCATCGTGCTGGACTCT
human_ACTA2(αSMA)	GATCTCGGCCAGCCAGATC
human_EP300_F	TTGTGAAGAGCCCCATGGAT
human_EP300_R	GCTTTGCATCACTGGGTCAA
human_FN1_F	AAGACCAGCAGAGGCATAAGG
human_FN1_R	TGTAGGGGTCAAAGCACGAG
human_GAPDH_F	TGACCGGTGCCATGGAATTTG
human_GAPDH_R	GTCGGAGTCAACGGATTTGG

human_Vimentin_F	GGAAGAGAACTTTGCCGTTGAA
human_Vimentin_R	GTGACGAGCCATTTCCTCCTT
human_PAI1_F	CCCCACTTCTTCAGGCTGTT
human_PAI1_R	GCCGTTGAAGTAGAGGGCAT
human_tie2_F	GGTCAAGCAACCCAGCCTTTTC
human_tie2_R	CAGGTCATTCCAGCAGAGCCAA
human_PECAM1(CD31)_F	AAGTGGAGTCCAGCCGCATATC
human_PECAM1(CD31)_R	ATGGAGCAGGACAGGTTCAGTC
mouse_COL1A1_F	ATGGATTCCCGTTCGAGTACG
mouse_COL1A1_R	TCAGCTGGATAGCGACATCG
mouse_COL3A1_F	CTAAAATTCTGCCACCCCGAA
mouse_COL3A1_R	AGGATCAACCCAGTATTCTCCACTC
mouse_ACTA2(αSMA)	GTGACTCACAACGTGCCTATC
mouse_ACTA2(αSMA)	CTCGGCCAGTAGTCACGAAGG
mouse_FN1_F	AAGACCATACCTGCCGAATG
mouse_FN1_R	GAACATGACCGATTTGGACC
mouse_EP300_F	CTGTGAACCAACATGAGTGCTAGTCC
mouse_EP300_R	TGAGCTGCTGTTGGCAAAGG
mouse_GAPDH_F	CGACTTCAACAGCAACTCCCACTCTTCC

mouse_GAPDH_R	TGGGTGGTCCAGGGTTTCTTACTCCTT
mouse_Vimentin_F	CCCTCACCTGTGAAGTGGAT
mouse_Vimentin_R	TCCAGCAGCTTCCTGTAGGT
mouse_PAI1_F	AGGGTTGCACTAAACATGTCAG
mouse_PAI1_R	GACACCCTCAGCATGTTCATC
mouse_FSP1_F	TGAGCAACTTGGACAGCAACA
mouse_FSP1_R	TTCCGGGGTTCCTTATCTGGG
mouse_PECAM1(CD31)_F	CCAAAGCCAGTAGCATCATGGTC
mouse_PECAM1(CD31)_R	GGATGGTGAAGTTGGCTACAGG
mouse_tie2_F	GAACTGAGGACGCTTCCACATTC
mouse_tie2_R	TCAGAAACGCCAACAGCACGGT
mouse_CD144_F	GAACGAGGACAGCAACTTCACC
mouse_CD144_R	GTTAGCGTGCTGGTTCCAGTCA

Abbreviations: RT-qPCR, real-time quantitative poly chain reaction

Table 3. The antibodies

	Antibody information (aplication, manufactur, product no.)
Anti-p300	IHC,IF(tissue), Cell signalling Technology, 86377s
Anti-p300	IF(cell),PLA,Western blot, Santacruz biotech, SC48343
Anti-PPM1K	IHC(human tissue), Invitrogen, PA5-21658
Anti-PPM1K	IHC,IF(mouse tisseue),Western blot,PLA, Abcam, ab135286
Anti-AQP1	IHC, IF, Western blot, Merck millipore ,ab2219
Anti-AQP2	IHC, Cell signalling Technology, 3487s
Anti-WT1	IHC, Abcam, ab89901
Anti-CD31	IHC,IF, Abcam, ab28364
Anti-p-p300(S1834)	IHC,Western blot, Invitrogen, PA5-64531
Anti-AKT	Western blot, Cell signalling Technology, 4691s
Anti-p-AKT(S473)	Western blot, Cell signalling Technology, 4060s
Anti-COL1A	IF(cell), Western blot, Santacruz biotech, SC59772
Anti-CTGF	Western blot, Santacruz biotech, SC365970
Anti-FSTL1	IHC,IF,Western blot, Abclonal, A15789
Anti-FSCN1	IHC,IF,Western blot, Abclonal, A9566
Anti-POSTN	IHC,IF,Western blot, Cell signalling Technology, 20302s

Anti-VIMENTIN	IF, Santacruz biotech, SC32322
Anti-KIM1	IHC, Invitrogen, PA1-86790
Anti-ALBUMIN	IHC, Cell signalling Technology, 4929s
Anti-ACTA2	IHC,IF, Western blot, Abcam, ab5694
Anti-ZO1	IF, Cell signalling Technology, 8193p
Anti-p53	Westernblot, Santacruz biotech, SC6243
LTL	IF,Cell sorting, Vector, FL-1321

Abbreviations: S, serine; p, phospho; LTL, lotus tetragonolobus lectin; IHC, immunohistochemistry; IF, immunofluorescence.

3. RESULTS

3.1. PTC-specific upregulation of p300 in CKD and murine fibrosis models

To investigate the clinical relevance of p300 in chronic kidney disease (CKD) with fibrosis. First, the expression of the p300 protein in renal tissues of CKD patients, including minimal change disease (MCD), focal segmental glomerulosclerosis (FSGS), and IgA nephropathy (IgAN) patients, was examined using immunohistochemistry (IHC) staining. Via histopathological analysis, a significant increase in p300 protein expression was observed in kidney tissues from FSGS and IgAN patients compared to normal tissues (Figure 1A). In addition, using three widely used mouse models (Unilateral Ureteral Obstruction (UUO), Streptozotocin-unilateral nephrectomy (UNZ-STZ), and Folic acid (FA)) to induce renal fibrosis, different fibrotic conditions of CKD patients were mimicked and revealing a significant increase in p300 protein levels in all three models (Figure 1B-D). Throughout this process, an elevation of p300 protein was observed during fibrosis development, particularly in renal epithelial cells. To identify specific cells with increased p300 expression, various cellular markers of kidney constituent cells were stained, and p300 expression changes in those cells were evaluated by H-scoring for assessment. Immunostaining was performed to distinguish components of the renal cortex, including proximal tubules (Aquaporin-1, AQP1), collecting ducts (Aquaporin-2, AQP2), glomeruli (Wilms tumor protein, WT1), and blood vessels (PECAM1, CD31). Specifically, in the UUO-induced renal fibrosis model, a significant increase in p300 was observed within the proximal tubule region identified by AQP1 (Figure 2A-E). To verify the increased expression of p300 in proximal tubular cell, Co-Immunofluorescence staining was

used to demonstrate that co-expression of p300 and AQP1 was increased but not in AQP2 stained cells (Figure 3A-B). To demonstrate the correlation between p300 of PTCs and fibrosis progression, p300 expression was assessed using mouse tissues sacrificed 2, 4, 6, 8, and 14 days after UUO surgery. It was demonstrated that p300 protein increased with the progression of fibrosis until 8 days after surgery (Figure 4). In addition, p300 of PTCs was increased in UNX-STZ induced fibrosis model (Figure 5).

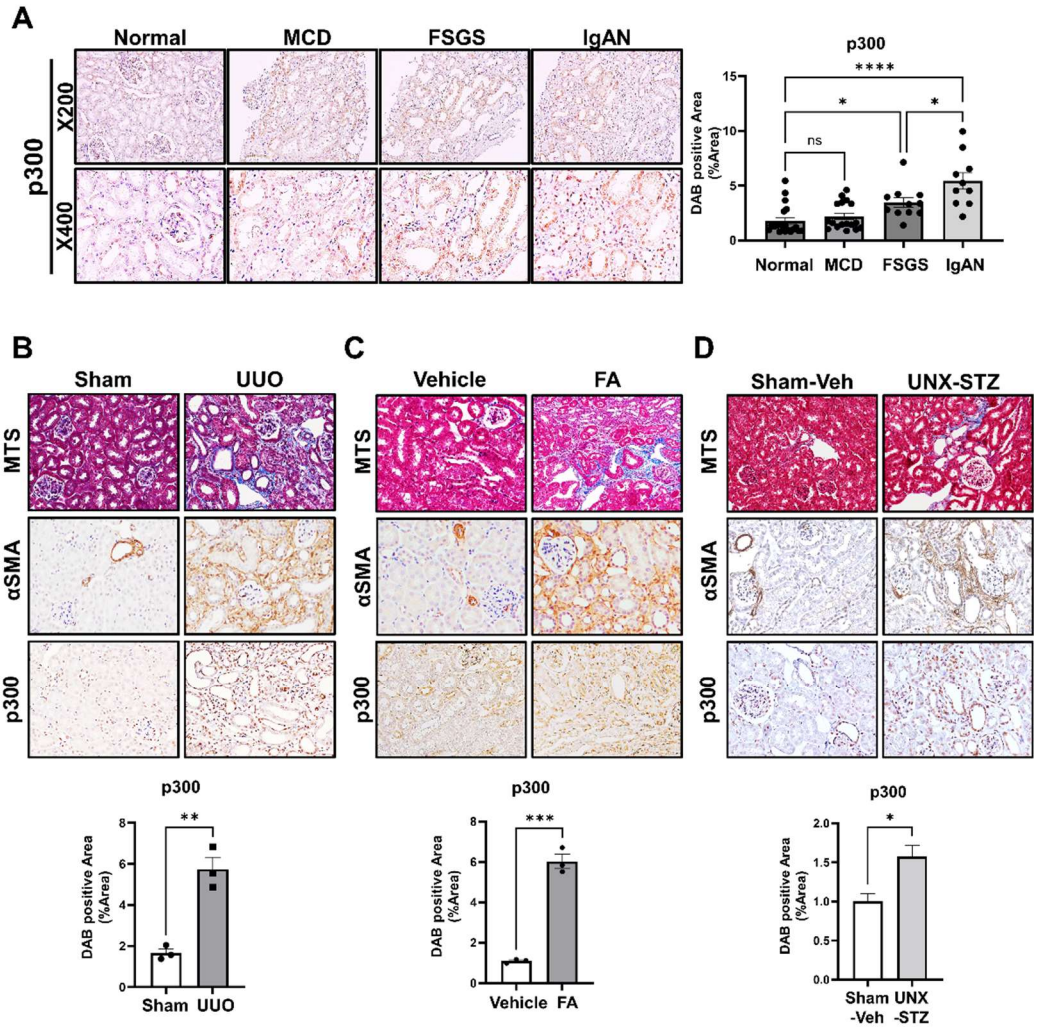

Figure 1. Elevation of p300 identified in Chronic kidney disease (CKD) patients and mouse fibrosis models. (A) Representative image of p300 immunohistochemistry (IHC) in kidney tissue from Minimal Change Disease (MCD), Focal segmental glomerulosclerosis (FSGS), IgA nephropathy (IgAN) patients and normal donor. The graph represents quantification of DAB area in histological staining images. Data are represented as mean ± SEM, *P < 0.05, and ****P < 0.0001 by ordinary one-way ANOVA test. (B) Representative image of Masson trichrome staining (MTS) and p300, αSMA immunohistochemistry (IHC) in mouse kidney tissue from UUO-induced mouse fibrosis model. The graph represents quantification of histological staining images. Data are represented as mean ± SEM, **P < 0.01 by t-test. (C) Representative image of Masson trichrome staining (MTS) and p300, αSMA immunohistochemistry (IHC) in mouse kidney tissue from FA-induced mouse fibrosis model. The graph represents quantification of histological staining images. Data are represented as mean ± SEM, ***P < 0.001 by t-test. (D) Representative image of Masson trichrome staining (MTS) and p300, αSMA immunohistochemistry (IHC) in mouse kidney tissue from UNZ-STZ-induced mouse fibrosis model. The graph represents quantification of histological staining images. Data are represented as mean ± SEM, *P < 0.05 by t-test.

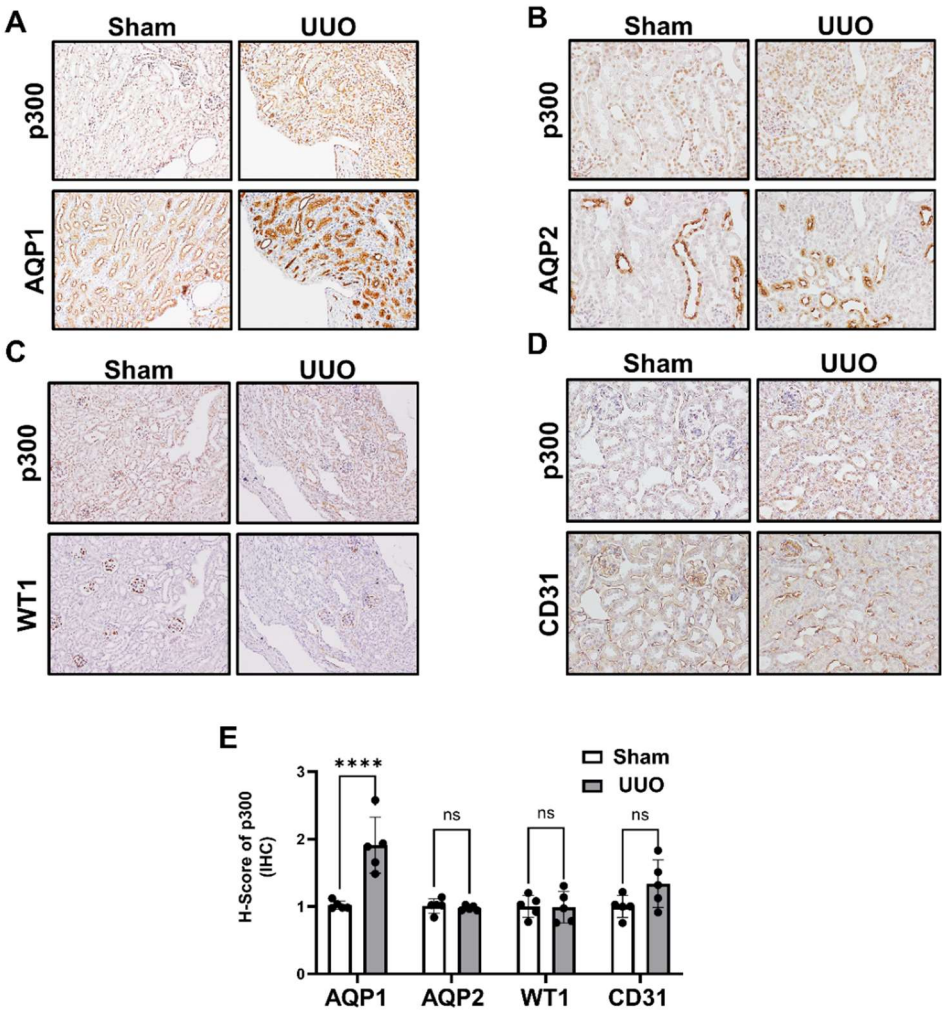

Figure 2. Identify the cells with increased p300 expression during fibrosis progression. (A) Representative image of p300 and AQP1 immunohistochemistry using serially sectioned samples. (B) Representative image of p300 and AQP2 immunohistochemistry using serially sectioned samples. (C) Representative image of p300 and WT1 immunohistochemistry using serially sectioned samples. (D) Representative image of p300 and CD31 immunohistochemistry using serially sectioned samples. (E) The graph represents p300 expression in AQP1, AQP2, WT1, and CD31+ cells using H-scoring. Data are represented as mean ± SEM, ****P < 0.0001 by t-test.

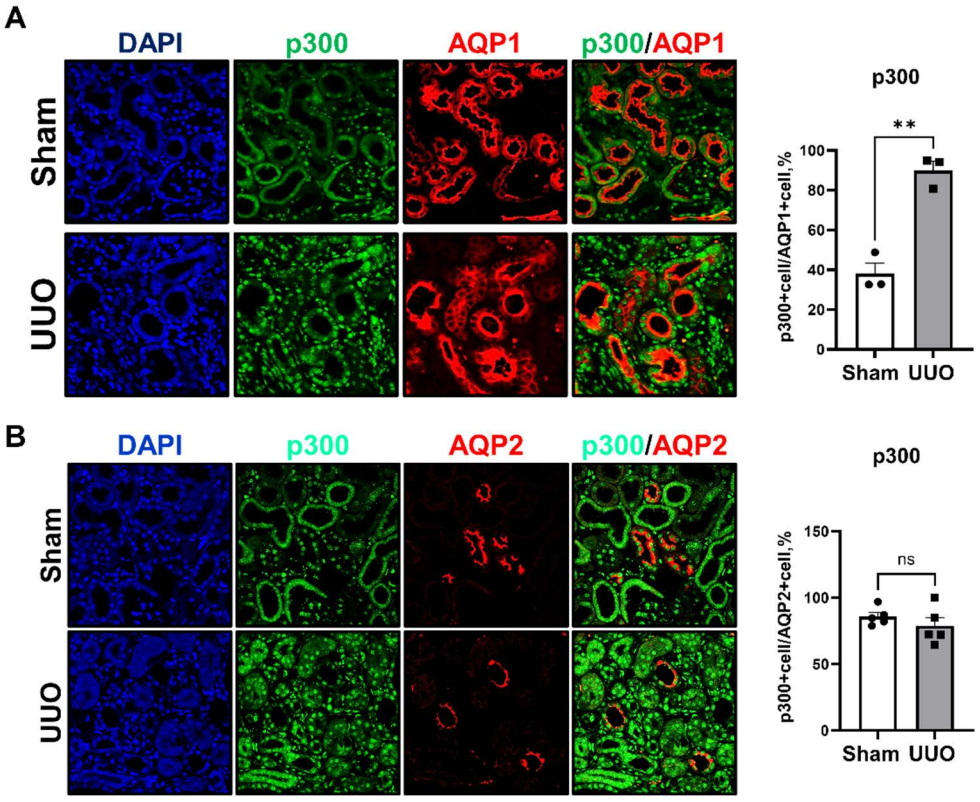

Figure 3. Identification of increased p300 in renal tubular epithelial cell during fibrosis progression. (A) Representative image of p300 and AQP1 co-immunofluorescence (IF) in mouse kidney tissue from UUO-induced mouse fibrosis model. The graph represents proportion of p300 positive cell among APQ1 positive cells. Data are represented as mean ± SEM, **P < 0.01 by t-test. (B) Representative image of p300 and AQP2 co-immunofluorescence (IF) in mouse kidney tissue from UUO-induced mouse fibrosis model. The graph represents proportion of p300 positive cell among APQ1 positive cells. Data are represented as mean ± SEM, n.s. not significant by t-test.

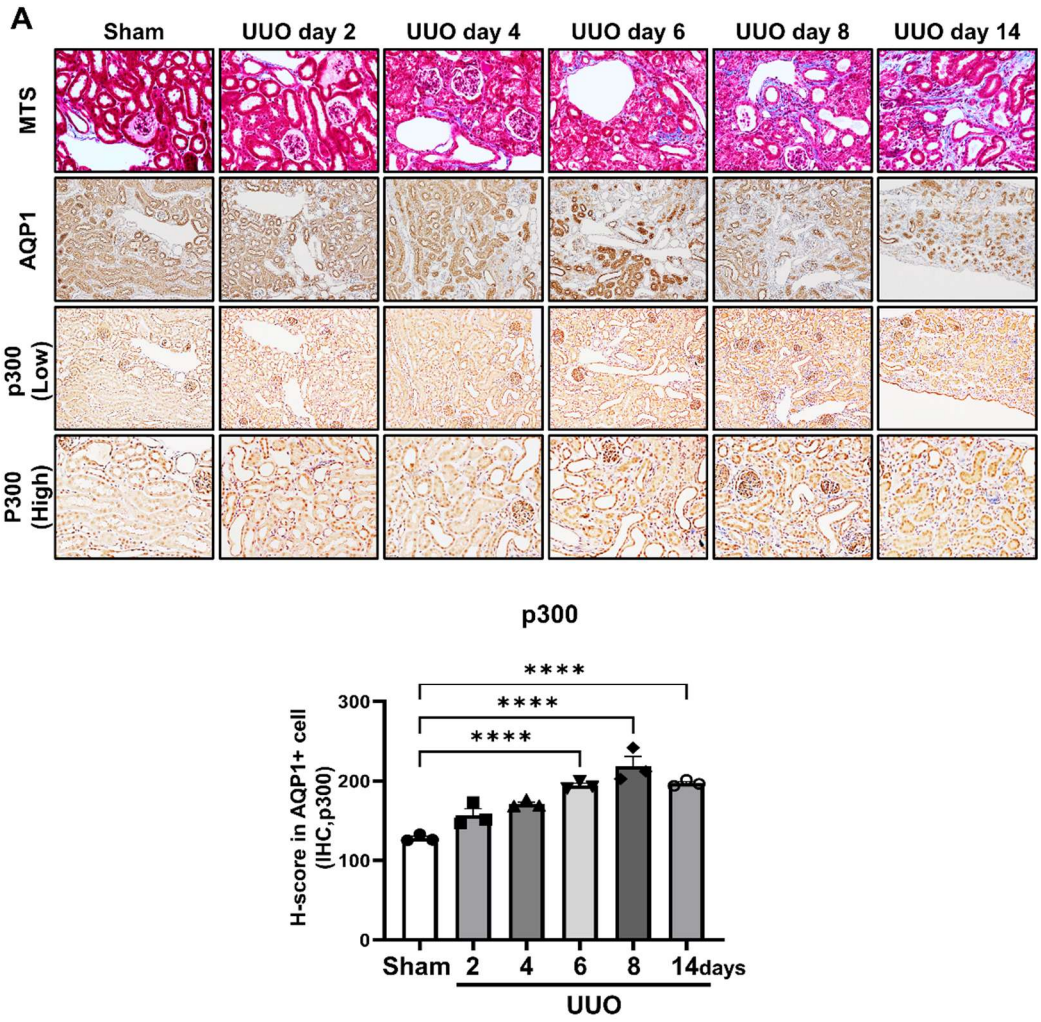

Figure 4. Elevation of p300 during UUO-induced fibrosis progression in renal proximal tubule cells. Representative image of Masson trichrome staining (MTS), and p300 and AQP1 immunohistochemistry using serially sectioned samples. Samples from UUO-induced mouse kidney 2, 4, 6, 8, 14, days after surgery. The graph represent expression of p300 in AQP1 positive cell analyzed by H-scoring. Data are represented as mean ± SEM, ****P < 0.0001 by ordinary one-way ANOVA test.

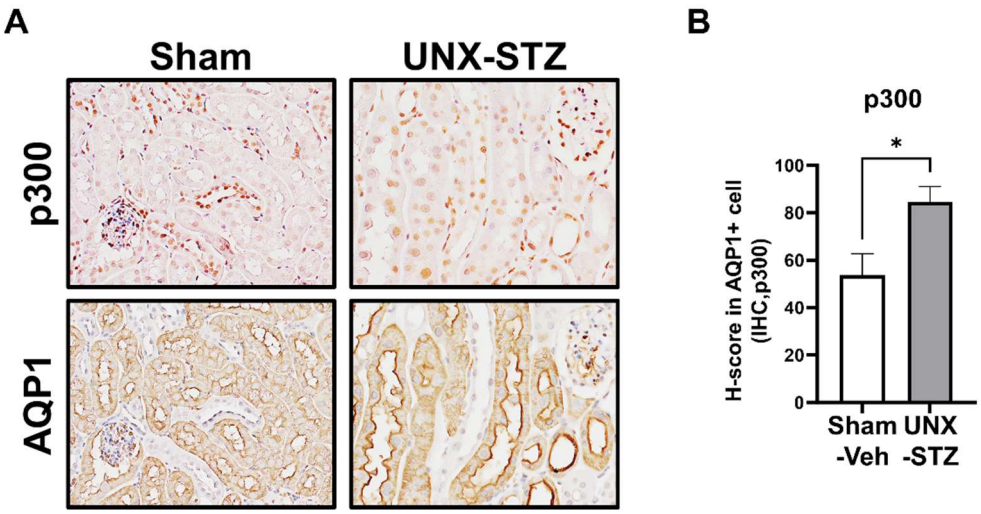

Figure 5. Elevation of p300 during UNZ-STZ induced fibrosis progression in renal proximal tubule cells. (A) Representative image of p300 and AQP1 immuno-histochemistry using serially sectioned samples. Samples from UNX-STZ induced-diabetic fibrosis mouse kidney. (B) The graph represent expression of p300 in AQP1 positive cell analyzed by H-scoring. Data are represented as mean ± SEM, *P < 0.05 by t-test.

3.2. PTC-specific p300 knock-out attenuates fibrosis development in a murine renal fibrosis model

To investigate the function of p300 in the fibrosis development. Mouse with genetically deleted p300 in renal proximal tubular cells were generated using gammaGT-1-cre mice and p300-floxed mice. The knock-out of p300 was confirmed through renal tissue immunostaining and isolation of proximal tubule cells for cellular immunofluorescence and RT-qPCR to verify the knock-out effect of p300 (Figure 6A-F). Subsequently, UUO surgery was performed on p300 knock-out and wild-type mice, and fibrosis progression was assessed. The results showed that significant attenuation of fibrosis progression was observed in knock-out mice compared to wild-type mice by Masson trichrome staining, and Sirius red (Figure 7A). The decreased expression of fibrosis-related genes and proteins in p300 knock-out mouse kidney tissues compared to wild-type mouse kidney tissues was demonstrated by RT-qPCR and western blot analysis (Figure 7B-C). In addition, kidney functional markers (serum creatinine and blood urea nitrogen (BUN)), kidney injury marker (KIM1) and myofibroblast activation were decreased in p300 knock-out mice compared with wild-type mice (Figure 8A-C). To clarify the function of p300 in renal fibrosis, Folic acid injection, known for causing substantial damage to the renal proximal nephron, was applied to p300 knock-out mice, and similar results to the UUO model were found (Figure 9A-D).

These results demonstrate that expression of p300 is increased in patients with fibrosis-associated CKD (FSGS, IgAN). In addition, elevation of p300 was observed in three different mouse models (UUO, FA, UNX-STZ) mimicking human renal fibrosis. Taken together, the results show that the p300 protein was specifically increased in renal proximal tubule cells. Moreover, it was verified that reduced fibrosis and kidney damage were observed in UUO and FA mouse models using proximal

tubule cell-specific p300 knockout mice compared with wild-type mice.

.

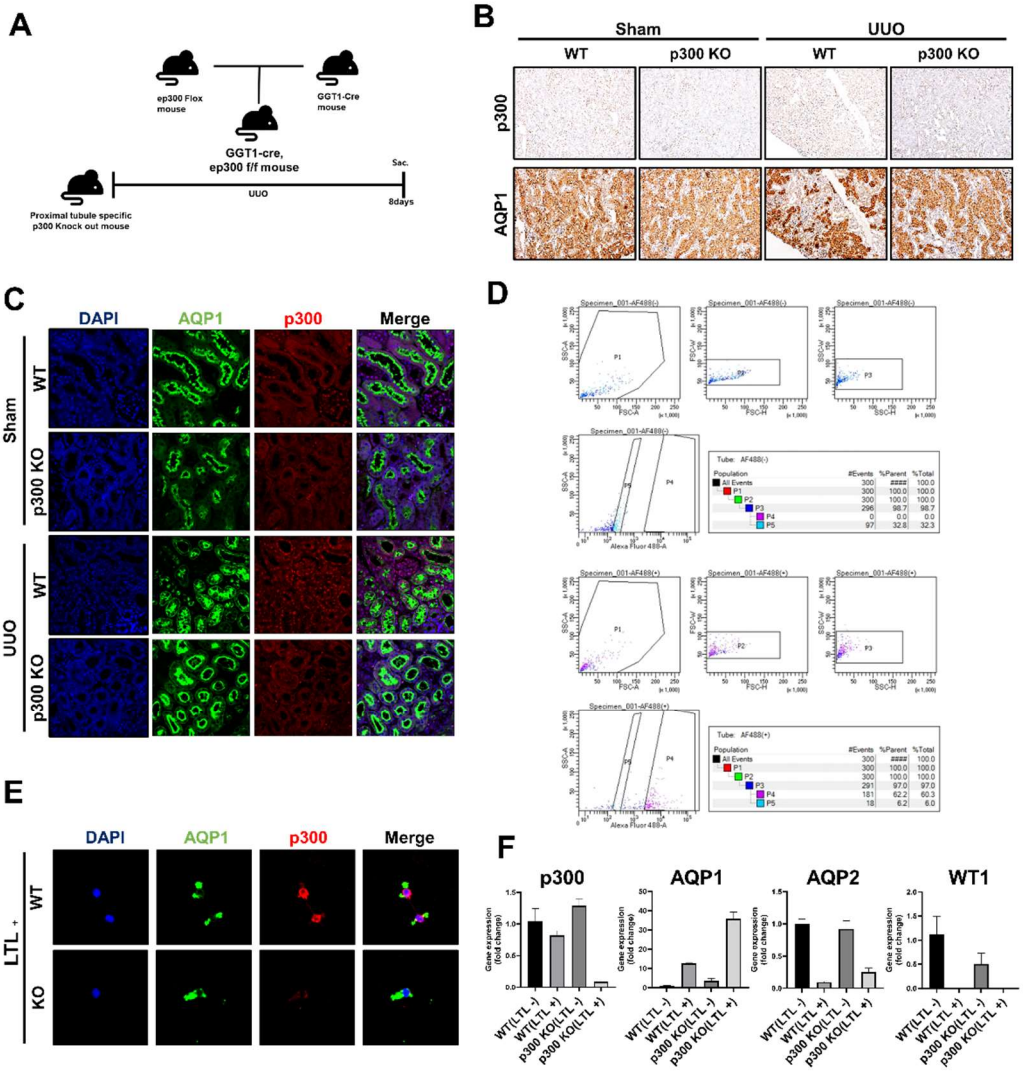

Figure 6. Generation of proximal tubular cell specific p300 knock-out mice. (A) Schematic image of the mouse generation process (B) Representative image of p300 and AQP1 immunohistochemistry using serially sectioned samples. Samples from UUO-induced fibrosis mouse model using wild-type and p300 knock-out (KO) mouse. (C) Representative image of p300 and AQP1 co-immunofluorescence (IF) in mouse kidney samples. Samples from UUO-induced fibrosis mouse model using wild-type and p300 knock-out mouse. (D) Gating for cell sorting with BD ARIA 3 device. The P5 region of the upper graph shows that the LTL negative cells. The P4 region of the bottom graph shows that the LTL positive cells (E) Representative image of p300 and AQP1 co-immunofluorescence (IF) in sorted LTL positive cell from wild-type and p300 knock-out mouse. (F) mRNA levels of p300 and kidney cell specific marker genes of LTL positive and negative cell from wild-type and p300 knock-out mouse.

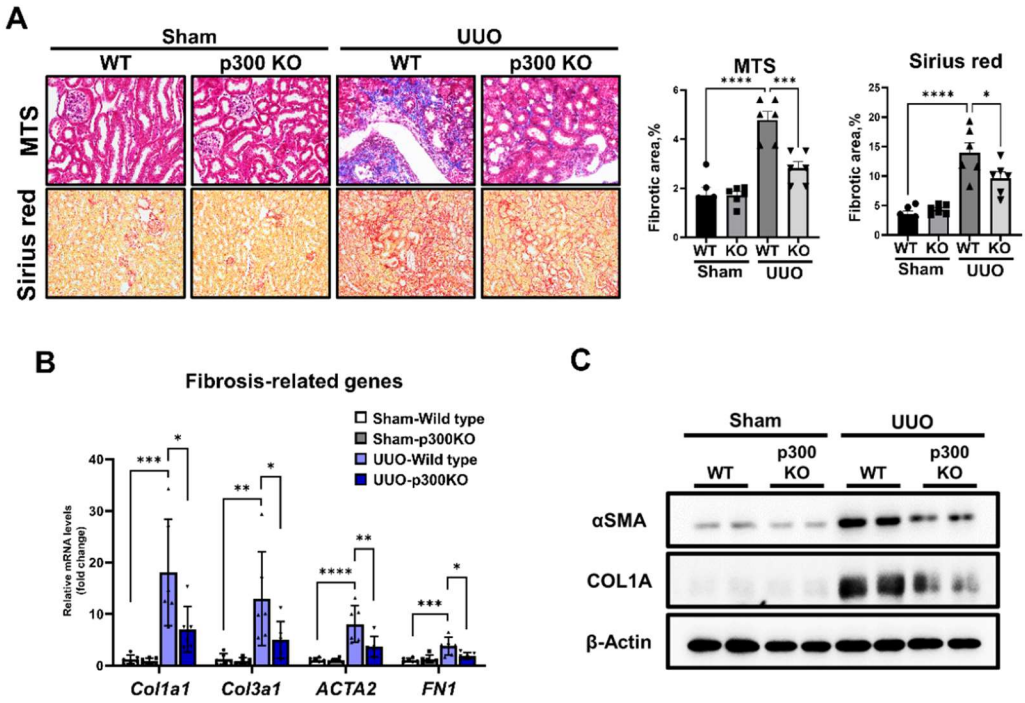

Figure 7. Proximal tubular cell-specific p300 knock-out attenuates fibrosis progression in UUO-induced renal fibrosis mouse model. (A) Representative image of Masson trichrome staining (MTS) and Sirius red staining using kidney samples. Samples from UUO-induced fibrosis mouse model using wild-type and p300 knock-out (KO) mouse. The graph represents quantification of fibrotic area in histological staining images. Data are represented as mean ± SEM, *P < 0.05, **P < 0.01, and ****P < 0.0001 by ordinary one-way ANOVA test. (B) mRNA levels of fibrosis-related genes of kidney tissue from UUO-induced fibrosis mouse model using wild-type and p300 knock-out mouse. Data are represented as mean ± SEM, *P < 0.05, **P < 0.01, ***P < 0.001 and ****P < 0.0001 by ordinary one-way ANOVA test. (C) Protein levels of fibrosis indicate protein αSMA and COL1A. β-actin was used as the sample loading control.

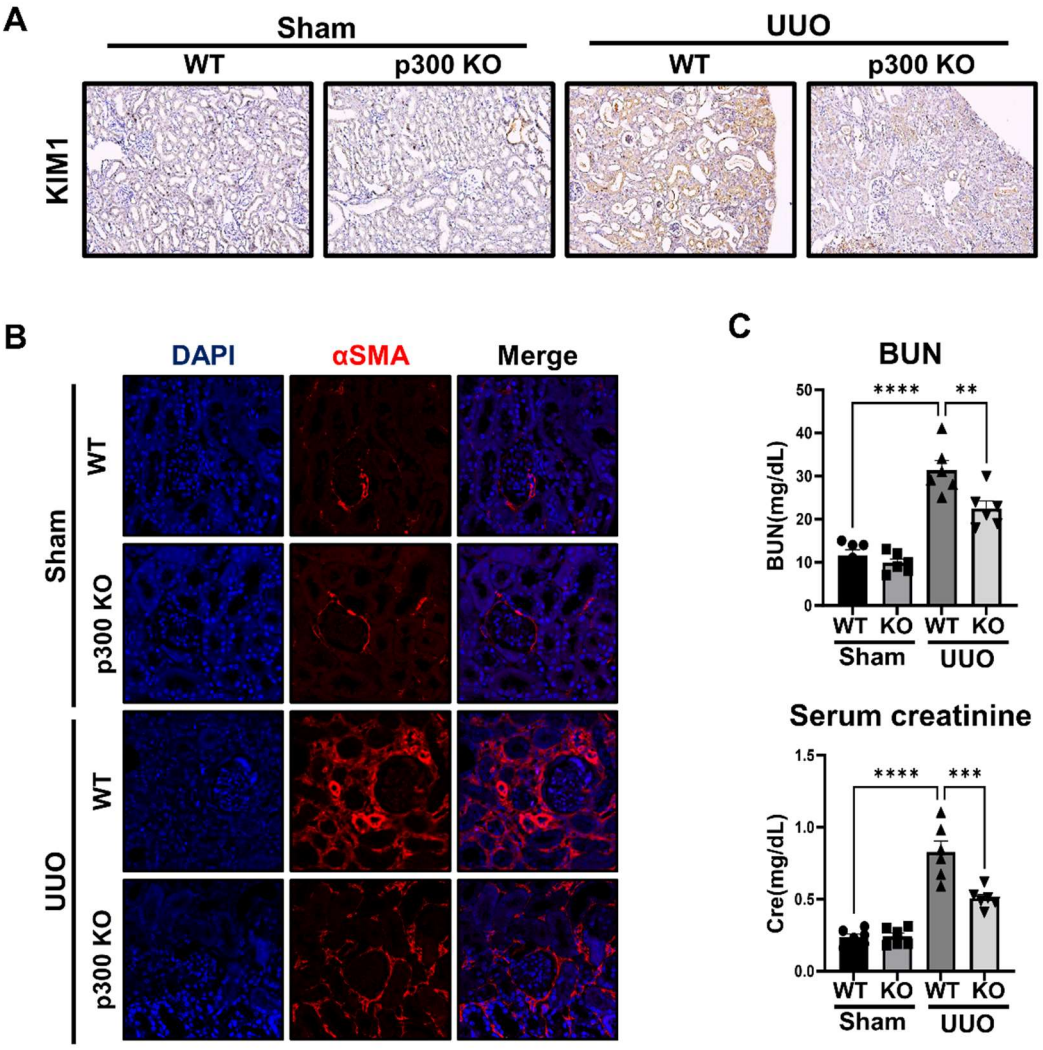

Figure 8. Proximal tubular cell-specific p300 knock-out attenuates kidney injury and myofibroblast activation in UUO-induced renal fibrosis mouse model. (A) Representative image of KIM1 immunohistochemistry (IHC) using kidney samples. Samples from UUO-induced fibrosis mouse model using wild-type and p300 knock-out (KO) mouse. (B) Representative image of αSMA immunofluorescence (IF) using kidney samples. Samples from UUO-induced fibrosis mouse model using wild-type and p300 knock-out mouse. (C) Renal function test by biochemical test of Blood urea nitrogen (BUN) and serum creatinine. Serums from UUO-induced fibrosis mouse model using wild-type and p300 knock-out mouse. Data are represented as mean ± SEM, **P < 0.01, ***P < 0.001 and ****P < 0.0001 by ordinary one-way ANOVA test.

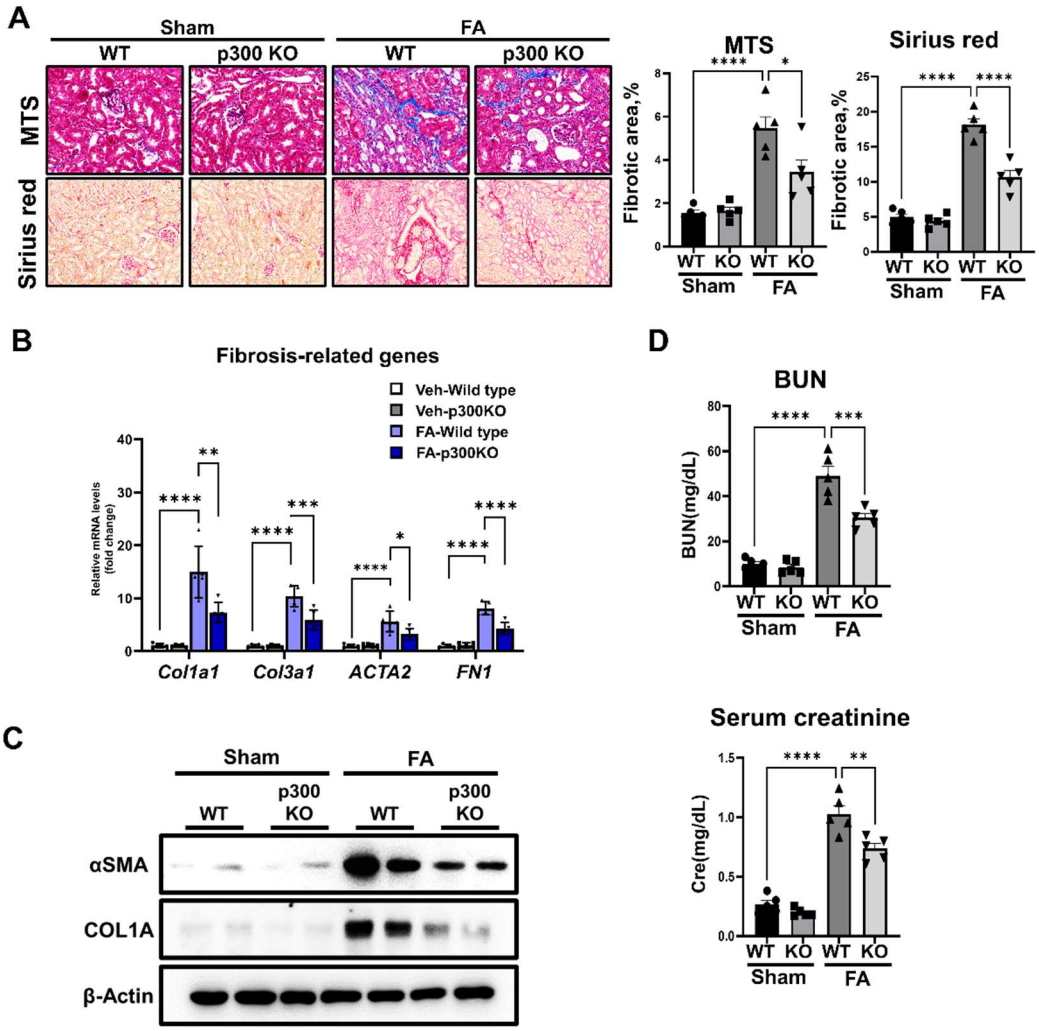

Figure 9. Proximal tubular cell-specific p300 knock-out attenuates kidney fibrosis and injury in FA-induced renal fibrosis mouse model. (A) Representative image of Masson trichrome staining (MTS) and Sirius red staining using kidney samples. Samples from FA-induced fibrosis mouse model using wild-type and p300 knock-out (KO) mouse. The graph represents quantification of fibrotic area in histological staining images. Data are represented as mean ± SEM, *P < 0.05, and ****P < 0.0001 by ordinary one-way ANOVA test. (B) mRNA levels of fibrosis-related genes of kidney tissue from FA-induced fibrosis mouse model using wild-type and p300 knock-out (KO) mice. Data are represented as mean ± SEM, *P < 0.05, **P < 0.01, ***P < 0.001 and ****P < 0.0001 by ordinary one-way ANOVA test. (C) Protein levels of fibrosis indicate protein αSMA and COL1A. β-actin was used as the sample loading control. (D) Renal function test by biochemical test of Blood urea nitrogen (BUN) and serum creatinine. Serums from FA-induced fibrosis mouse model using wild-type and p300 knock-out mice. Data are represented as mean ± SEM, **P < 0.01, ***P < 0.001 and ****P < 0.0001 by ordinary one-way ANOVA test.

3.3. The protein stability of p300 is regulated by AKT signaling-induced phosphorylation at Serine 1834 site

To identify the molecular mechanisms that regulate p300 in renal proximal tubule cells, first, primary renal proximal tubular cells (PTEC) isolated from mouse kidneys were treated with TGF-beta, a well-known fibrotic stimulus. A time-dependent increase of p300 protein levels was observed in TGF-beta-treated cells (Figure 10A). To further explore particular physiological regulatory pathways of p300, the human renal proximal tubular cell line HK-2 was used. Using Western blot analysis and cellular immunofluorescence staining, it was verified that p300 protein expression was increased by TGF-beta treatment in HK-2 cells (Figure 10B-C). But, RT-qPCR analysis failed to observe significant changes in mRNA levels at 6, 12, 24, and 48 hours post-TGF-beta treatment (Figure 10D). Recent studies propose that p300 protein levels are regulated through protein stabilization, a mechanism of regulating protein level, as demonstrated in the lungs and liver. To investigate the p300 in renal proximal tubular cells undergoes similar regulation of protein stability, HK-2 cells were treated with MG132 and cycloheximide. (CHX). Moreover, the increase of p300 protein stability by TGF-beta stimuli was observed (Figure 10E-F). Recent research highlights that the stability of p300 is regulated by phosphorylation at Serine 1834 site through the AKT signaling pathway. A time-dependent increase of p300 phosphorylation at Serine 1834 by TGF-beta stimulation was observed in HK-2 cells. In addition, TGF-beta stimulation led to the phosphorylation of AKT, resulting in elevated p300 phosphorylation (Figure 11A-B). To investigate whether TGF-beta-induced p300 phosphorylation is mediated by the AKT pathway, HK-2 cells were treated with TGF-beta and the TGF-beta inhibitor LY2157299, and the Pan-AKT inhibitor LY294002. Blockade the TGF-beta and AKT signal led to a decrease in p300 phosphorylation and p300 protein levels (Figure 11C). To elucidate the function of serine 1834 site of p300 during

stability regulation, a mutant construct replacing Serine 1834 with Alanine in p300 was generated and transfected to HK-2 cells for overexpression, where endogenous p300 was knocked down using shRNA. Unlike the wild-type p300, the S1834A mutant-p300 was decreased its level and phosphorylation upon TGF-beta stimulation (Figure 12A). In addition, in the CHX chase assay, reduced protein stability was verified in the p300(S1834) mutant form (Figure 12B). To elucidate whether AKT signaling regulates protein stabilization of p300, CHX-chase assay was performed with LY294002, an AKT inhibitor, and a decrease in the stability of the p300 mutant (S1834A) compared to the wild type p300 was observed (Figure 12C). Furthermore, an increase of the phosphorylation of the p300 Serine 1834 site in a UUO-induced fibrosis mouse model was demonstrated by immunohistochemistry and immunofluorescence staining (Figure 13A-B).

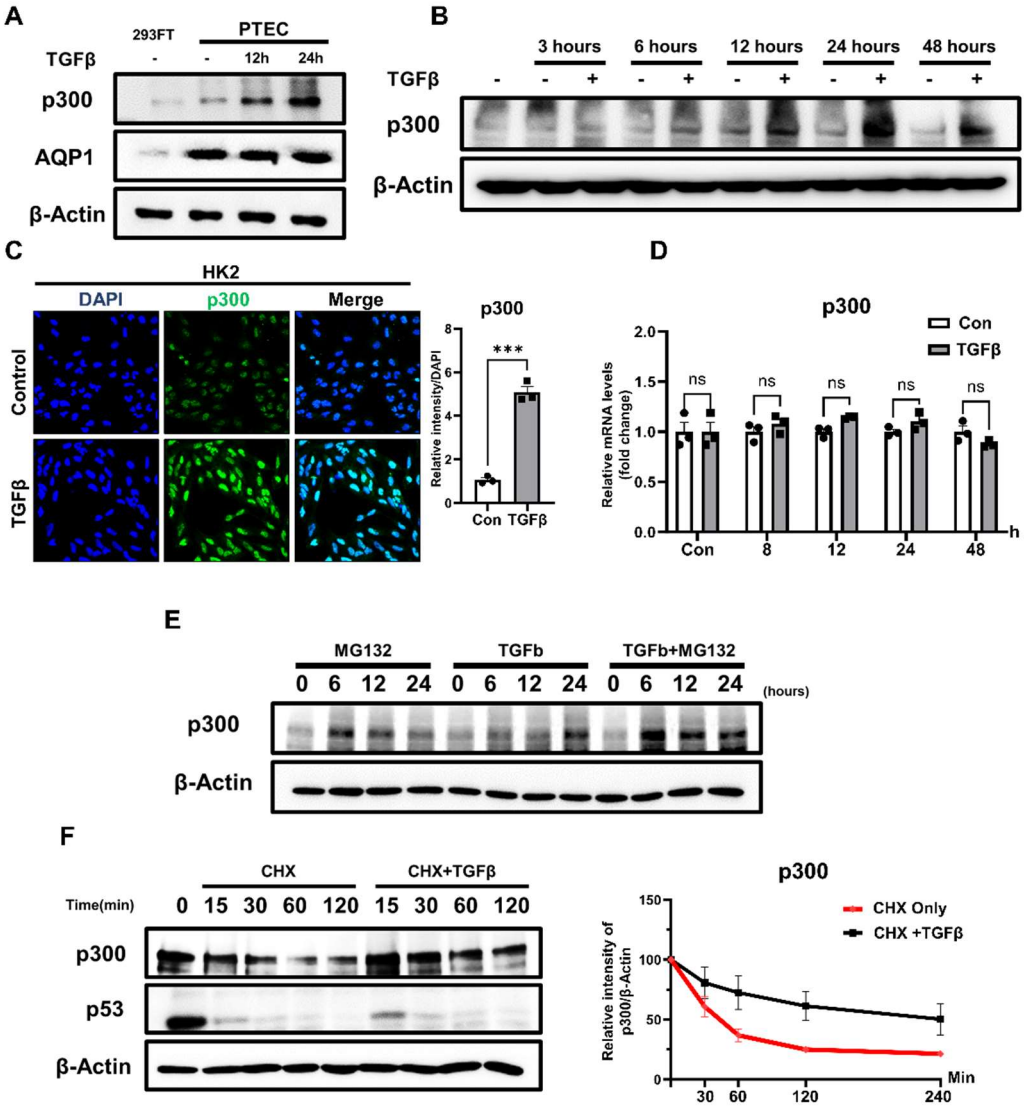

Figure 10. p300 elevated at the protein level, not the mRNA level, in fibrotic condition. (A) Protein levels of p300 in primary proximal tubular epithelial cell (PTEC) treated with TGFβ. (B) Protein levels of p300 in HK2 cell line treated with TGFβ. (C) Representative image of p300 immunofluorescence in HK2 cell line treated with TGFβ. The graph represent quantification of p300 immunofluorescence image (normalized by DAPI). Data are represented as mean ± SEM, ***P < 0.001 by ordinary one-way ANOVA test. (D) mRNA levels of p300 in HK2 cell line treated with TGFβ. Data are represented as mean ± SEM, ns, not-significant. by t-test. (E) Protein levels of p300 in HK2 cell line treated with TGFβ and MG132 (proteasome inhibitor). (F) Protein levels of p300 in HK2 cell line treated with TGFβ and Cycloheximide (CHX, protein synthesis inhibitor). The graph represent quantification of p300 intensity in western blot image (normalized by β-Actin).

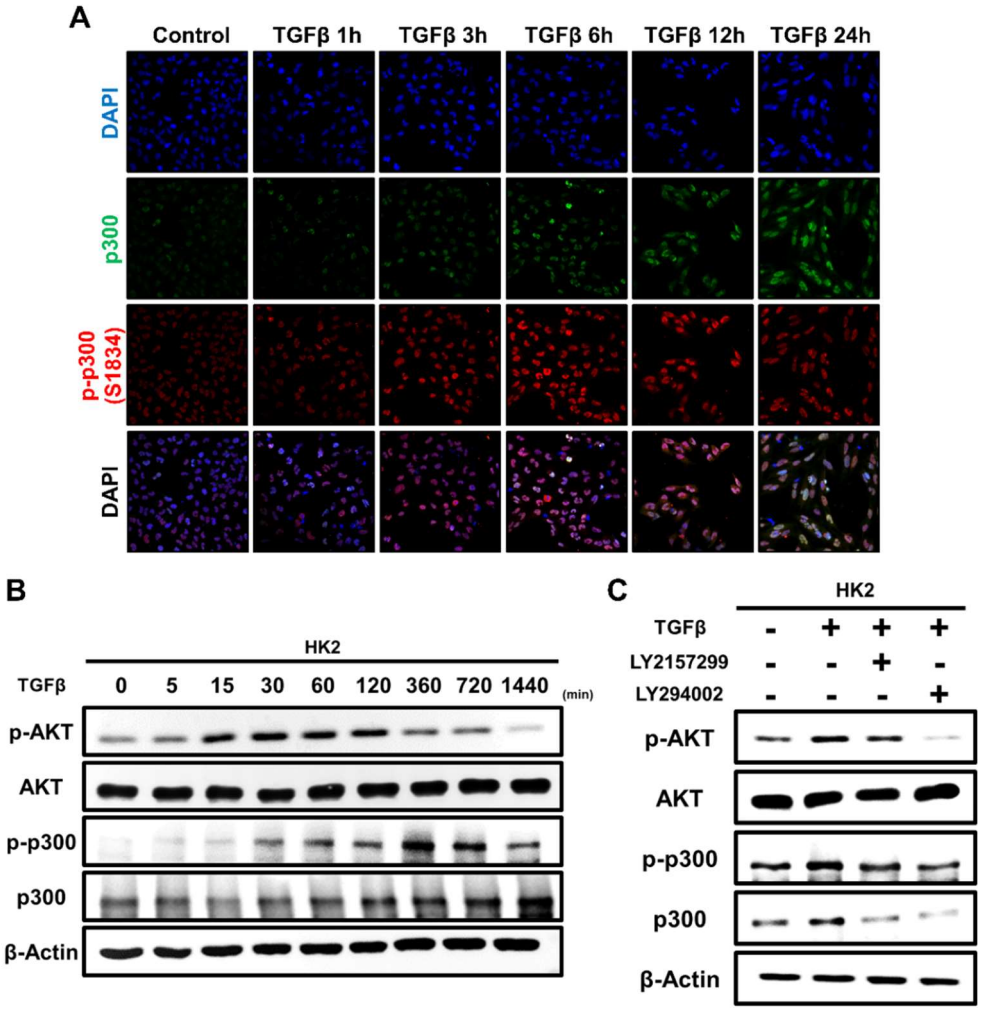

Figure 11. Increase of phosphorylation of p300 Serine 1834 site in fibrotic condition. (A) Representative image of p300 and p-p300 immunofluorescence in HK2 treated with TGFβ for the indicated time. (B) Protein levels of AKT, phosphorylated AKT at Serine 473 (p-AKT), p300 and phosphorylated p300 at Serine 1834 (p-p300) in HK2 treated with TGFβ for the indicated time. (C) Protein levels of AKT, p-AKT, p300 and p-p300 in HK2 treated with TGFβ, LY2157299 (TGFβ inhibitor) and LY294002(AKT inhibitor).

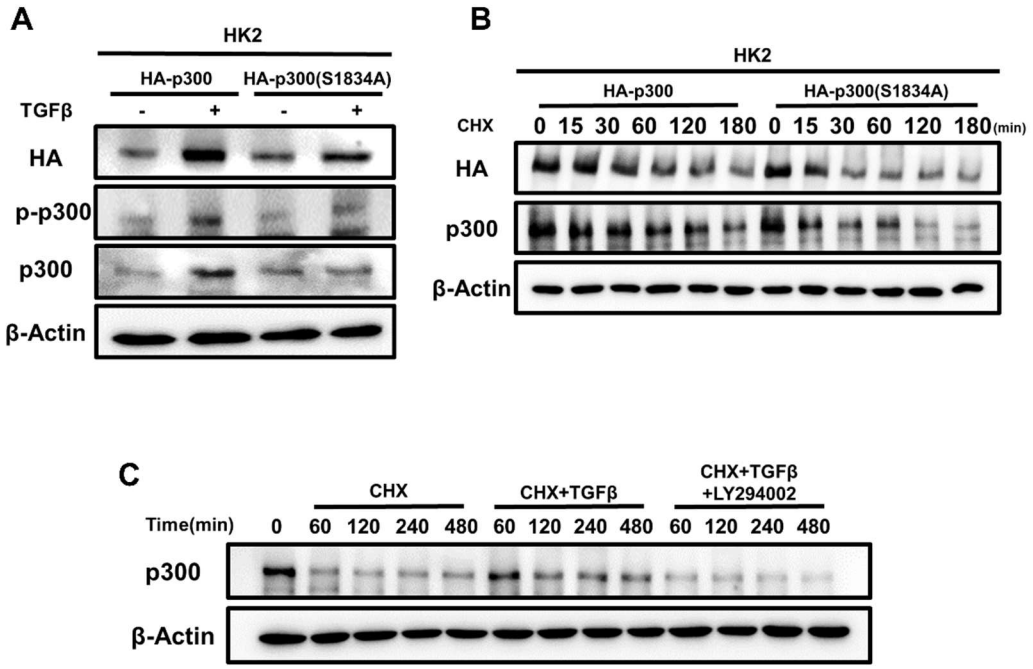

Figure 12. Regulation of p300 stability via AKT-p-p300 axis in fibrotic condition. (A) Protein level of HA, phosphorylated p300 at Serine 1834 and p300 in HA-p300 and HA-p300 Serine to Alanine mutation construct transfected HK2 cell treated with TGFβ. (B) Protein level of HA and p300 in HA-p300 and HA-p300 Serine to Alanine mutation construct transfected HK2 cell treated with Cycloheximide (CHX, protein synthesis inhibitor) for the indicated time. (C) Protein level of p300 in HK2 cell treated with TGFβ, CHX and LY294002 (AKT inhibitor) for the indicated time.

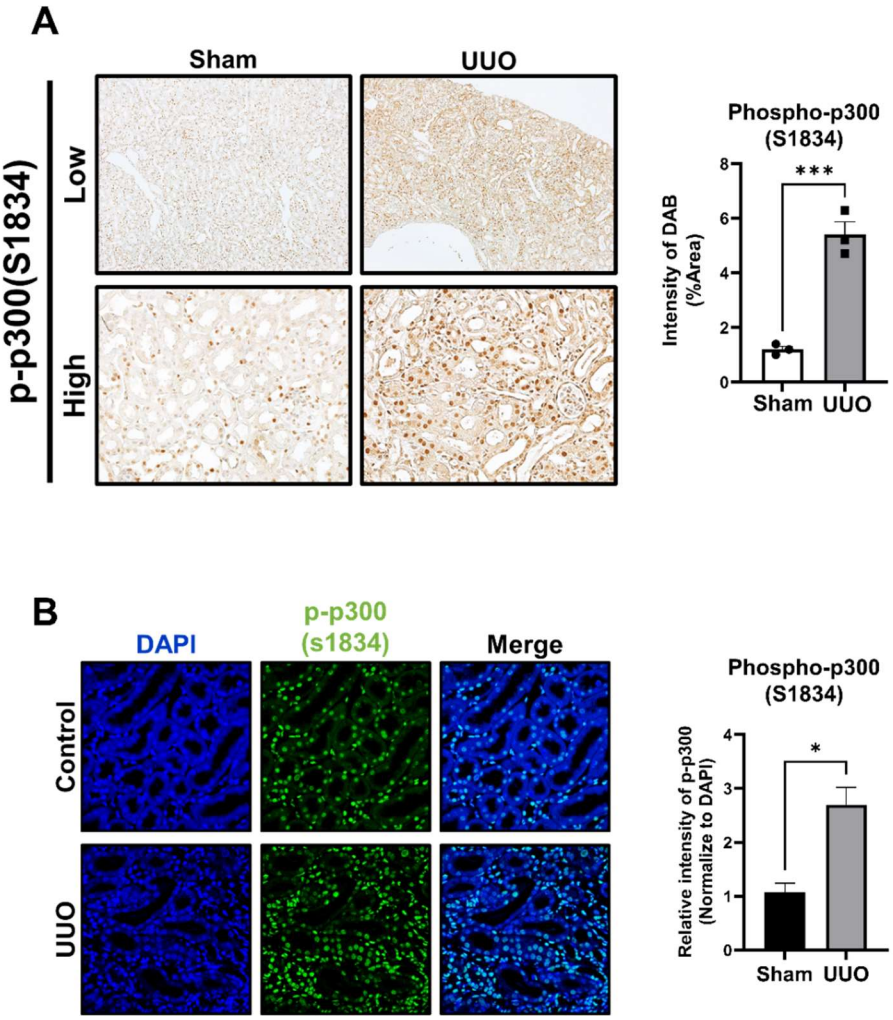

Figure 13. Increase of p300 phosphorylation at Serine 1834 in UUO-induced mouse fibrosis model kidney. (A) Representative image of phosphorylated p300 immunohistochemistry (IHC) in mouse kidney tissues from UUO-induced mouse fibrosis model. The graph represents quantification of histological staining images. Data are represented as mean ± SEM, ***P < 0.001 by t-test. (B) Representative image of phosphorylated p300 immunofluorescence (IF) in mouse kidney tissues from UUO-induced mouse fibrosis model. The graph represents quantification of intensity of p-p300 S1834 (normalized by DAPI). Data are represented as mean ± SEM, *P < 0.05 by t-test.

3.4. PPM1K diminishes the stability of p300 by interacting with p300 to regulate the de-phosphorylation of the serine1834 site

To identify the partner phosphatase of p300 that induces de-phosphorylation of p300 at serine 1834, twelve phosphatases were screened, and the binding of PPP6C, PPM1D, PPM1M, PPM1K, and PPEF1 to p300 was validated through *in vitro* transcription and immunoprecipitation assays (Figure 14A). Among the phosphatases that bind to p300, specifically, PPM1K was identified to significantly reduce p300 protein levels and phosphorylation levels upon its overexpression in HK-2 cells (Figure 14B). Furthermore, the de-phosphorylation function of PPM1K were validated using the PPM1K malfunctioning mutant, PPM1K N94K construct (Figure 14C). To elucidate the region of biding with PPM1K, a partial fragment of p300 was generated to screen the binding region between p300 and PPM1K (Figure 15A). Immunoprecipitation assay with fragmented constructs of p300 and PPM1K revealed that the 4348-5796 amino acid region of p300, including Serine 1834 amino acid, is crucial for binding region with PPM1K (Figure 15B). Furthermore, to verify the interaction of p300 and PPM1K in fibrotic state, p300 and PPM1K were overexpressed in HK-2 cells and the interaction between p300 and PPM1K was diminished by TGF-beta treatment in particular the p300 4348-5896 amino acid fragment (Figure 15C-D). In addition, proximity ligation assays (PLA) in HK-2 cells (Figure 15E), and UUO mouse kidney tissues was performed (Figure 16). The interaction between p300 and PPM1K was reduced in UUO mouse tissues and TGF-beta stimulated HK2 cell line. In conclusion, these findings indicate that TGF-beta induces an increase in p300 protein levels in renal proximal tubular cells, regulated by protein stability rather than mRNA levels. The stability of p300 is regulated by phosphorylation at Serine 1834 through the AKT signaling pathway.

Taken together, PPM1K was identified as a phosphatase that dephosphorylates p300 at Serine 1834, and the interaction between p300 and PPM1K decreased under fibrotic conditions.

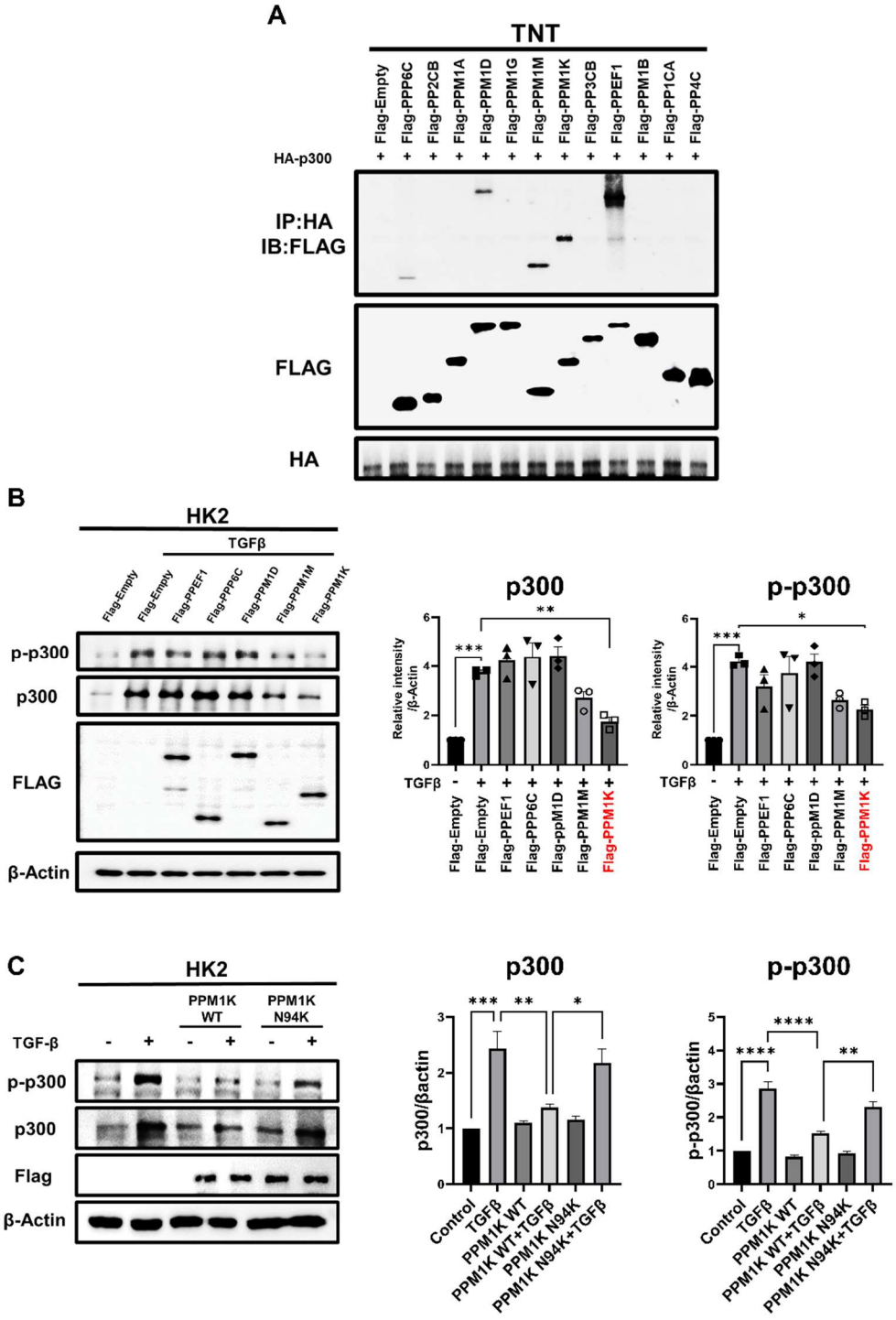

Figure 14. PPM1K dephosphorylate p300 Serine 1834 site via protein interaction. (A) Screening of p300 partner phosphatase that de-phosphorylate Serine 1834 site via immunoprecipitation assay. (B) Protein level of p300 and phosphorylated p300 at Serine 1834 in phosphatases transfected HK2 cell treated with TGFβ. The graph represent quantification of p300 and phosphorylated p300 at Serine 1834 intensity in western blot image (normalized by β-Actin). Data are represented as mean ± SEM, *P < 0.05, **P < 0.01, ***P < 0.001 and ****P < 0.0001 by ordinary one-way ANOVA test. (C) Protein level of p300 and phosphorylated p300 at Serine 1834 in PPM1K and PPM1K Asparagine to Lysine mutation construct transfected HK2 cell treated with TGFβ. The graph represent quantification of p300 and phosphorylated p300 at Serine 1834 intensity in western blot image (normalized by β-Actin). Data are represented as mean ± SEM, *P < 0.05, **P < 0.01, ***P < 0.001 and ****P < 0.0001 by ordinary one-way ANOVA test.

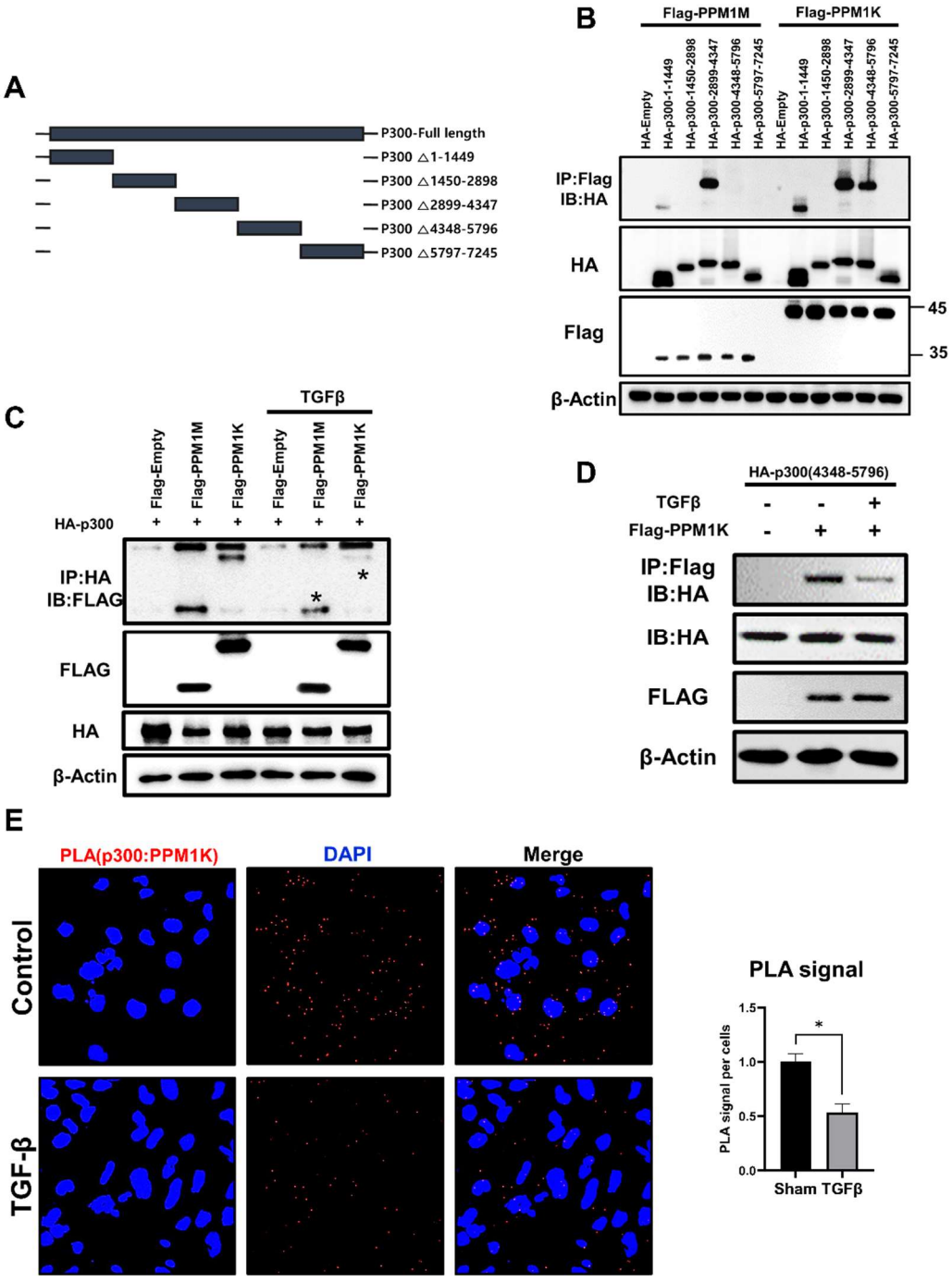

Figure 15. PPM1K has diminished interaction with the p300 4348-5796 amino acid site in fibrotic condition. (A) Schematic image of partial construct of the p300. (B) Screening of PPM1K biding site on p300 by Immunoprecipitation assays using p300 partial construct. (C) Interaction of p300 and PPM1M, PPM1K in HK2 cell treated with TGFβ (D) Interaction of PPM1K at p300 4348-5796 amino acid region in HK2 cell treated with TGFβ (E) Representative image of Proximity Ligation assay (PLA) in HK2 cell treated with TGFβ. The graph represents quantification of PLA signal (normalized by DAPI). Data are represented as mean ± SEM, *P < 0.05 by t-test.

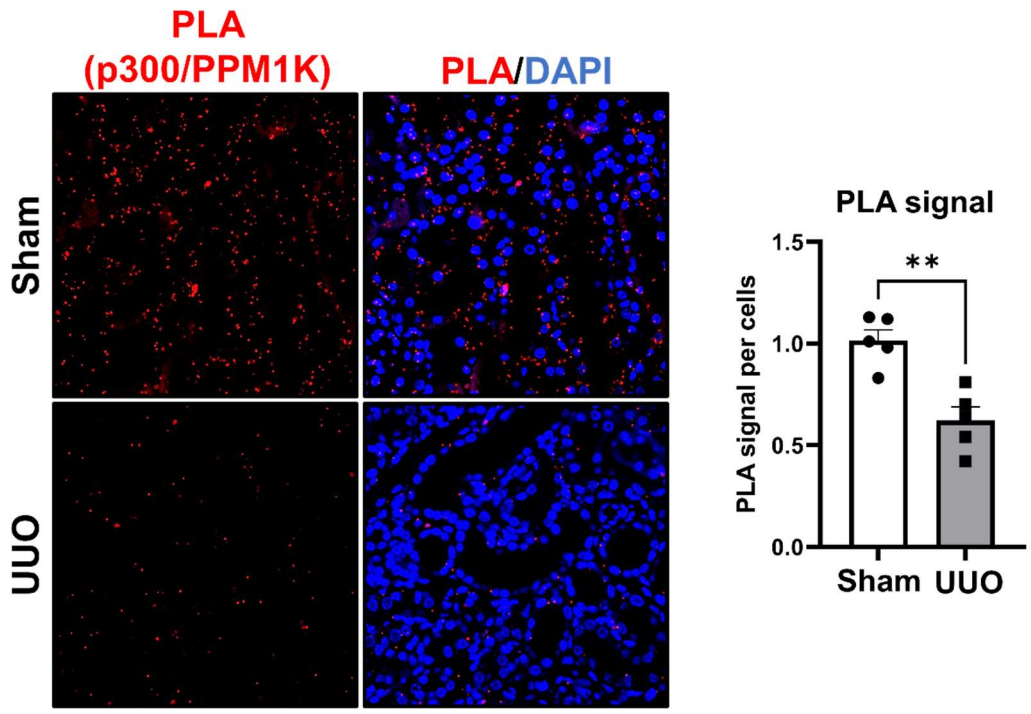

Figure 16. PPM1K has diminished interaction with the p300 in UUO-induced mouse kidney. Representative image of Proximity Ligation assay (PLA) in mouse kidney tissue from UUO-induced mouse fibrosis model. The graph represents quantification of PLA signal (normalized by DAPI). Data are represented as mean ± SEM, **P < 0.01 by t-test.

3.5. Down-regulation of PPM1K in CKD and murine fibrosis models

First, the clinical relevance of phosphatase PPM1K in chronic kidney disease (CKD) was investigated, particularly focusing on diabetic nephropathy (DM), the major type of CKD. Analysis of the Gene Expression Omnibus (GEO) dataset (GSE142025) revealed a significant decrease in PPM1K expression in DM patients (Figure 17A), and single-cell RNA sequencing analysis of CKD patients (GSE183279) demonstrated a reduction of PPM1K expression levels and the proportion of PPM1K expression cells in PTCs (Figure 17B). IHC of CKD patients' kidneys revealed a substantial decrease in PPM1K expression, particularly in FSGS and IgAN patients (Figure 17C). Furthermore, the decrease of PPM1K expression was observed in the UUO mouse fibrosis model at 2, 4, 6, 8, and 14 days after surgery (Figure 18A), in addition, mRNA level of PPM1K was downregulated in UUO kidney fibrosis model (Figure 18B). In the UUO mouse model, opposite expression trend of p300 and PPM1K. were observed in immunofluorescence staining. In addition, the inverse correlation of p300 and PPM1K expression was confirmed by correlation analysis ($R2=0.793$, $p<0.0001$) and western blot assay (Figure 19A-C). To assess the physiological change of PPM1K in PTCs, primary PTCs isolated from mice and the HK-2 cell line were treated with TGFβ (Figure 19D-E).

As a results, the expression of PPM1K was shown to decrease in CKD patients and mouse fibrosis models, and the expression of PPM1K and p300 in PTCs demonstrated an inverse correlation. Moreover, mRNA levels of PPM1K showed a decreasing trend in UUO and FA models.

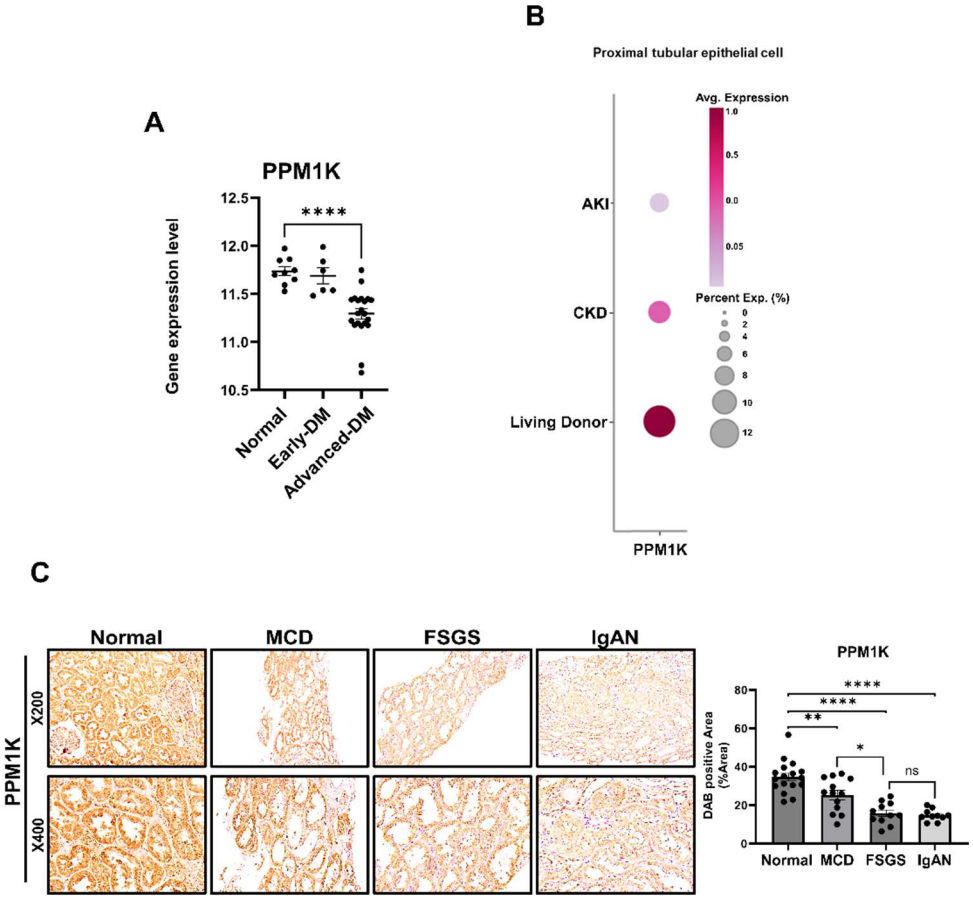

Figure 17. Reduction of PPM1K in patients with CKD. (A) mRNA levels of PPM1K in diabetes mellitus (DM) patient's kidney. (B) mRNA levels of PPM1K in CKD and AKI patient's kidney proximal tubular epithelial cell. (C) Representative image PPM1K immunohistochemistry (IHC) in kidney tissue from Minimal Change Disease (MCD), Focal segmental glomerulosclerosis (FSGS), IgA nephropathy (IgAN) patients and normal donor. The graph represents quantification of DAB area in histological staining images. Data are represented as mean ± SEM, *P < 0.05, **P < 0.01 and ****P < 0.0001 by ordinary one-way ANOVA test.

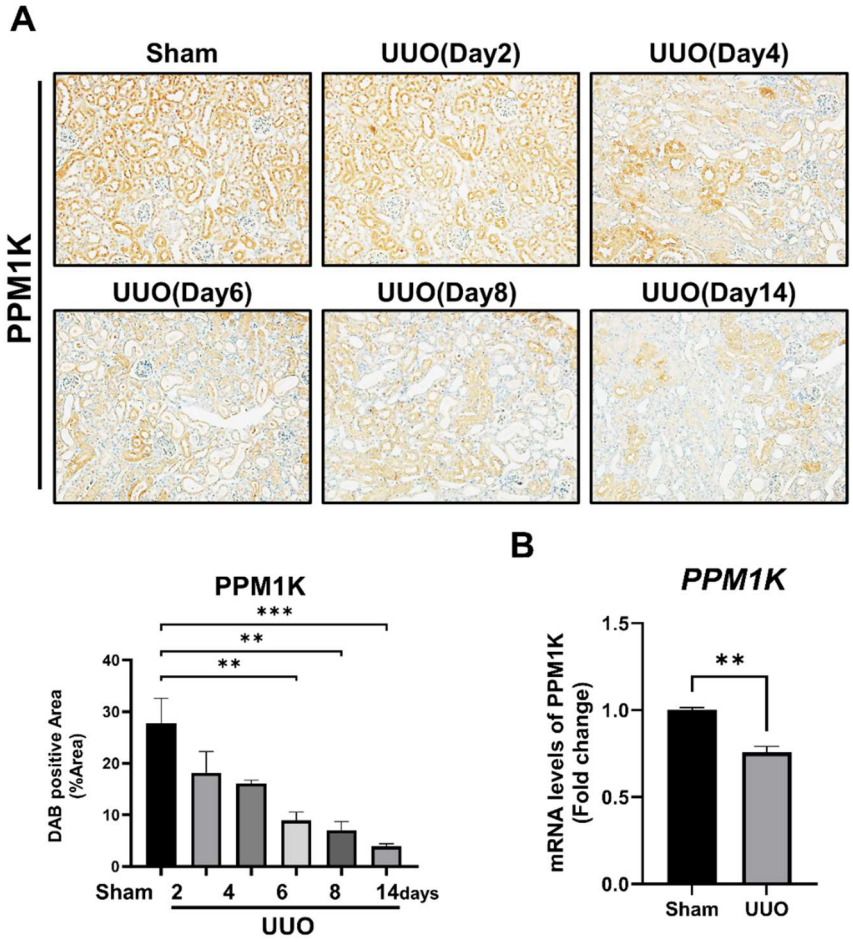

Figure 18. Reduction of PPM1K in UUO-induced mouse fibrosis model kidney. (A) Representative image PPM1K immunohistochemistry (IHC) in kidney tissue sample. Samples from UUO-induced mouse kidney 2, 4, 6, 8, and 14 days after surgery. The graph represents quantification of DAB area in histological staining images. Data are represented as mean ± SEM, **P < 0.01 and ***P < 0.001 by ordinary one-way ANOVA test. (B) mRNA level of PPM1K in UUO-induced mouse fibrosis model kidney (8 days after surgery). Data are represented as mean ± SEM, **P < 0.01 by t-test.

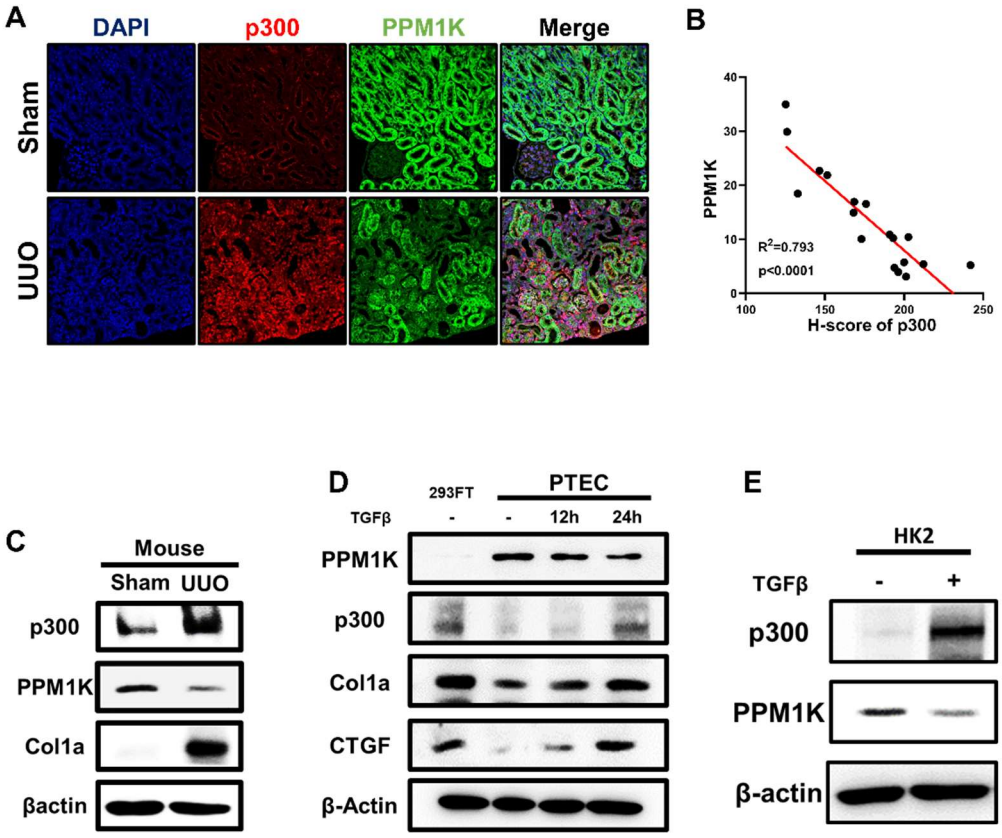

Figure 19. Inverse correlation of p300 and PPM1K in fibrotic condition. (A) Representative image of p300 and PPM1K co-immunofluorescence (IF) in mouse kidney tissues from UUO-induced mouse fibrosis model. (B) Correlation analysis of H-score of p300 and PPM1K expression in immunohistochemistry (IHC) of UUO-induced mouse kidneys. (C) Protein levels of p300, PPM1K and Col1a in UUO-induced mouse fibrosis model kidney (8 days after surgery). (D) Protein levels of p300, PPM1K, Col1a and CTGF in primary proximal tubular epithelial cell (PTEC) treated with TGFβ. (E) Protein levels of p300, PPM1K in HK2 cell treated with TGFβ.

3.6. PPM1K negatively regulates fibrosis in the development of renal fibrosis

To reveal the physiological roles of PPM1K on renal fibrosis, the RNA-sequencing dataset of the PPM1K-overexpressing HK-2 cell line (GSE212681) was analyzed, and reductions of fibrosis-related genes such as Col1A1, Col2A1, CTGF, Vimentin, and FN1 were identified (Figure 20A). Furthermore, PPM1K-overexpressed HK-2 cells treated with TGF-beta led to a decrease of fibrosis-related targets expression at both protein and mRNA levels compared with control HK-2 cells but not in PPM1K-N94K-overexpressed HK-2 cells (Figure 20B-C). Conversely, as a result of PPM1K knockdown using siRNA, fibrosis-related genes and proteins increased by TGF were further increased.in HK-2 cell (Figure 20D-F). Furthermore, to investigate the effect of PPM1K on fibrosis development *in vivo*, Adenovirus serotype 5 (Ad5) carrying PPM1K sequence tagged with GFP and Flag was generated. The virus was introduced via sub-capsular (SC) injection into UUO-operated mouse kidneys, and successful viral introduction was confirmed by observing GFP fluorescence (Figure 21A). SC injection of PPM1K-Ad5 into UUO kidney showed a decrease in p300 and p-p300 expression compared to Empty-Ad5 injection (Figure 21 B-D), accompanied by reduced fibrosis observed through MTS and Sirius red staining (Figure 22A). Moreover, protein and mRNA levels of fibrosis-related targets decreased in UUO mouse kidneys with PPM1K overexpression, and kidney functional markers (serum creatinine and BUN) were restored (Figure 22B-D). But there is no change of PPM1K expression in PTCs specific p300 knock-out mice compared with wild-type mice with or without UUO surgery (Figure 23).

In summary. it was revealed that PPM1K plays an important role in the development of renal fibrosis through overexpression and knockdown experiments in HK-2 cells. Furthermore, the anti-

fibrotic roles of PPM1K were demonstrated *in vivo* via PPM1K-Ad5 virus transduction into the UUO mouse renal fibrosis model.

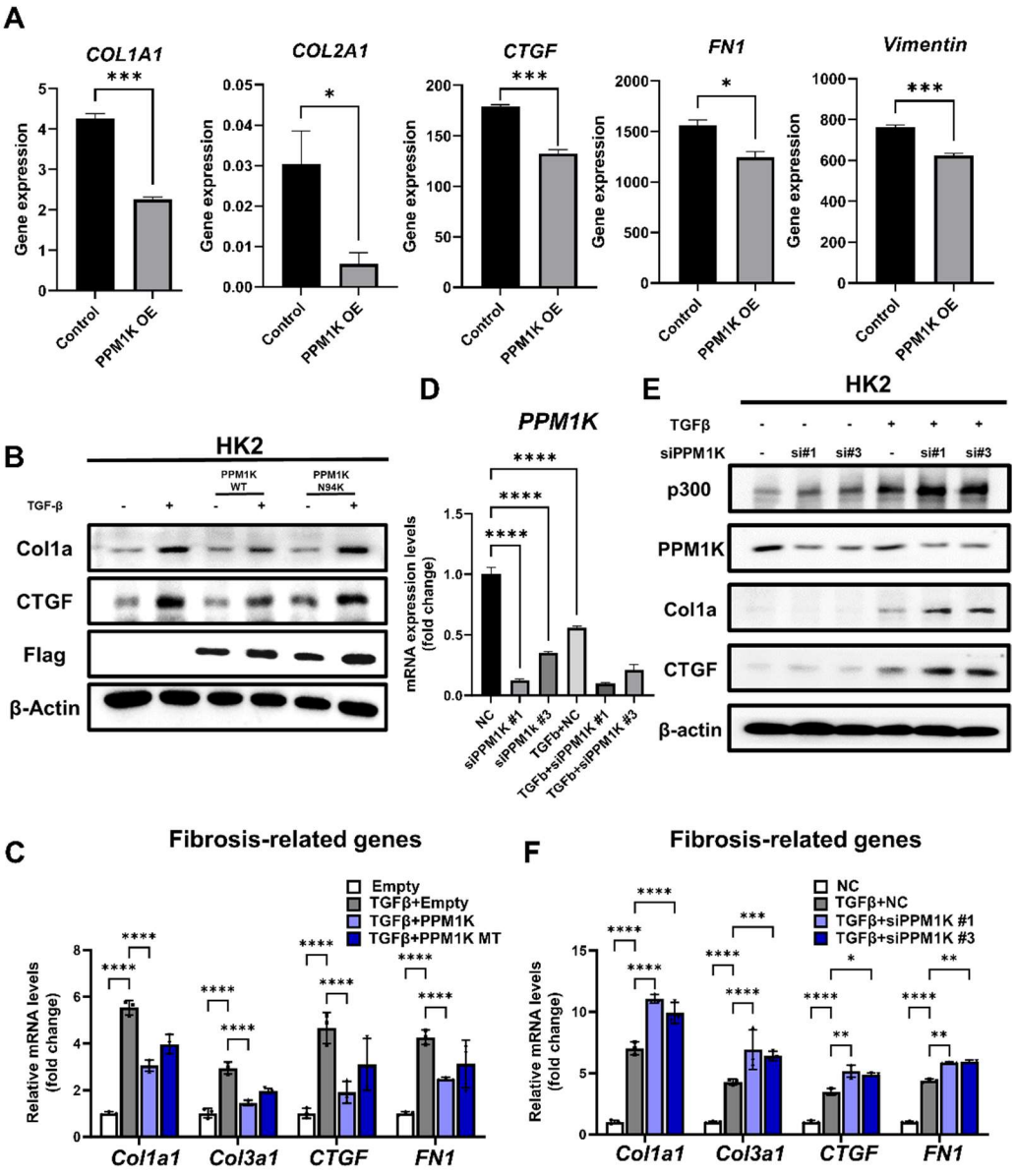

Figure 20. PPM1K reduced fibrosis-related gene and protein. (A) mRNA levels of fibrosis related gene in HK2 cell. RNA-sequencing data from Gene expression omnibus (GEO) data base. Data are represented as mean ± SEM, *P < 0.05 and ***P < 0. by ordinary t-test. (B) Protein levels of Col1a and CTGF in Flag-PPM1K and Flag-PPM1K N94K transfected HK2 cell treated with TGFβ. (C) mRNA levels of fibrosis-related genes in PPM1K and PPM1K N94K transfected HK2 cell treated with TGFβ. Data are represented as mean ± SEM, ****P < 0.0001 by ordinary one-way ANOVA test. (D) mRNA levels of PPM1K in siPPM1K induced PPM1K knocking down HK2 cell. Data are represented as mean ± SEM, ****P < 0.0001 by ordinary one-way ANOVA test. (E) Protein levels of p300, PPM1K, Col1a and CTGF in siPPM1K transfected HK2 cell treated with TGFβ. (F) mRNA levels of fibrosis-related genes in siPPM1K #1 and #3 transfected HK2 cell treated with TGFβ. Data are represented as mean ± SEM, *P < 0.05, **P < 0.01 and ****P < 0.0001 by ordinary one-way ANOVA test.

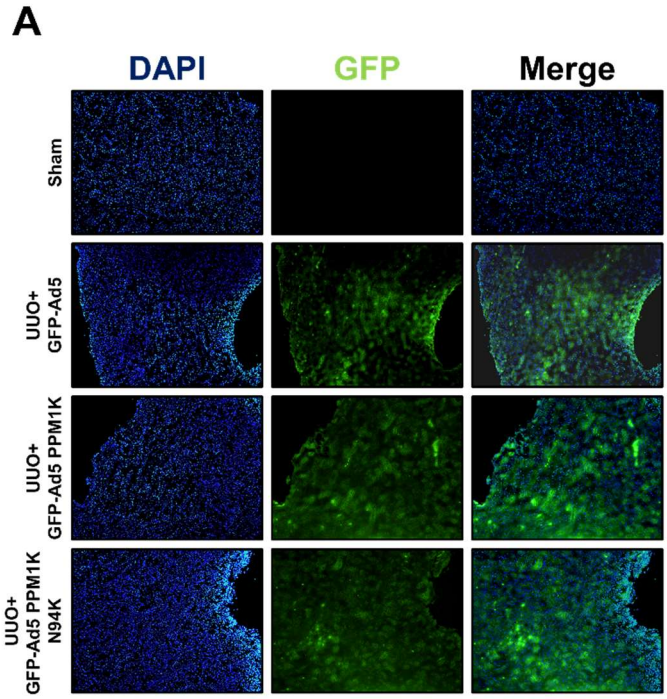

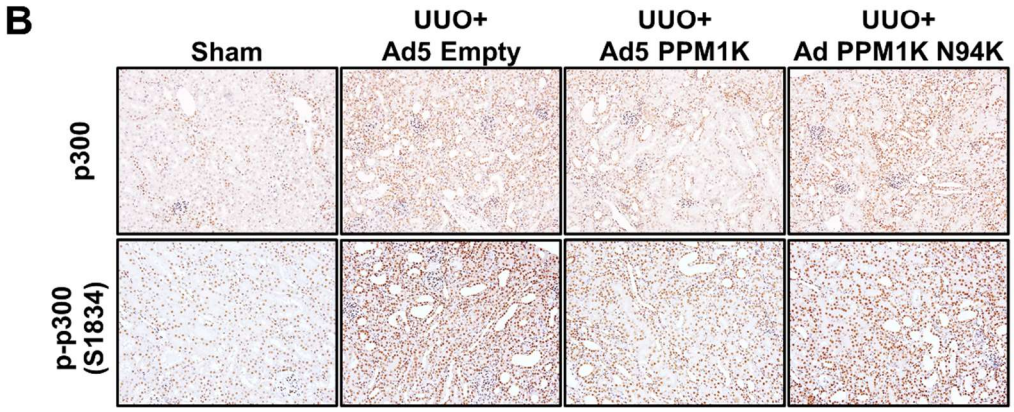

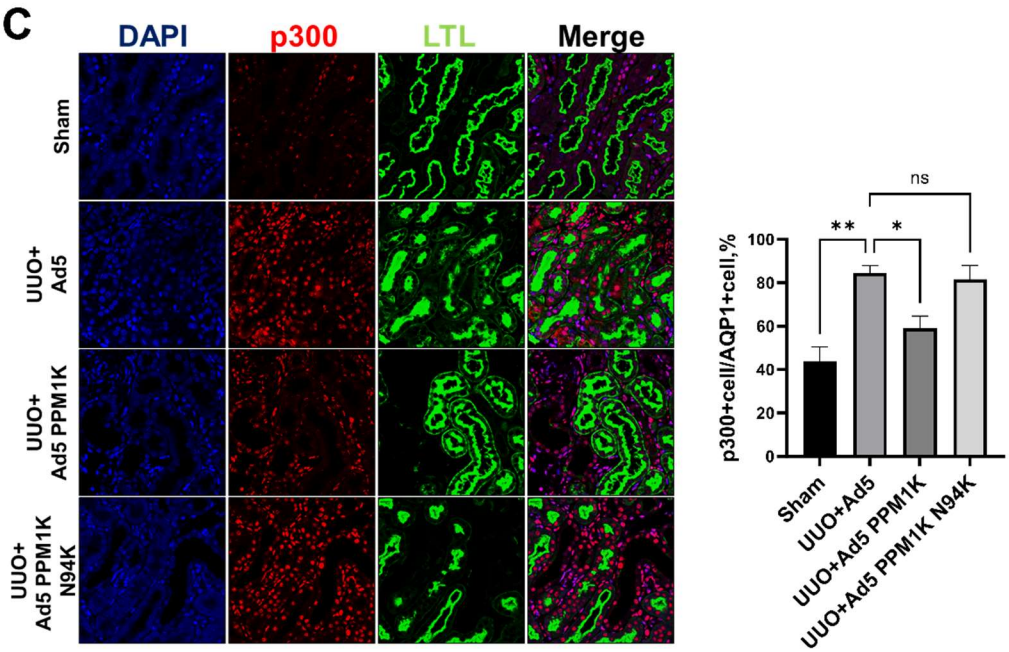

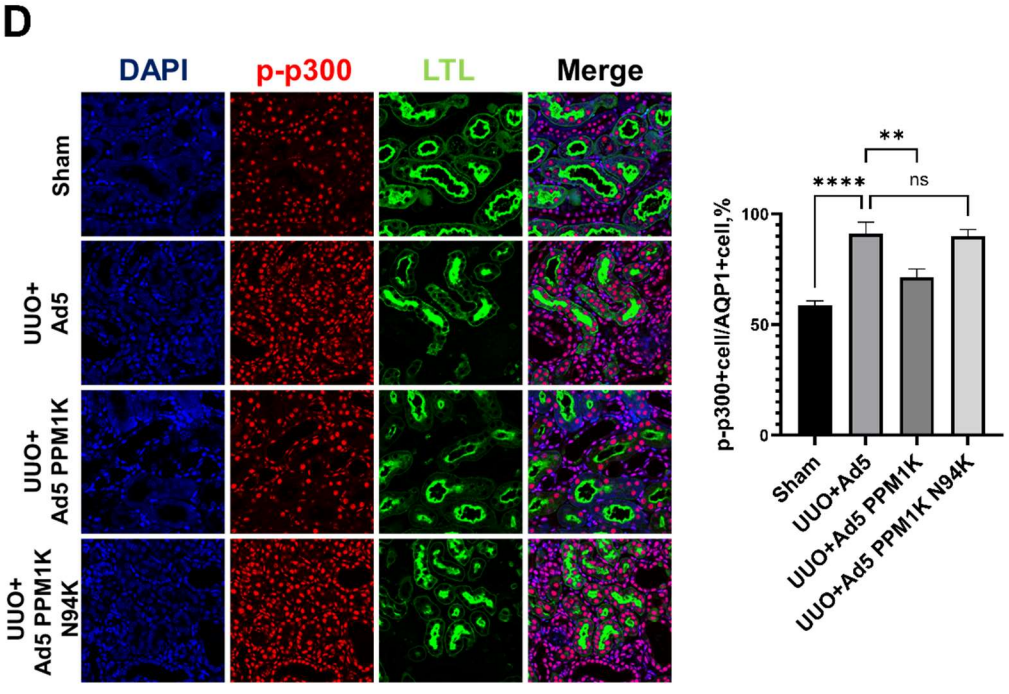

Figure 21. Ad5-PPM1K introduction reduced p300 and phosphorylated p300 at Serine 1834 in UUO-induced mouse kidney fibrosis model. (A) Confirmation of intrarenal introduction via immunofluorescence imaging. (B) Representative image of p300 and phosphorylated p300 at serine 1834 (p-p300) immunohistochemistry (IHC) in kidney tissue sample. Samples from UUO after Ad5-PPM1K and Ad5-PPM1K N94K injected mouse kidneys. (C) Representative image of p300 and Lotus Tetragonolobus Lectin (LTL) Co-immunofluorescence (IF) in kidney tissue sample. Samples from UUO after Ad5-PPM1K and Ad5-PPM1K N94K injected mouse kidneys. The graph represents proportion of p300 positive cell among LTL positive cells. Data are represented as mean ± SEM, *P < 0.05 and **P < 0.01 by ordinary one-way ANOVA test. (D) Representative image of p-p300 and Lotus Tetragonolobus Lectin (LTL) Co-immunofluorescence (IF) in kidney tissue sample. Samples from UUO after Ad5-PPM1K and Ad5-PPM1K N94K injected mouse kidneys. The graph represents proportion of p-p300 positive cell among LTL positive cells. Data are represented as mean ± SEM, **P < 0.01 and ****P < 0.0001 by ordinary one-way ANOVA test.

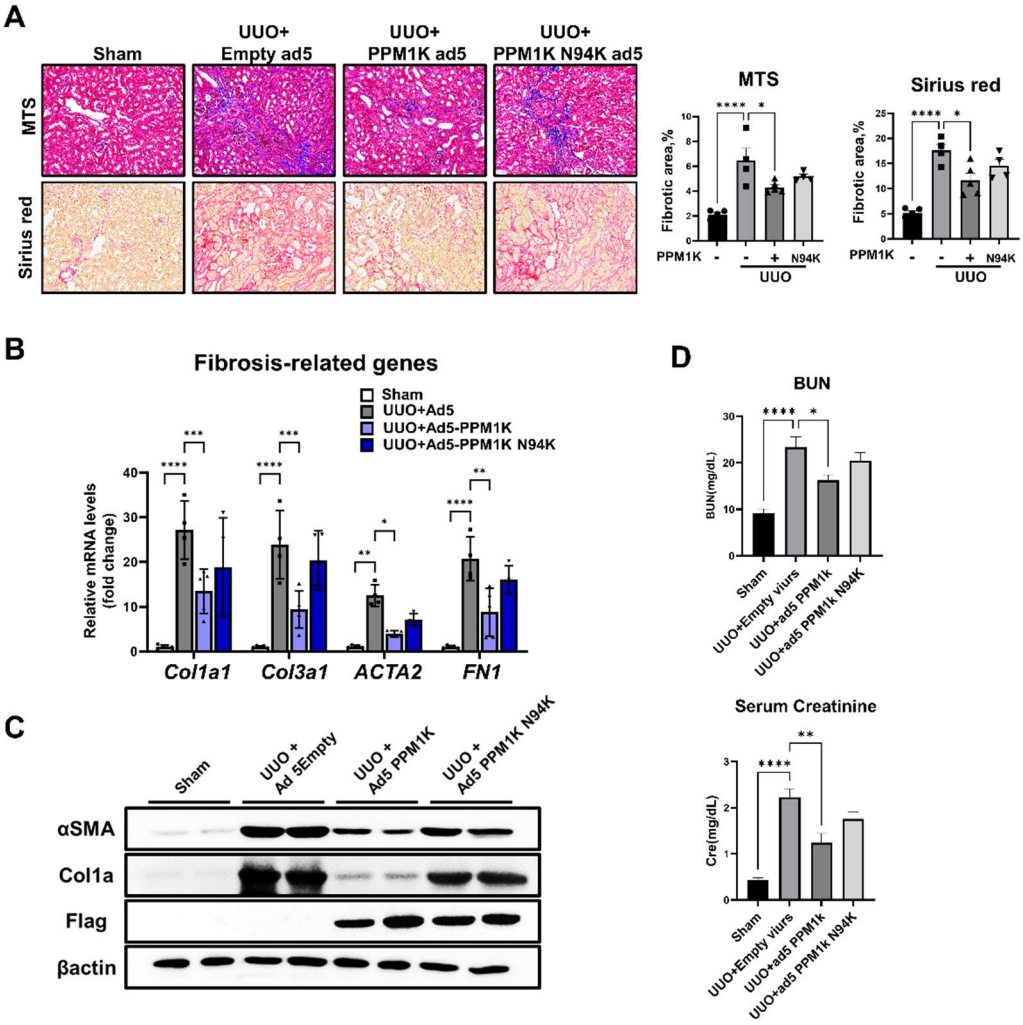

Figure 22. Ad5-PPM1K introduction alleviate kidney fibrosis in UUO-induced mouse kidney fibrosis model. (A) Representative image of Masson trichrome staining (MTS) and Sirius red staining using kidney sample. Samples from Ad5-PPM1K and Ad5-PPM1K N94K introduced UUO-induced mouse model kidney. The graph represents quantification of fibrotic area in histological staining images. Data are represented as mean ± SEM, *P < 0.05 and ****P < 0.0001 by ordinary one-way ANOVA test. (B) mRNA levels of fibrosis-related gene in Ad5-PPM1K and Ad5-PPM1K N94K introduced UUO-induced mouse model kidney. Data are represented as mean ± SEM, *P < 0.05, **P < 0.01, ***P < 0.001 and ****P < 0.0001 by ordinary one-way ANOVA test. (C) Protein levels of fibrosis-related protein αSMA and COL1A. β-actin was used as the sample loading control. (D) Renal function test by biochemical test of Blood urea nitrogen (BUN) and serum creatinine. Serums from Ad5-PPM1K and Ad5-PPM1K N94K introduced UUO-induced mouse model. Data are represented as mean ± SEM, *P < 0.05, **P < 0.01 and ****P < 0.0001 by ordinary one-way ANOVA test.

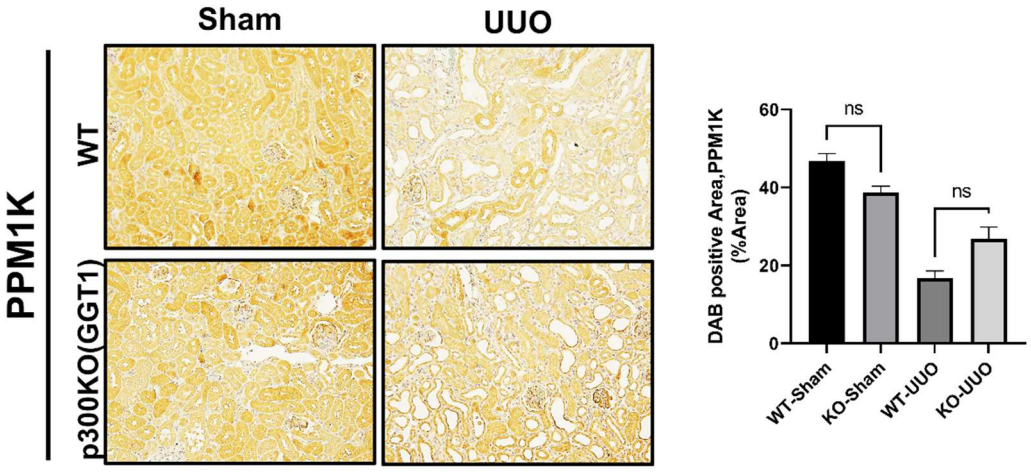

Figure 23. No alterations of PPM1K expression in proximal tubular cell-specific p300 knock-out mouse kidney. Representative image PPM1K immunohistochemistry (IHC) in kidney tissue sample. Samples from UUO-induced fibrosis mouse model using wild-type and p300 knock-out (KO) mice. The graph represents quantification of DAB positive area in histological staining images. Data are represented as mean ± SEM, ns, not significant by ordinary one-way ANOVA test.

3.7. PTC-specific p300 knock-out modulates mesenchymal transition in renal fibrosis development

Previous results showed that Co-transcription factor, p300 in the proximal tubule involved in the development of renal fibrosis. Therefore, to reveal the molecular mechanism involved in p300, RNA-sequencing was performed using kidney tissue from UUO surgery on PTC-specific p300 knock-out mice, and Anti-p300 CUT&TAG-sequencing was performed using primary kidney proximal tubule cells isolated from PTCs specific p300 knock-out mouse kidney tissues to identify genes transcriptionally regulated by p300. The RNA-sequencing analysis identified 702 genes down-regulated in PTCs specific p300 knock-out mice with UUO surgery compared to the wild type mice with UUO surgery (fold-change > 1.5, 2Log2). Furthermore, comparative analysis of CUT&TAG data between wild-type and PTCs specific p300 knock-out mice with UUO surgery identified more than 800 genes expected to be regulated by p300 in fibrosis. Then, twenty-eight commonly regulated genes were identified in RNA-sequencing and CUT&TAG-sequencing data (Figure 24A, D). To investigate change of biological pathways in PTCs specific p300 knock-out mice, GO Enrichment Analysis performed using PANTHER revealed that Epithelial-Mesenchymal transition (EMT) and angiogenesis were the major regulated pathways (Figure 24B). Gene set enrichment analysis (GSEA) demonstrated significant change of EMT genes regulated by p300 (Figure 24C). Recent studies have reported that EMT, a myofibroblast-derived process that has been considered important in the progression of renal fibrosis, does not have a significant effect as expected. Recent studies have reported that EMT, the process by which myofibroblasts are derived, known to play a role in the progression of renal fibrosis, does not have a significant effect as expected[34]. Therefore, EndoMT, which has similar characteristics to EMT and shares many regulatory mechanisms has been proposed as an alternative pathway for myofibroblast derivation in

the development of renal fibrosis. Another pathway regulated by p300, angiogenesis, suggests that there are alterations in the maintenance and formation of vasculature in renal tissue during fibrosis development, Therefore, this could be considered further evidence for EndoMT. In addition, the public dataset of single-cell RNA-sequencing of CKD patients was investigated and it showed that the expression rate of Vimentin, a representative mesenchymal cell marker, was increased in epithelial cells and endothelial cells of CKD patients compared to normal (Figure 24E). Moreover, an increase of the expression rate and relative mRNA levels of mesenchymal cell markers such as Fn1, SNAI2, and Vimentin in endothelial cells was verified (Figure 24F).

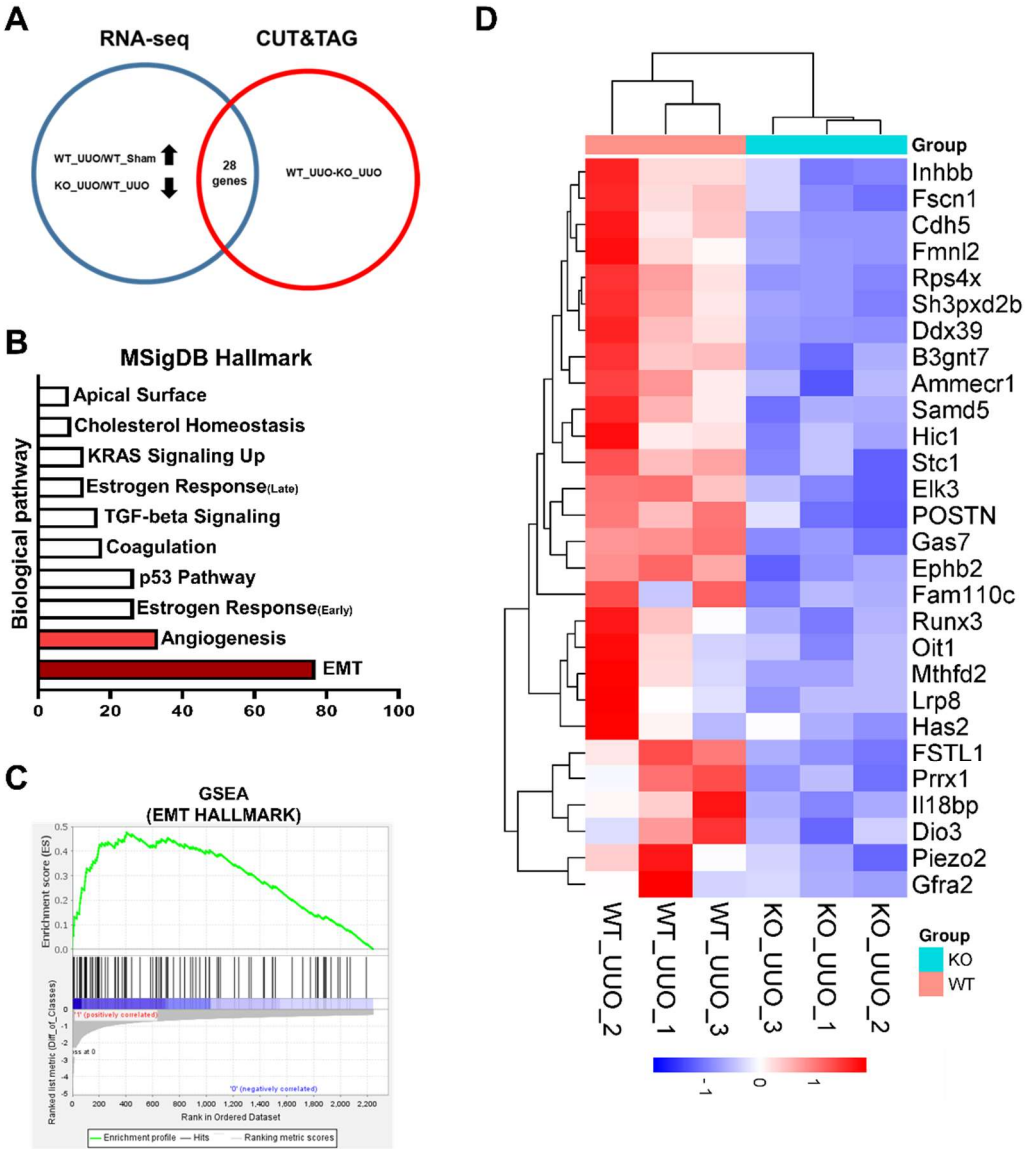

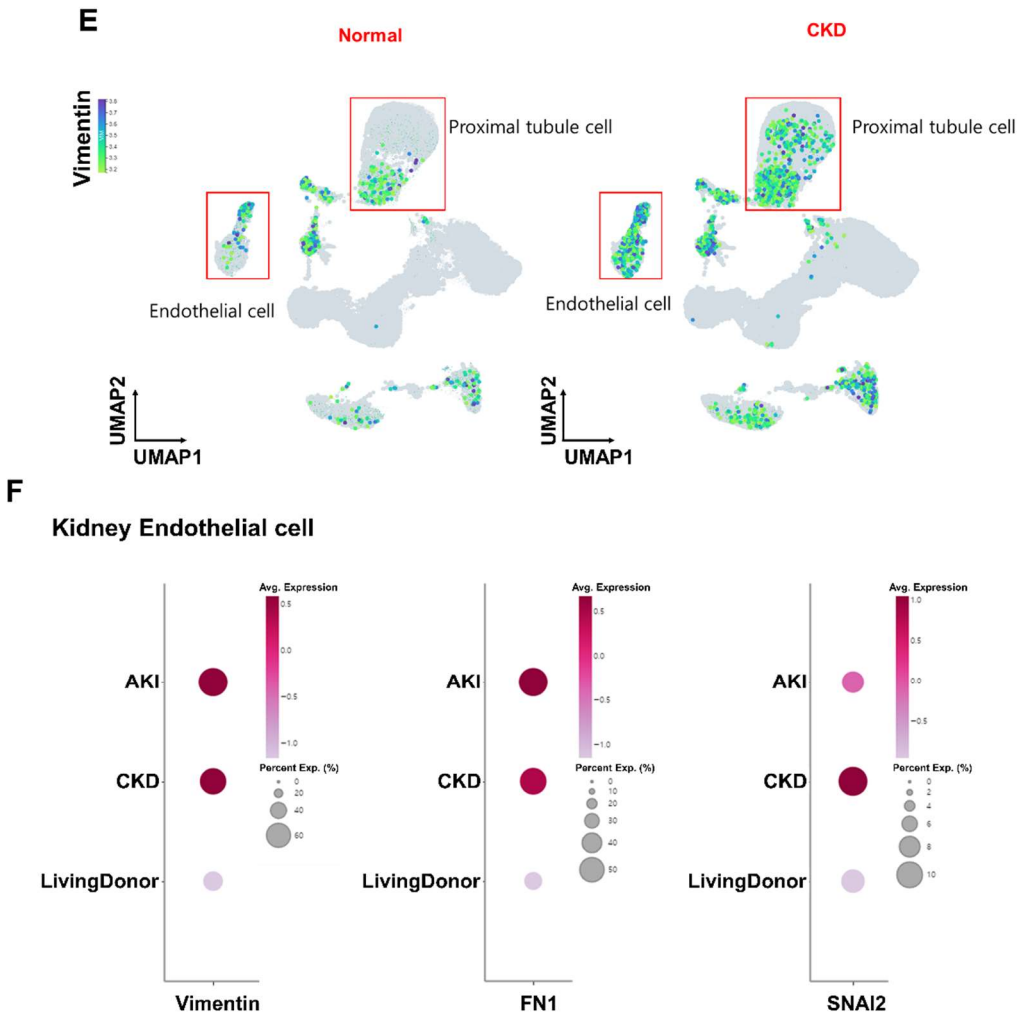

Figure 24. p300 of proximal tubular cell regulate mesenchymal transition related gene expression. (A) The Venn diagram shows the overlap between differentially expressed genes and direct target genes common to the RNA-sequencing and CUT&TAG-sequencing. (B) Pathway analysis using MSigDB Hallmark for the differentially expressed genes in proximal tubular cell-specific p300 knock-out (KO) mouse kidneys versus wild-type mouse kidneys. (C) Epithelial-to-Mesenchymal transition (EMT) related Gene Set Enrichment Analysis (GSEA) for the differentially expressed genes in proximal tubular cell-specific p300 knock-out mouse kidneys versus wild-type mouse kidneys. (D) 28 genes identified in common in both RNA sequencing and CUT&TAG sequencing. (E) UMAP representation of cell cluster from CKD patients' samples. Expression of Vimentin in proximal tubule cell and endothelial cell population (red box) were represent by green to blue dots. Single cell-RNA sequencing data from public database. (F) Expression level of mesenchymal marker gene in endothelial cell. CKD patients Single cell-RNA sequencing data from public database.

3.8. p300 regulates the expression of the mesenchymal transition-associated secreted proteins POSTN, FSTL1, and FSCN1 in renal fibrosis

Among the genes predicted to be regulated by p300 in proximal tubule cells during renal fibrosis, the POSTN, FSTL1, and FSCN1 genes were focused on, which encode secreted proteins that mediate cross-talk with surrounding cells and are known to affect mesenchymal transition. First, the public dataset of CKD was analyzed to identify POSTN, FSTL1, and FSCN1 gene expression in CKD patients. As a result, increased expression of these three genes was found in DM patients (Figure 25A) and single-cell RNA sequencing analysis of CKD patients showed that the expression of POSTN, FSTL1, and FSCN1 was increased in PTCs (Figure 25B). Furthermore, ATAC-sequencing analysis of PTCs of mouse ischemia-reperfusion injury(IRI) fibrosis model kidneys revealed increased chromatin accessibility in the promoter regions of POSTN, FSTL1, and FSCN1 genes during the progression of renal fibrosis (Figure 25C). Thus, POSTN, FSTL1, and FSCN1 secreted proteins from HK-2 cultured media and mRNA of HK-2 cells were examined to verify whether protein and gene expression were regulated by TGF-beta-induced fibrotic conditions in proximal tubule cells. The results show that both mRNA and secreted protein are increased upon TGF-beta treatment in a time-dependent manner as p300 was increased (Figure 25D-E). In addition, to confirm that the selected genes are regulated by p300, public datasets were analyzed. A p300 Chromatin-immunoprecipitation (ChIP)-sequencing analysis in the human fetal kidney cortex confirmed enrichment of p300 near the transcription start site (TSS) of the POSTN, FSTL1, and FSCN1 genes (Figure 26A). To investigate that the p300 regulates the expression of the three genes and secretory proteins, using genetically-engineered p300 knock-out HK-2 cells, it was

demonstrated that the secretion of POSTN, FSTL1, and FSCN1, which was increased by TGF-beta stimulation, was reduced from the HK-2 cell culture media, and the mRNA levels were decreased (Figure 26B, D). Then, UUO surgery on PTC-specific p300 knock-out mice was performed, and the expression levels of FSTL1, FSCN1, and POSTN were investigated by immunohistochemistry. The results showed that the expression of these three proteins increased by UUO and decreased by p300 knock-out (Figure 26C). In addition, overexpression of p300 promoted the mRNA expression of the three genes POSTN, FSTL1, and FSCN1 in HK-2 cell (Figure 26E). Moreover, to verify the regulation of the three genes by PPM1K, the expression of POSTN, FSTL1, and FSCN1 genes was examined upon overexpression of PPM1K in TGF-beta-induced fibrotic conditions and RT-qPCR analysis showed that the expression of POSTN, FSTL1, and FSCN1 genes decreased by PPM1K overexpression (Figure 26F). Finally, to investigate whether PPM1K regulates the expression of POSTN, FSTL1, and FSCN1 *in vivo* under fibrotic conditions, the mRNA levels were examined in the kidney tissues of UUO-induced renal fibrosis model mice overexpressing PPM1K via adenovirus. It was observed that the expression of POSTN, FSTL1, and FSCN1 was reduced in the PPM1K-overexpressed UUO-induced kidneys (Figure 26G).

In conclusion, these result suggests that p300 deficiency in renal proximal tubular cells supposed to regulate mesenchymal transition and angiogenesis and these implies that p300 regulates EMT or EndoMT via modulate the expression of mesenchymal transition-related secretory proteins, POSTN, FSTL1, and FSCN1. Moreover, these three genes were verified to be increased in CKD patients, and it was demonstrated that p300 regulates their expression via *in vivo* and *in vitro* studies using p300 overexpression and knock-out systems and PPM1K adenoviral vector.

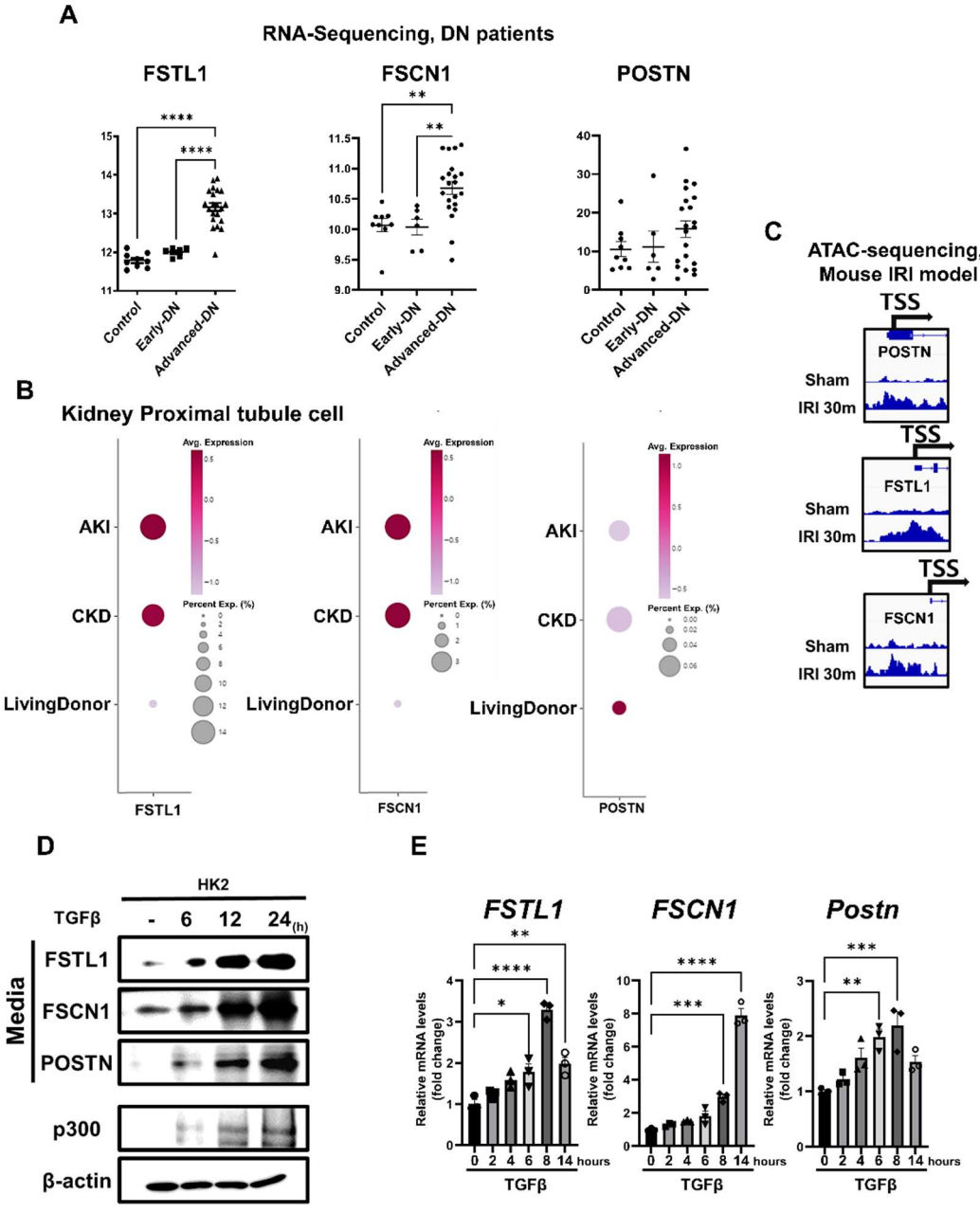

Figure 25. Increased expression levels of FSTL1, FSCN1 and POSTN during fibrosis progression. (A) mRNA levels of FSTL1, FSCN1 and POSTN. RNA-sequencing data of Diabetes nephropathy patients from Gene Expression Omnibus (GEO). (B) Expression of FSTL1, FSCN1 and POSTN in kidney proximal tubular cell. Single cell RNA-sequencing data of CKD and AKI patients from public data base. (C) Chromatin accessibility of POSTN, FSTL1, and FSCN1 promoter region in Ischemia Reperfusion Injury (IRI) model mouse kidneys. ATAC-sequencing data from public data base. (D) Protein levels of FSTL1, FSCN1 and POSTN in HK2 cultured medium and p300 from HK2 cell lysates. HK2 cells were stimulated by TGFβ. β-actin was used as the sample loading control. (E) mRNA levels of FSTL1, FSCN1 and Postn in HK2 cells treated with TGFβ. Data are represented as mean ± SEM, *P < 0.05, **P < 0.01, ***P < 0.001 and ****P < 0.0001 by ordinary one-way ANOVA test.

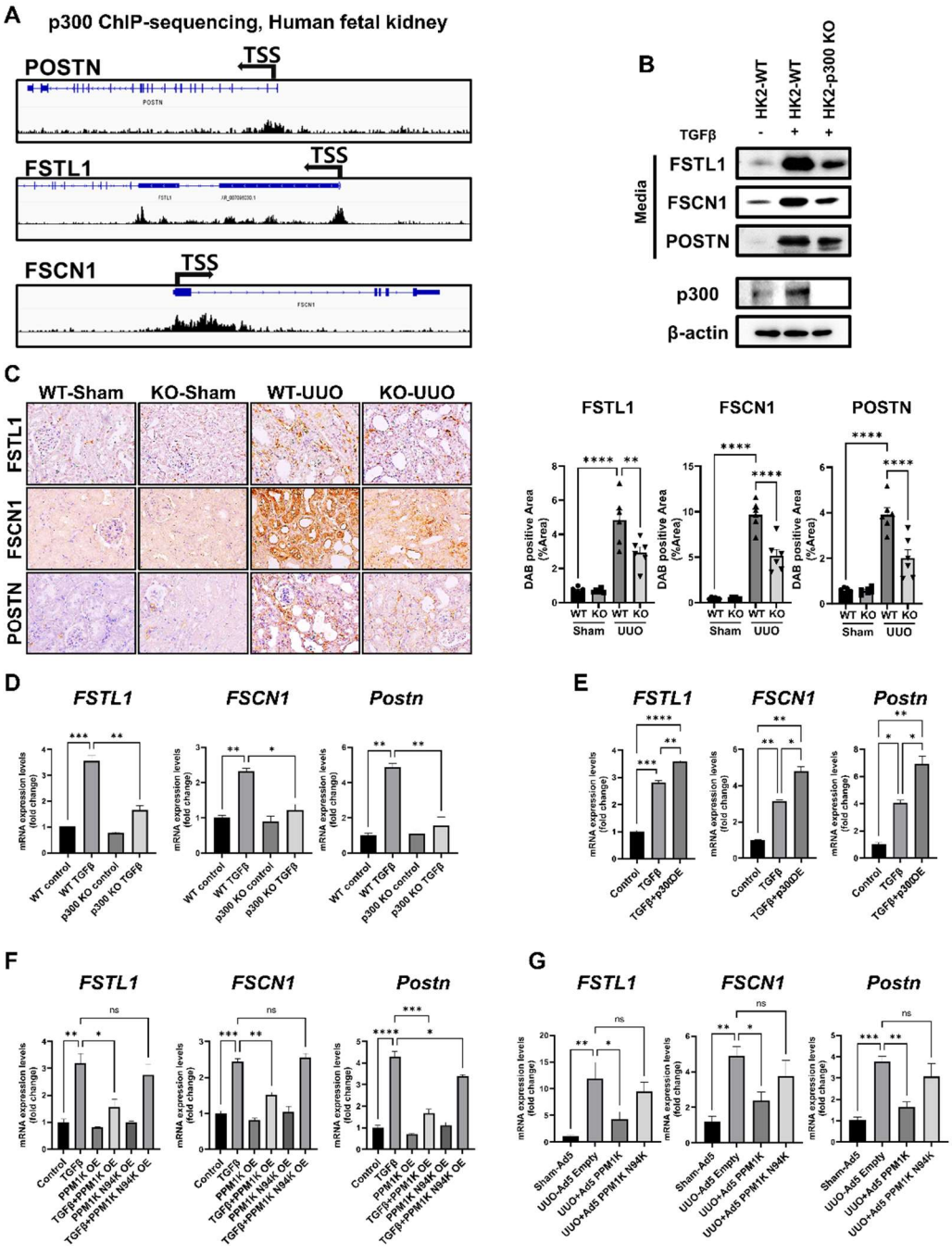

Figure 26. p300 regulate expression of FSTL1, FSCN1, POSTN in kidney proximal tubular cell. (A) p300 enrichment in POSTN, FSTL1, and FSCN1 promoter region. Chromatin immunoprecipitation (ChIP)-Sequencing data of human fetal kidney from public data base. (B) Protein levels of FSTL1, FSCN1 and POSTN in HK2 cultured medium and p300 from HK2 cell lysates. Wild type and p300 knock-out (KO) HK2 cells were stimulated by TGFβ. β-actin was used as the sample loading control. (C) Representative image of FSTL1, FSCN1, POSTN immunohistochemistry (IHC) in kidney tissue sample. Samples from UUO-induced fibrosis mouse model using wild-type and p300 knock-out mice. The graph represents quantification of DAB area in histological staining images. Data are represented as mean ± SEM, **P < 0.01 and ****P < 0.0001 by ordinary one-way ANOVA test. D, E, F, G mRNA levels of FSTL1, FSCN1 and Postn. (D) p300 knock-out and wild-type HK2 cells treated with TGFβ. (E) p300 overexpressed HK2 cell treated with TGFβ. (F) PPM1K and PPM1K N94K overexpressed HK2 cell treated with TGFβ. (G) Ad5-PPM1K and Ad5-PPM1K N94K introduced UUO-induced mouse model kidney. Data are represented as mean ± SEM, *P < 0.05, **P < 0.01, ***P < 0.001 and ****P < 0.0001 by ordinary one-way ANOVA test.

3.9. p300 in PTCs promotes EndoMT via regulation of protein secretion during renal fibrosis development

The possibility that p300 in the PTCs may regulate the expression of secreted proteins that can induce EndoMT was verified from the previous RNA-sequencing and CUT&TAG-sequencing analysis results. Therefore, to determine whether proximal tubule cells could directly induce mesenchymal transition of HUVECs, HK2 cells were co-cultured with human vascular endothelial cells, HUVEC cells. The protein and mRNA levels of endothelial and mesenchymal markers in HUVECs co-cultured with TGF-beta-stimulated HK-2 cells were observed by immunofluorescence (IF) and RT-qPCR. The results showed that EndoMT was derived in HUVECs co-cultured with TGF-beta stimulated HK2 cells (Figure 27A-C). Therefore, to determine whether EndoMT is regulated by p300 in renal fibrosis, first, quantitative changes of endothelial cells were identified by immunohistochemistry for the endothelial cell marker, CD31 in renal proximal tubule-specific p300 knock-out UUO mice. The results showed that the number of endothelial cells decreased in UUO-induced wild type mice, but the UUO-induced decrease was restored in p300 knock-out mice. Furthermore, endothelial cell integrity of blood vessels was validated by examining albumin leakage. The results showed that increased albumin leakage in UUO was significantly reduced in p300 knock-out mouse kidneys compared with wild-type mice (Figure 28A). To assess the mesenchymal transition of endothelial cells, Zo-1, an intercellular tight junction marker, was identified in CD31-positive cells by immunofluorescence staining. As a result, the intercellular junction of endothelial cells reduced by UUO induced EndoMT, but was restored in UUO induced PTCs specific p300 knock-out mice compared to wild-type mice (Figure 28B). To clarify that p300 deficiency in the proximal tubule regulates EndoMT in fibrosis development, expression of the endothelial cell marker, CD31 and the mesenchymal cell marker Vimentin were verified by Co-immunofluorescence

staining. These results showed that the co-expression of Vimentin and CD31, increased by UUO, was significantly reduced in PTC specific p300 knock-out mice compared to wild-type mice (Figure 28C). Furthermore, the mRNA levels of the mesenchymal cell markers Vimentin, PAI-1, and FSP-1, and the endothelial cell markers CD31, Tie-2, and CD144, were examined by RT-qPCR. It was demonstrated that EndoMT was reduced in UUO-induced PTC-specific p300 knock-out mice compared to wild-type mice (Figure 28D). To determine whether p300 in proximal tubule cells directly affects EndoMT, Wild-type and p300 knock-out HK-2 cells were stimulated by TGF-beta and then switched to non-serum medium to obtain HK-2-derived secreted proteins. The medium was concentrated and treated to HUVECs. The results showed that HUVECs treated with medium collected from TGF-beta-stimulated HK2 cells induced EndoMT, but EndoMT progression was significantly reduced in HUVECs treated with medium collected from p300 knock-out HK2 cells, as verified by RT-qPCR of endothelial cell and mesenchymal cell markers (Figure 28E), and observation of HUVEC morphologic change (mesenchymal character ex. Sharp and long shape) (Figure 28F). Finally, to determine whether p300-induced increases in EndoMT impaired vascular structure maintenance, three-dimensional imaging of UUO-induced wild-type mouse and PTC-specific p300 knock-out mouse kidneys was performed to determine the microvascular structure. This results demonstrated that impaired micro vascular structure via UUO-induced fibrosis, was restored by PTCs-specific p300 knock-out (Figure 29). Moreover, to verify that proximal tubule cells affect the mesenchymal transition in epithelial cells (EMT), HK-2 cells were co-cultured with TGF-beta-stimulated HK-2 cells, and it was observed that mesenchymal transition occurred similarly to HUVEC cells (Figure 30).

In summary, these results suggest that renal fibrosis involves not only Epithelial-to-Mesenchymal transition (EMT) but also Endothelial-to-Mesenchymal transition (EndoMT). Furthermore, the

knock-out of p300 in renal proximal tubular cells leads to a reduction of EndoMT, contributing to the preservation of microvascular integrity in the kidney.

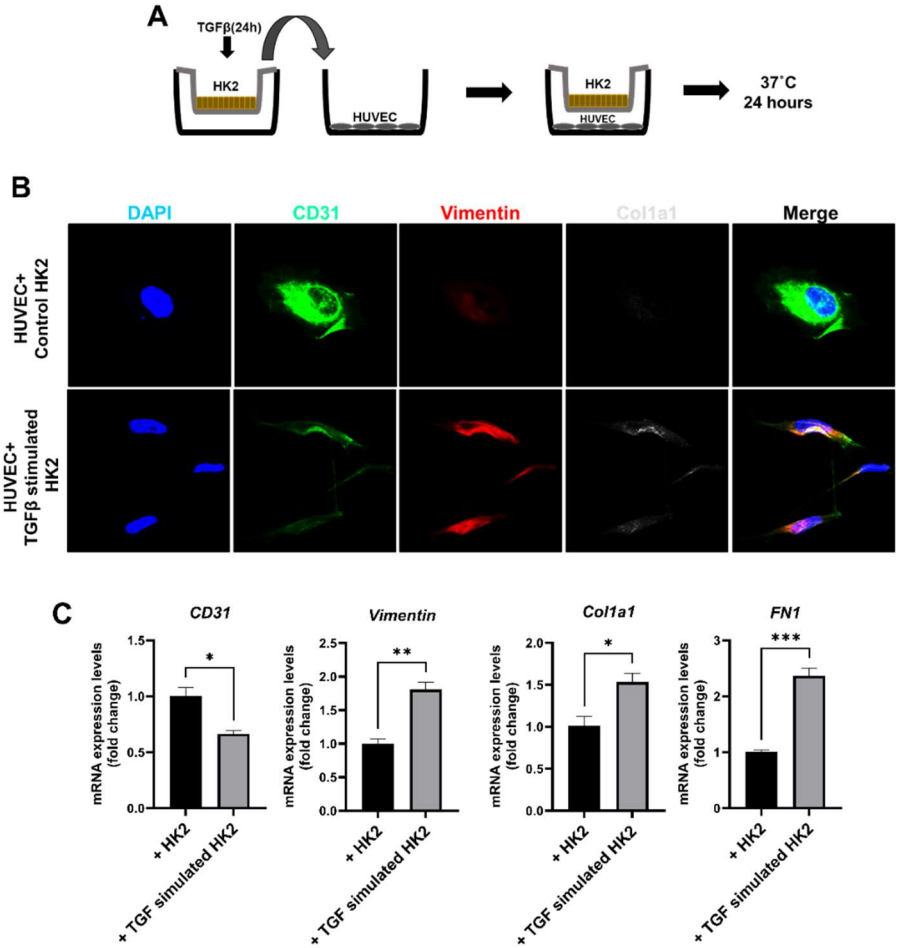

Figure 27. Proximal tubule cell promotes Endothelial-to-Mesenchymal transition directly in fibrotic condition. (A) Schematic image of the Co-culture method. TGFβ stimulated HK2 cells were transferred to HK2 cells or HUVEC cells and cultured for 24 hours. (B) Representative image of endothelial and mesenchymal cell marker co-immunofluorescence (IF) in HUVEC cells co-cultured with TGFβ stimulated HK2 cells. (C) mRNA levels of endothelial and mesenchymal cell marker genes in HUVEC cells co-cultured with TGFβ. Data are represented as mean ± SEM, *P < 0.05, **P < 0.01 and ***P < 0.001 by t-test.

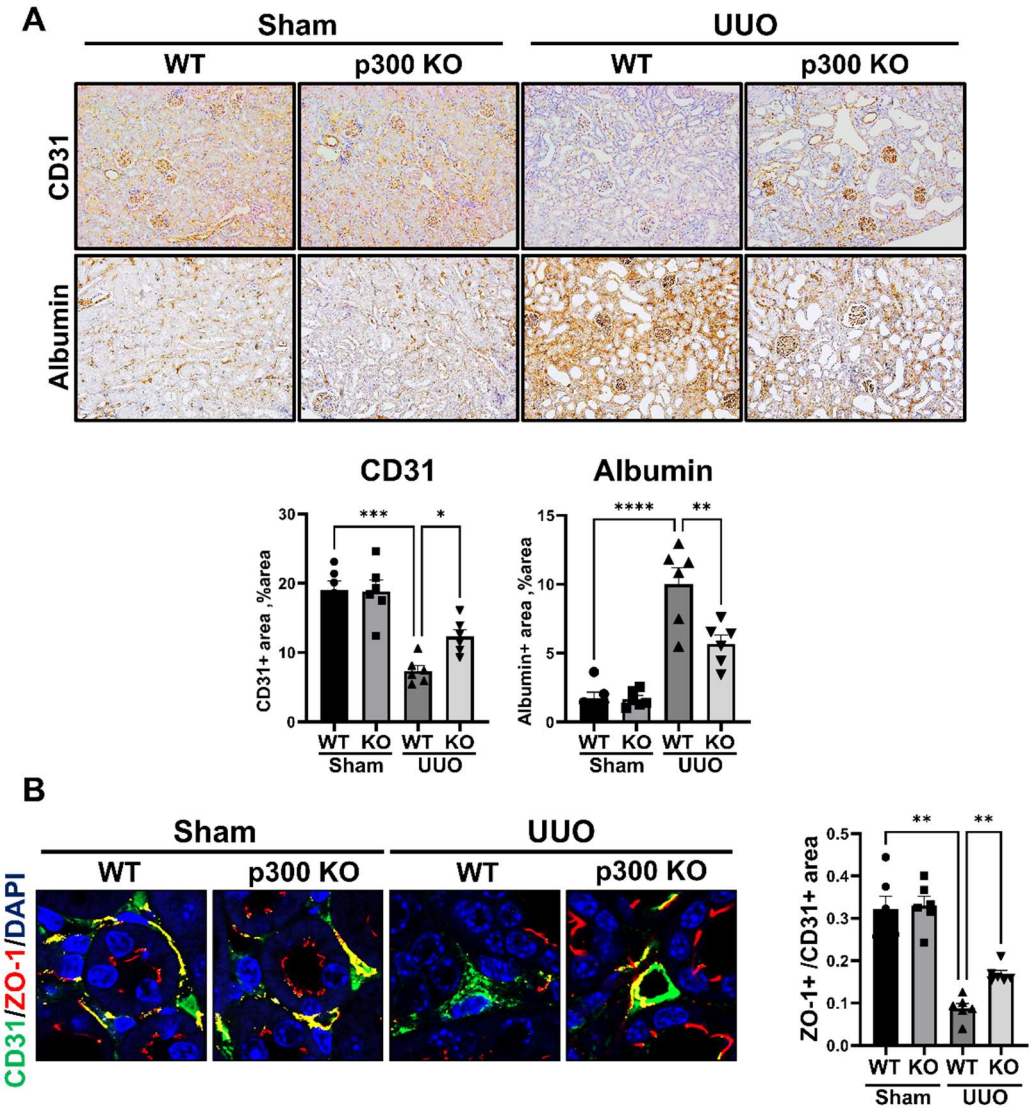

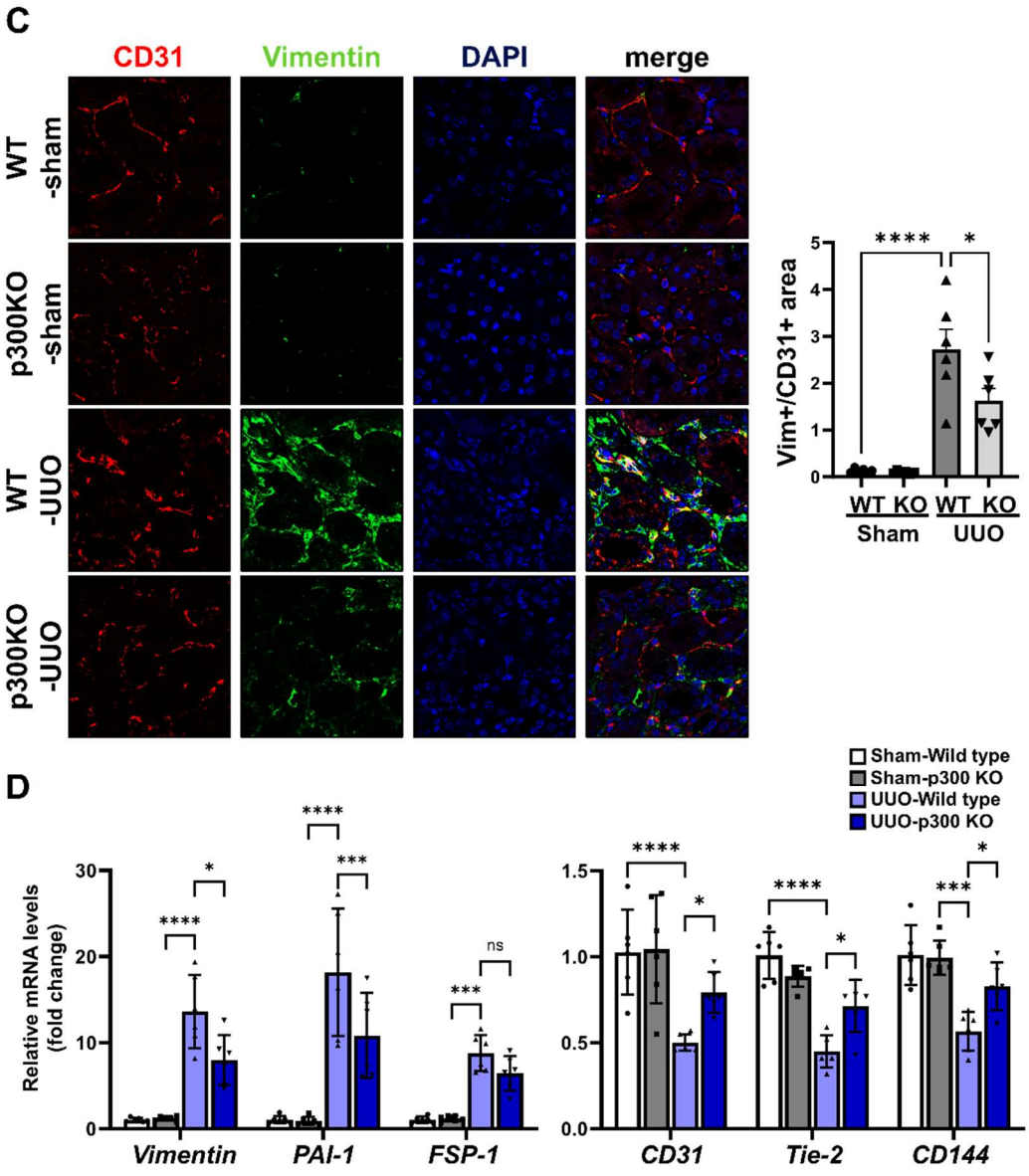

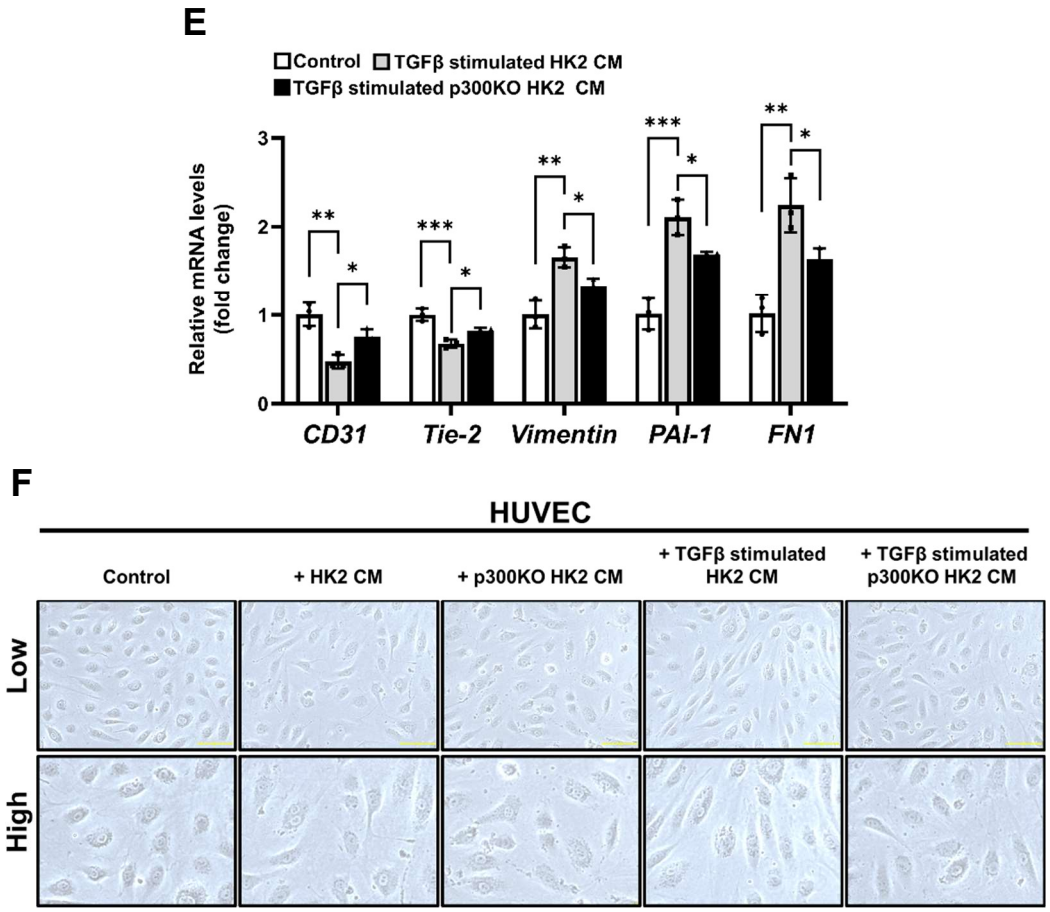

Figure 28. p300 in kidney proximal tubule cell modulate Endothelial-to-Mesenchymal transition in fibrotic condition. (A) Representative image CD31 and Albumin immunohistochemistry (IHC) in kidney tissue sample. Samples from UUO-induced fibrosis mouse model using wild-type and p300 knock-out mice. The graph represents quantification of DAB area in histological staining images. Data are represented as mean ± SEM, *P < 0.05, **P < 0.01, ***P < 0.001 and ****P < 0.0001 by ordinary one-way ANOVA test. (B) Representative image of CD31 and Zo-1 co-immunofluorescence (IF) in kidney tissue sample. Samples from UUO-induced fibrosis mouse model using wild-type and p300 knock-out mice. The graph represents quantification of Co-localized area in images. Data are represented as mean ± SEM, **P < 0.01 by ordinary one-way ANOVA test. (C) Representative image of CD31 and Vimentin co-immunofluorescence (IF) in kidney tissue sample. Samples from UUO-induced fibrosis mouse model using wild-type and p300 knock-out mice. The graph represents quantification of Co-localized area in images. Data are represented as mean ± SEM, *P < 0.05 and ****P < 0.0001 by ordinary one-way ANOVA test. (D) mRNA levels of endothelial and mesenchymal cell marker genes in kidney tissue sample. Samples from UUO-induced fibrosis mouse model using wild-type and p300 knock-out mice. Data are represented as mean ± SEM, *P < 0.05, ***P < 0.001 and ****P < 0.0001 by ordinary one-way ANOVA test. (E) mRNA levels of endothelial and mesenchymal cell marker genes in HUVEC cell with TGFβ stimulated HK2 cell conditioned medium. Data are represented as mean ± SEM, *P < 0.05, **P < 0.01 and ***P < 0.001 by ordinary one-way ANOVA test. (F) morphologic change of HUVEC cell with TGFβ stimulated HK2 cell conditioned medium.

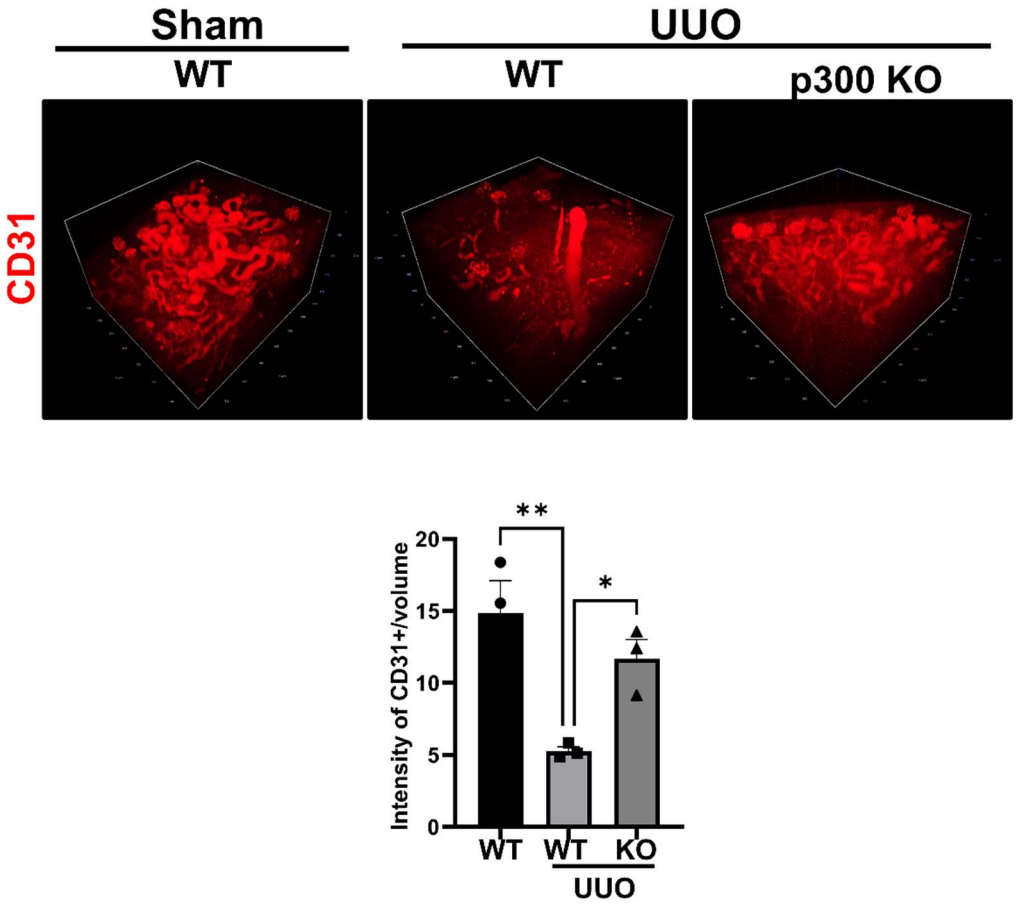

Figure 29. p300 knock-out in kidney proximal tubule cells attenuates fibrosis-induced microvasculature destruction. (A) Representative 3-D image of microvascular structure (CD31) in kidney tissue sample. Samples from UUO-induced mouse fibrosis model using wild-type and p300 knock-out (KO) mice. The graph represents quantification of CD31 intensity in 3-D images (normalized by tissue volume). Data are represented as mean ± SEM, *P < 0.05 and **P < 0.01 by ordinary one-way ANOVA test.

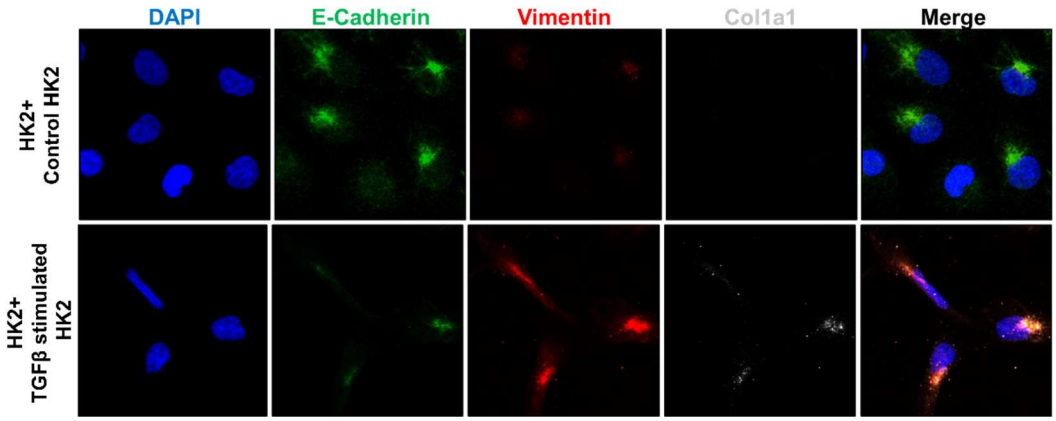

Figure 30. Proximal tubule cell promotes Epithelial-to-Mesenchymal transition via autocrine in fibrotic condition. Representative image of epithelial and mesenchymal cell marker co-immunofluorescence (IF) in HK2 cells co-cultured with TGFβ stimulated HK2 cells.

3.10. p300-specific inhibitor, attenuates the development of renal fibrosis *in vivo* and *in vitro*

Previous results indicate that p300 protein in renal proximal tubule cells induces renal fibrosis by leading to mesenchymal transition of renal constituent cells during the development of renal fibrosis. Therefore, using A6 and C646, a p300-specific inhibitor that has recently been shown to inhibit p300 in the lung and liver, to determine its anti-fibrotic effect in the progression of renal fibrosis. It was demonstrated that treatment with A6 and C646 in a UUO-induced renal fibrosis model mice significantly inhibited fibrosis progression, as assessed by MTS, Sirius red staining, and soluble collagen assay (Figure 31A, C). In addition, p300 protein expression in PTCs, elevated in UUO, was significantly reduced by A6 and C646 treatment. (Figure 31B). The expression of fibrosis-related genes and proteins of inhibitor treated kidney tissues was assessed by RT-qPCR and western blot, which showed that increased expression of fibrosis-related genes and proteins by UUO was significantly reduced by A6 treatment (Figure 31D-E). To investigate the anti-fibrotic effects of p300 selective inhibitors in HK-2 cells, cells were treated with A6 and C646 before TGF-beta treatment. The results demonstrated that the increase of fibrosis-related genes and p300 protein induced by TGF-beta was reduced by the treatment of A6 and C646, as verified by RT-qPCR and Western blot. These results showed that inhibition of p300 led to suppression of fibrotic function via EMT in PTCs (Figure 32A-B).

Previous in vivo and in vitro results demonstrated that p300 regulates the expression of POSTN, FSTL1, and FSCN1 in renal proximal tubule cells in the development of fibrosis. Therefore, A6 and C646 administration was investigated to determine whether it inhibits the expression of the three target proteins in a UUO-induced mouse renal fibrosis model through p300 inhibition. The results

showed that the expression of the three proteins increased by UUO induction was significantly reduced by A6 treatment, especially in the interstitium between PTCs (Figure 33A). Furthermore, in HK2 cells, the secretion of POSTN, FSTL1, and FSCN1 upon p300-selective inhibitor treatment was examined. It was observed that A6 and C646 inhibited the secretion of these three proteins, which had been increased by TGF-beta (Figure 33B). Finally, to verify the alleviation of tubular cell injury and reduction of EndoMT after p300-selective inhibitors treatment, KIM1 expression, albumin leakage, and intercellular connections of endothelial cells were verified. The results showed that KIM1 expression and Albumin leakage, which were increased by UUO, were alleviated by p300-seletive inhibitors and the intercellular connections of endothelial cells that were reduced upon UUO were alleviated by p300-selective inhibitors treatment (Figure 34 A-B).

Taken together, these results demonstrate that A6 and C646 a p300-specific inhibitor, prevents the progression of renal fibrosis by inhibiting p300 in PTC. In particular, it inhibited the expression of POSTN, FSTL1, and FSCN1, which are downstream regulatory proteins of p300 in PTC, leading to inhibition of renal injury and EndoMT.

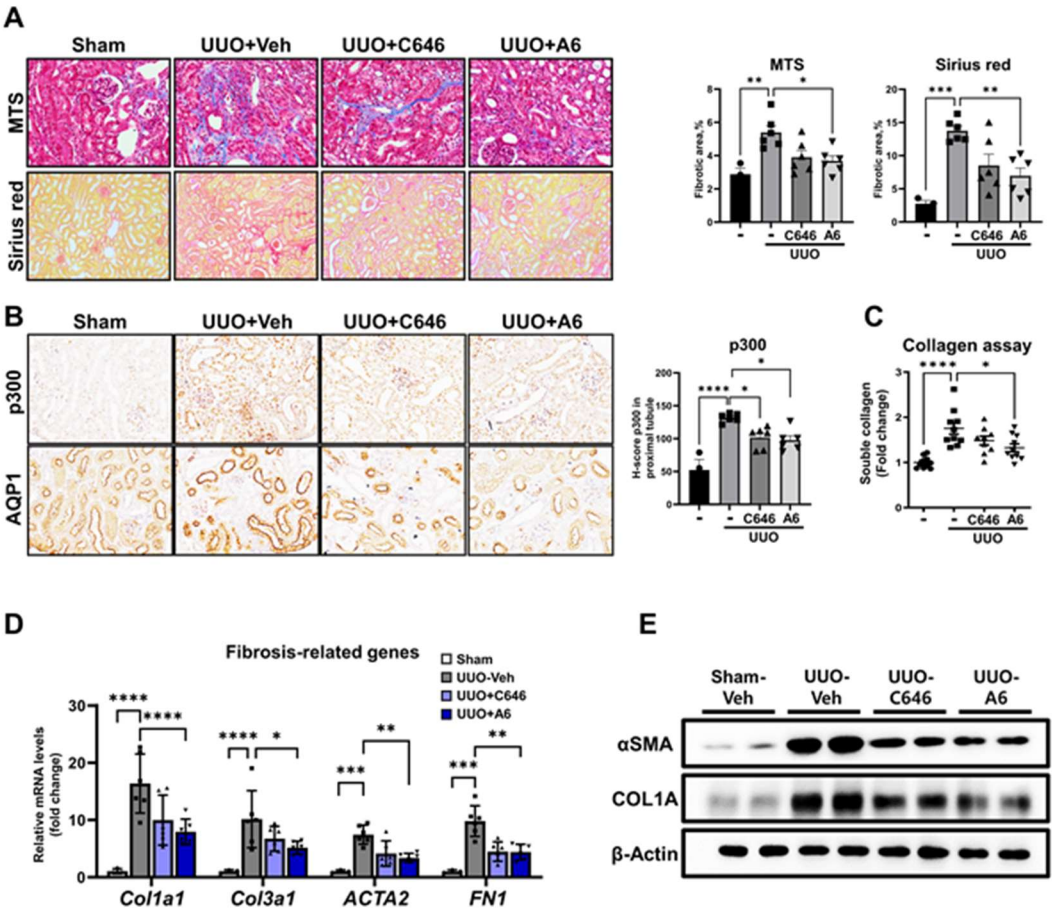

Figure 31. p300-selective inhibitors attenuate kidney fibrosis in mouse fibrosis model. (A) Representative image of Masson trichrome staining (MTS) and Sirius red staining using kidney samples. Samples from UUO-induced mouse fibrosis model injected with C646 and A6. The graph represents quantification of fibrotic area in histological staining images. Data are represented as mean ± SEM, *P < 0.05, **P < 0.01 and ***P < 0.001 by ordinary one-way ANOVA test. (B) Representative image of p300 and AQP1 immunohistochemistry using serially sectioned samples. Samples from UUO-induced mouse fibrosis model injected with C646 and A6. The graph represents H-score in histological staining images. Data are represented as mean ± SEM, *P < 0.05 and ****P < 0.0001 by ordinary one-way ANOVA test. (C) Soluble collagen assay using kidney samples. Samples from UUO-induced fibrosis mouse fibrosis model injected with C646 and A6. Data are represented as mean ± SEM, *P < 0.05 and ****P < 0.0001 by ordinary one-way ANOVA test. (D) mRNA levels of fibrosis-related genes in kidney samples from UUO-induced fibrosis mouse injected with C646 and A6. Data are represented as mean ± SEM, *P < 0.05, **P < 0.01, ***P < 0.001 and ****P < 0.0001 by ordinary one-way ANOVA test. (E) fibrosis-related protein αSMA and COL1A in kidney samples from UUO-induced fibrosis mouse injected with C646 and A6. β-actin was used as the sample loading control.

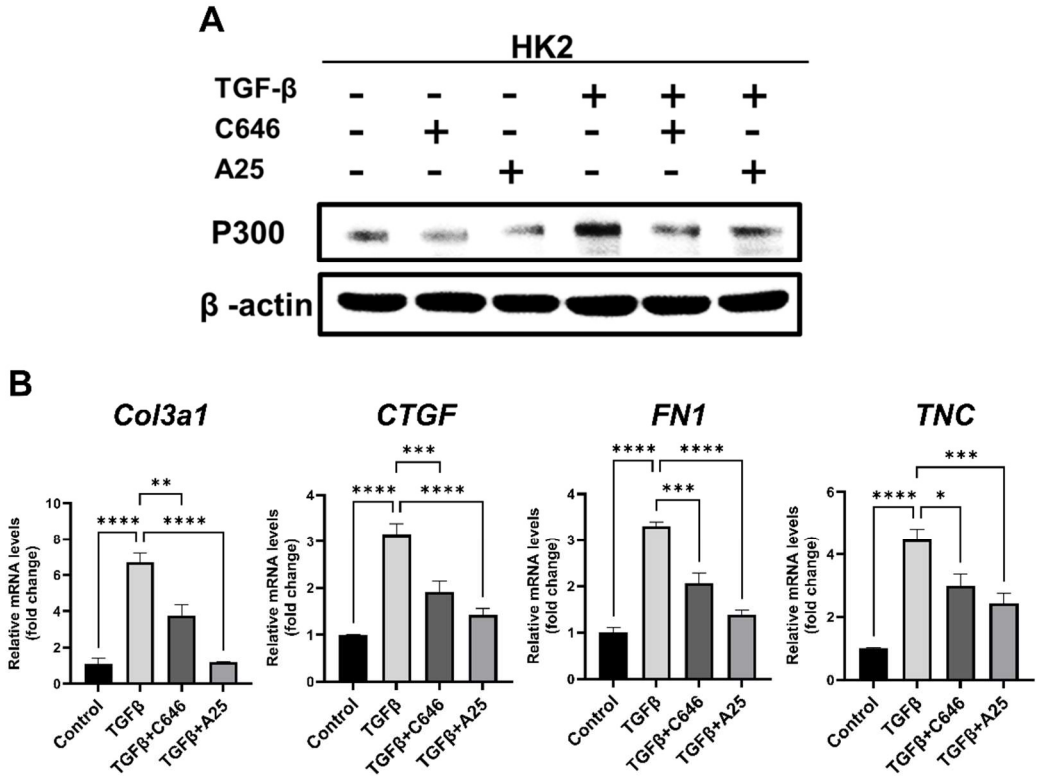

Figure 32. p300-selective inhibitors alleviate fibrosis in HK2 cells via inhibition of p300. (A) Protein level of p300 HK2 cells treated with TGFβ, C646 and A6. β-actin was used as the sample loading control. (B) mRNA levels of fibrosis-related genes in HK2 cells treated with TGFβ, C646 and A6. Data are represented as mean ± SEM, *P < 0.05, **P < 0.01, ***P < 0.001 and ****P < 0.0001 by ordinary one-way ANOVA test.

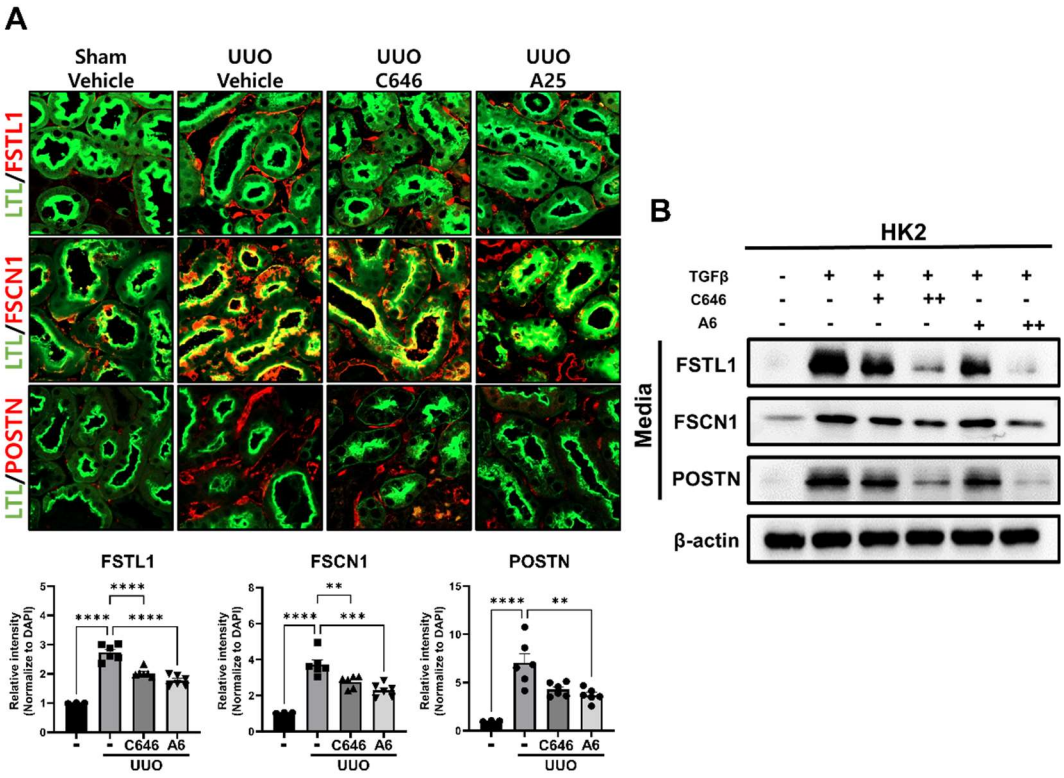

Figure 33. p300-selective inhibitors reduced expression of FSTL1, FSCN1 and POSTN. (A) Representative image of FSTL1, FSCN1 and POSTN Co-immunofluorescence (IF) in kidney samples. Samples from UUO-induced fibrosis mouse fibrosis model injected with C646 and A6. The graph represents quantification of intensity of FSCTL1, FSCN1, and POSTN (normalized by DAPI). Data are represented as mean ± SEM, **P < 0.01, ***P < 0.001 and ****P < 0.0001 by ordinary one-way ANOVA test. (B) Protein levels of FSTL1, FSCN1 and POSTN in HK2 cultured medium. HK2 cells were treated by TGFβ with C646 and A6. β-actin was used as the sample loading control.

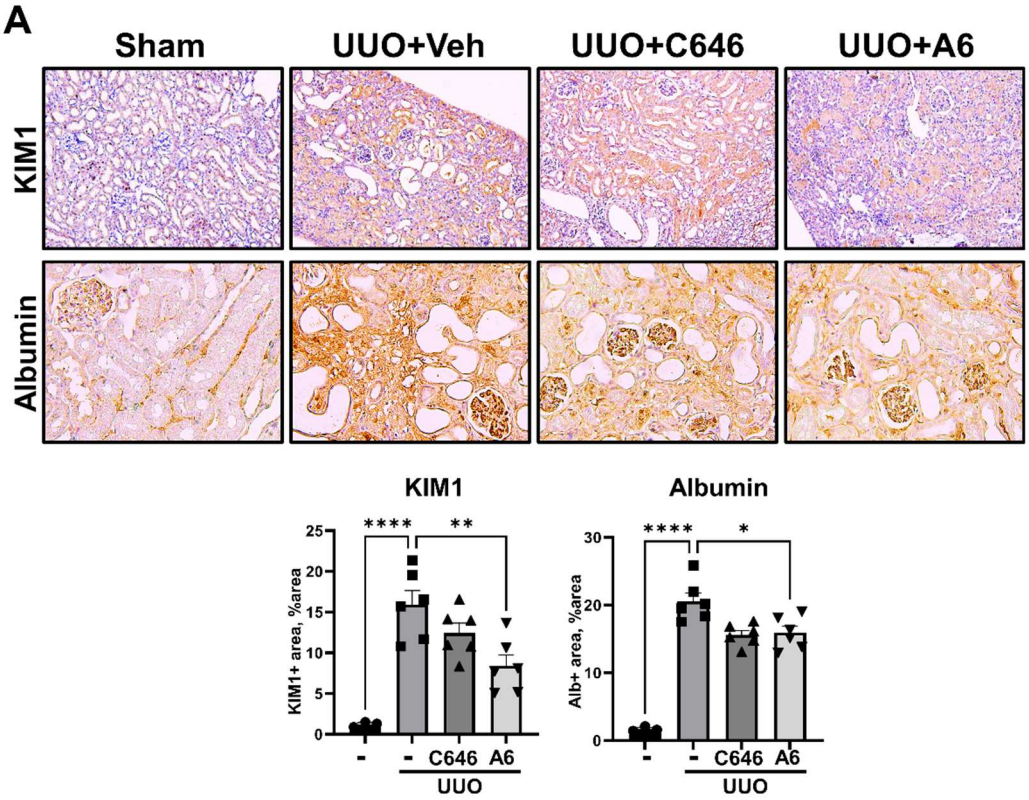

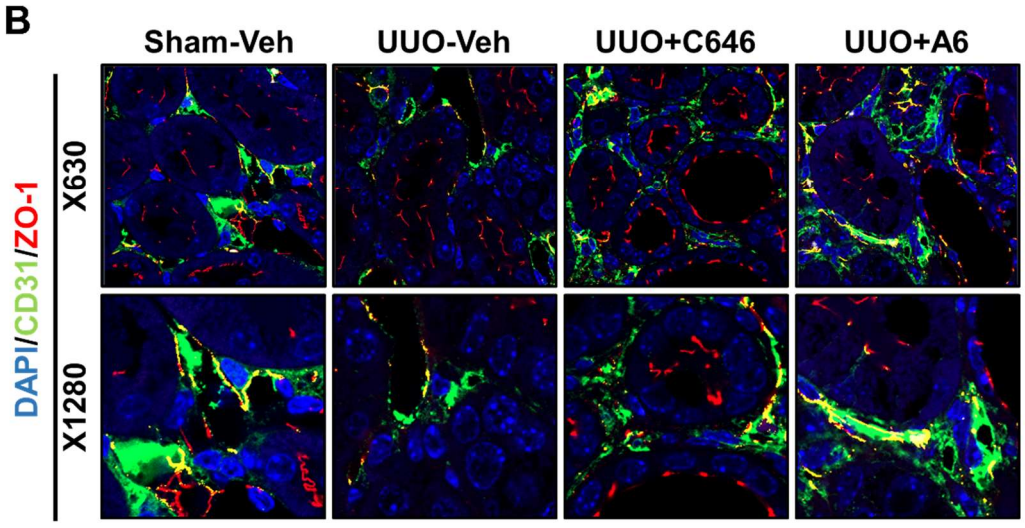

Figure 34. p300-selective inhibitors inhibit Endothelial-to-Mesenchymal transition in fibrotic condition. (A) Representative image of KIM1 and albumin immunohistochemistry (IHC) in kidney tissue sample. Samples from UUO-induced fibrosis mouse fibrosis model injected with C646 and A6. The graph represents quantification of DAB positive area. Data are represented as mean ± SEM, *P < 0.05, **P < 0.01 and ****P < 0.0001 by ordinary one-way ANOVA test. (B) Representative image of CD31 and Zo-1 co-immunofluorescence (IF) in kidney tissue sample. Samples from UUO-induced fibrosis mouse fibrosis model injected with C646 and A6.

4. DISCUSSION

Chronic kidney disease (CKD) has a high prevalence and impairs patient's quality of life. Especially, the fibrosis is characterized in patients with advanced CKD. However, despite the majority of patients with CKD eventually progress to kidney failure by kidney fibrosis, the pathogenesis and mechanisms for the progression of kidney fibrosis are currently unclear. Therefore, fundamental research on the pathogenesis of kidney fibrosis was conducted by targeting p300, an epigenetic regulator in kidney fibrosis. Histone acetyltransferase p300, an epigenetic regulator, is a crucial co-transcription factor that regulates the expression of various genes and has been studied as a factor associated with poor prognosis in cancer, fibrosis, and inflammation. In particular, in fibrotic diseases, p300 is known to play an important role in pathogenesis in various organs and tissues. It is known that p300 protein is upregulated in stellate cells during liver fibrosis by regulating its stability through phosphorylation of Serine 1834 site and plays an important role in fibrosis development[86]. In the heart, high levels of lactate induce cardiac fibrosis by regulating EndoMT via inducing p300 binding to snail1[100]. In addition, p300 protein is upregulated in IPF patients, and in pulmonary fibrosis progression, p300 expression is specifically increased in AT2 cells. p300 in AT2 cells induces transcriptional activation of chemokines such as CCL7 and CCL12 and promotes polarization of macrophages[92]. However, there are only a few studies on the cell-specific role of p300 in renal fibrosis and detailed pathogenesis. Therefore, in this study, increased expression of p300 protein was identified in CKD patients with fibrosis and in three different mouse models of renal fibrosis, and a specific increase of p300 in proximal tubular epithelial cells (PTCs), which constitute the major proportion of the kidney, was further identified during fibrosis progression. This study focused on the proximal tubular epithelial cell (PTC)-specific function of p300 in the

development of renal fibrosis and proposed that the level of p300 protein in renal proximal tubule cells is regulated by the partner phosphatase PPM1K. In particular, high levels of p300 expression were found in FSGS and IgAN patients, suggesting its potential as a differential marker for early, clinically indistinguishable MCD. Finally, in p300 knock-out mice, fibrosis progression was attenuated in both UUO and folic acid fibrosis models compared to wild type mice, therefore, it was demonstrated that an elevation of p300 protein plays an important role in the development of renal fibrosis.

PPM1K is a phosphatase in the PPM family, and unlike PPM1A, which is known to be a regulator of kidney, liver, and lung fibrosis, and PPM1D, PPM1G, and PPM1B, which have been associated with various type of cancer, PPM1K has rarely been reported to be associated with clinical disease and has only been reported in some branched-chain amino acids-related ischemic stroke or metabolic disorders such as polycystic ovary syndrome and maple syrup urine disease. Intriguingly, with regard to renal disease, it has been reported that the RNA sequencing analysis using PPM1K overexpressed HK2 human proximal tubule cell lines have shown that biological pathways such as apoptosis, angiogenesis, cell adhesion, and ECM organization are regulated by PPM1K. Interestingly, this study demonstrated the clinical relevance of PPM1K in CKD patients and proposed a novel molecular mechanism of PPM1K in association with p300 stability in the development of renal fibrosis. Therefore, this study verified that the PPM1K negatively regulated renal fibrosis. Since, there are only few studies on PPM1K in human diseases, further research is needed to clarify the patho-physiological roles of PPM1K in human disease.

In many cases of CKD, the End-stage of pathogenesis is accompanied by fibrosis. In most organs, fibroblasts, present in the tissue stroma are the major origin of ECM-secreting myofibroblasts. However, trans-differentiation to myofibroblasts via EMT and EndoMT also play an important role

in the progression of renal fibrosis. In the case of EMT, it is induced by various molecular pathways in response to signaling such as TGF-beta and TNA-alpha in the kidneys[31,36,93]. In particular, it is known that human proximal tubule cells HK-2 cells, which are widely used in renal fibrosis research, increase the expression of ECM proteins such as collagen 1 and collagen 3 as well as mesenchymal transition upon TGF-beta treatment[101,102]. In addition, it has been widely reported that various stimuli such as TGF-beta, wnt3a, IL-6, and Notch promote EndoMT upon induction of renal fibrosis[35,65,70]. Interestingly, it was reported that up-regulation of MYC protein in renal proximal tubule cells promotes EndoMT-mediated renal fibrosis[103]. Moreover, recent reports have demonstrated that EndoMT plays a more important role than EMT during development of renal fibrosis[34]. Therefore, this study focused on the changes in EndoMT via p300 regulation in the renal proximal tubule cell during renal fibrosis progression. First, it was observed that the elevation of p300 in proximal tubule cells promotes the secretion of mesenchymal-transition-associated secretory proteins (POSTN, FSTL1, and FSCN1), inducing EndoMT. Second, Low oxygen and low nutrient supply are well-known factors that promote fibrosis. Therefore, capillaries, the main source of oxygen and nutrients, are thought to play an important role in the development of fibrosis[104,105]. As a results, a collapse of the microvascular structure with EndoMT was observed during the development of fibrosis. However, EndoMT in kidney fibrosis was reversed by the inhibition of p300 function. These results suggest that the lack of tissue oxygen and nutrients supply via destruction of microvascular structure could be alleviated by p300 inhibition in kidney fibrosis condition. However, the exact function of each secreted protein (FSTL1, FSCN1, and POSTN) in EndoMT-mediated fibrosis progression is unclear, hence, additional detailed studies are necessary.

Notably, several clinical trials of anti-fibrotic therapies have been conducted in CKD patients in the past such as FG-3019, the CTGF targeting drug, Pirfenidone, TGF-β targeting drug, Bardoxolone

methyl, Nrf2 targeting dug[14]. However, they had the limitation of targeting a single sub-target and did not show any noticeable therapeutic effect. The development of renal fibrosis involves the cross-talk of various cell types, including fibroblasts, tubular cells, vascular endothelial cells, and immune cells, thus it is important to target common upstream regulators of fibrosis signaling in various cells, such as p300, as therapeutic targets. Therefore, inhibiting the function of p300 may be a promising therapeutic approach for CKD patients with renal fibrosis. Moreover, introducing p300-specific inhibitors, A6 and C646, which have been reported to have anti-fibrotic activity in other organs such as lung and liver, the anti-fibrotic effect of p300-selective inhibitors on the renal fibrosis was validated using *in vivo* and *in vitro* fibrosis models. Therefore, it was suggested that the selective inhibitor of p300 function could alleviate fibrosis not only kidney but other fibrotic organs.

5. CONCLUSION

In this study, it was demonstrated that the elevated expression levels of p300 protein in the renal proximal tubular cells in Chronic kidney disease patients with fibrosis and three different mouse kidney fibrosis models. Moreover, expression levels of p300 protein in renal proximal tubule cells are negatively regulated by PPM1K phosphatase via inhibition of AKT-mediated phosphorylation of p300 at Serine 1834. Importantly, depletion of p300 gene diminishes EndoMT-mediated renal fibrosis. Furthermore, selective inhibition of p300 activity attenuates kidney fibrosis progression in mouse kidney fibrosis models. Collectively, our finding identified that the functional significance of p300 in the progression of kidney fibrosis and proposed that p300 as therapeutic target for Chronic kidney disease patients with fibrosis.

REFERENCES

1. Adamczak M, Surma S. Metabolic Acidosis in Patients with CKD: Epidemiology, Pathogenesis, and Treatment. Kidney Dis (Basel) 2021;7:452-67.
2. Hamrahian SM, Falkner B. Hypertension in Chronic Kidney Disease. Adv Exp Med Biol 2017;956:307-25.
3. Reiss AB, Voloshyna I, De Leon J, Miyawaki N, Mattana J. Cholesterol Metabolism in CKD. Am J Kidney Dis 2015;66:1071-82.
4. de Cos M, Xipell M, Garcia-Herrera A, Lledo GM, Guillen E, Blasco M, et al. Assessing and counteracting fibrosis is a cornerstone of the treatment of CKD secondary to systemic and renal limited autoimmune disorders. Autoimmun Rev 2022;21:103014.
5. Anders HJ, Huber TB, Isermann B, Schiffer M. CKD in diabetes: diabetic kidney disease versus nondiabetic kidney disease. Nat Rev Nephrol 2018;14:361-77.
6. Devarajan P, Chertow GM, Susztak K, Levin A, Agarwal R, Stenvinkel P, et al. Emerging Role of Clinical Genetics in CKD.

Kidney Med 2022;4:100435.

7. Vehaskari VM. Genetics and CKD. Adv Chronic Kidney Dis 2011;18:317-23.

8. Kovesdy CP. Epidemiology of chronic kidney disease: an update 2022. Kidney Int Suppl (2011) 2022;12:7-11.

9. Flagg AJ. Chronic Renal Therapy. Nurs Clin North Am 2018;53:511-9.

10. Lv JC, Zhang LX. Prevalence and Disease Burden of Chronic Kidney Disease. Adv Exp Med Biol 2019;1165:3-15.

11. Wilkinson TJ, McAdams-DeMarco M, Bennett PN, Wilund K, Global Renal Exercise N. Advances in exercise therapy in predialysis chronic kidney disease, hemodialysis, peritoneal dialysis, and kidney transplantation. Curr Opin Nephrol Hypertens 2020;29:471-9.

12. Panizo S, Martinez-Arias L, Alonso-Montes C, Cannata P, Martin-Carro B, Fernandez-Martin JL, et al. Fibrosis in Chronic Kidney Disease: Pathogenesis and Consequences. Int J Mol Sci 2021;22.

13. Ruiz-Ortega M, Lamas S, Ortiz A. Antifibrotic Agents for the Management of CKD: A Review. Am J Kidney Dis 2022;80:251-63.

14. Huang R, Fu P, Ma L. Kidney fibrosis: from mechanisms to therapeutic medicines. Signal Transduct Target Ther 2023;8:129.

15. Meng XM, Nikolic-Paterson DJ, Lan HY. TGF-beta: the master regulator of fibrosis. Nat Rev Nephrol 2016;12:325-38.

16. Humphreys BD. Mechanisms of Renal Fibrosis. Annu Rev Physiol 2018;80:309-26.

17. Li L, Fu H, Liu Y. The fibrogenic niche in kidney fibrosis: components and mechanisms. Nat Rev Nephrol 2022;18:545-57.

18. Wynn TA. Cellular and molecular mechanisms of fibrosis. J Pathol 2008;214:199-210.

19. Zhou W, Wu WH, Si ZL, Liu HL, Wang H, Jiang H, et al. The gut microbe Bacteroides fragilis ameliorates renal fibrosis in mice. Nat Commun 2022;13:6081.

20. Zhang WJ, Chen SJ, Zhou SC, Wu SZ, Wang H. Inflammasomes and Fibrosis. Front Immunol 2021;12:643149.

21. Borthwick LA. The IL-1 cytokine family and its role in inflammation and fibrosis in the lung. Semin Immunopathol 2016;38:517-34.

22. Zhao X, Kong Y, Liang B, Xu J, Lin Y, Zhou N, et al.

Mechanosensitive Piezo1 channels mediate renal fibrosis. JCI Insight 2022;7.

23. Kang HM, Ahn SH, Choi P, Ko YA, Han SH, Chinga F, et al. Defective fatty acid oxidation in renal tubular epithelial cells has a key role in kidney fibrosis development. Nat Med 2015;21:37-46.

24. Lian YG, Zhou QG, Zhang YJ, Zheng FL. VEGF ameliorates tubulointerstitial fibrosis in unilateral ureteral obstruction mice via inhibition of epithelial-mesenchymal transition. Acta Pharmacol Sin 2011;32:1513-21.

25. Yuan Q, Tan RJ, Liu Y. Myofibroblast in Kidney Fibrosis: Origin, Activation, and Regulation. Adv Exp Med Biol 2019;1165:253-83.

26. Maremonti F, Meyer C, Linkermann A. Mechanisms and Models of Kidney Tubular Necrosis and Nephron Loss. J Am Soc Nephrol 2022;33:472-86.

27. Liu Y, Wang J. Ferroptosis, a Rising Force against Renal Fibrosis. Oxid Med Cell Longev 2022;2022:7686956.

28. Sanz AB, Sanchez-Nino MD, Ramos AM, Ortiz A. Regulated cell death pathways in kidney disease. Nat Rev Nephrol 2023;19:281-99.

29. Ballermann BJ, Obeidat M. Tipping the balance from angiogenesis to fibrosis in CKD. Kidney Int Suppl (2011) 2014;4:45-52.

30. Zhang Y, Shi C, Yang Y, Hu X, Ni H, Li L, et al. Identifying key genes related to the peritubular capillary rarefaction in renal interstitial fibrosis by bioinformatics. Sci Rep 2023;13:19611.

31. Sun YB, Qu X, Caruana G, Li J. The origin of renal fibroblasts/myofibroblasts and the signals that trigger fibrosis. Differentiation 2016;92:102-7.

32. Grgic I, Duffield JS, Humphreys BD. The origin of interstitial myofibroblasts in chronic kidney disease. Pediatr Nephrol 2012;27:183-93.

33. Loeffler I, Wolf G. Epithelial-to-Mesenchymal Transition in Diabetic Nephropathy: Fact or Fiction? Cells 2015;4:631-52.

34. LeBleu VS, Taduri G, O'Connell J, Teng Y, Cooke VG, Woda C, et al. Origin and function of myofibroblasts in kidney fibrosis. Nat Med 2013;19:1047-53.

35. Zeisberg EM, Potenta SE, Sugimoto H, Zeisberg M, Kalluri R. Fibroblasts in kidney fibrosis emerge via endothelial-to-mesenchymal

transition. J Am Soc Nephrol 2008;19:2282-7.

36. Li S, Yu L, He A, Liu Q. Klotho Inhibits Unilateral Ureteral Obstruction-Induced Endothelial-to-Mesenchymal Transition via TGF-beta1/Smad2/Snail1 Signaling in Mice. Front Pharmacol 2019;10:348.

37. Yao L, Liang X, Qiao Y, Chen B, Wang P, Liu Z. Mitochondrial dysfunction in diabetic tubulopathy. Metabolism 2022;131:155195.

38. Molitoris BA, Sandoval RM, Yadav SPS, Wagner MC. Albumin uptake and processing by the proximal tubule: physiological, pathological, and therapeutic implications. Physiol Rev 2022;102:1625-67.

39. Wallace MA. Anatomy and physiology of the kidney. AORN J 1998;68:800, 3-16, 19-20; quiz 21-4.

40. McMahon AP. Development of the Mammalian Kidney. Curr Top Dev Biol 2016;117:31-64.

41. Balzer MS, Rohacs T, Susztak K. How Many Cell Types Are in the Kidney and What Do They Do? Annu Rev Physiol 2022;84:507-31.

42. Ying KE, Feng W, Ying WZ, Sanders PW. Cellular antioxidant

mechanisms control immunoglobulin light chain-mediated proximal tubule injury. Free Radic Biol Med 2021;171:80-90.

43. Gwinner W, Deters-Evers U, Brandes RP, Kubat B, Koch KM, Pape M, et al. Antioxidant-oxidant balance in the glomerulus and proximal tubule of the rat kidney. J Physiol 1998;509 (Pt 2):599-606.

44. Chevalier RL. The proximal tubule is the primary target of injury and progression of kidney disease: role of the glomerulotubular junction. Am J Physiol Renal Physiol 2016;311:F145-61.

45. Ho KM, Morgan DJR. The Proximal Tubule as the Pathogenic and Therapeutic Target in Acute Kidney Injury. Nephron 2022;146:494-502.

46. Jobst-Schwan T, Knaup KX, Nielsen R, Hackenbeck T, Buettner-Herold M, Lechler P, et al. Renal uptake of the antiapoptotic protein survivin is mediated by megalin at the apical membrane of the proximal tubule. Am J Physiol Renal Physiol 2013;305:F734-44.

47. Su L, Zhang J, Gomez H, Kellum JA, Peng Z. Mitochondria ROS and mitophagy in acute kidney injury. Autophagy 2023;19:401-14.

48. Witzgall R. The proximal tubule phenotype and its disruption in acute

renal failure and polycystic kidney disease. Exp Nephrol 1999;7:15-9.

49. Gewin LS. Renal fibrosis: Primacy of the proximal tubule. Matrix Biol 2018;68-69:248-62.

50. MacMahon P, Blackie RA, House MJ, Risdon RA, Crawfurd MD. A further family with congenital renal proximal tubular dysgenesis. J Med Genet 1990;27:395-8.

51. Tang SC, Yiu WH, Lin M, Lai KN. Diabetic nephropathy and proximal tubular damage. J Ren Nutr 2015;25:230-3.

52. Martinez-Klimova E, Aparicio-Trejo OE, Tapia E, Pedraza-Chaverri J. Unilateral Ureteral Obstruction as a Model to Investigate Fibrosis-Attenuating Treatments. Biomolecules 2019;9.

53. Chevalier RL, Forbes MS, Thornhill BA. Ureteral obstruction as a model of renal interstitial fibrosis and obstructive nephropathy. Kidney Int 2009;75:1145-52.

54. Kashoor I, Batlle D. Proximal renal tubular acidosis with and without Fanconi syndrome. Kidney Res Clin Pract 2019;38:267-81.

55. Haraguchi R, Kohara Y, Matsubayashi K, Kitazawa R, Kitazawa S. New Insights into the Pathogenesis of Diabetic Nephropathy:

Proximal Renal Tubules Are Primary Target of Oxidative Stress in Diabetic Kidney. Acta Histochem Cytochem 2020;53:21-31.

56. Wang Y, Jin M, Cheng CK, Li Q. Tubular injury in diabetic kidney disease: molecular mechanisms and potential therapeutic perspectives. Front Endocrinol (Lausanne) 2023;14:1238927.

57. Sturtzel C. Endothelial Cells. Adv Exp Med Biol 2017;1003:71-91.

58. Trimm E, Red-Horse K. Vascular endothelial cell development and diversity. Nat Rev Cardiol 2023;20:197-210.

59. Kruger-Genge A, Blocki A, Franke RP, Jung F. Vascular Endothelial Cell Biology: An Update. Int J Mol Sci 2019;20.

60. Cerutti C, Ridley AJ. Endothelial cell-cell adhesion and signaling. Exp Cell Res 2017;358:31-8.

61. Yazdani S, Jaldin-Fincati JR, Pereira RVS, Klip A. Endothelial cell barriers: Transport of molecules between blood and tissues. Traffic 2019;20:390-403.

62. Salvador E, Shityakov S, Forster C. Glucocorticoids and endothelial cell barrier function. Cell Tissue Res 2014;355:597-605.

63. Rosemblatt M, Bono MR. Functional consequences of immune cell

adhesion to endothelial cells. Curr Pharm Des 2004;10:109-20.

64. Saito A. EMT and EndMT: regulated in similar ways? J Biochem 2013;153:493-5.

65. Cruz-Solbes AS, Youker K. Epithelial to Mesenchymal Transition (EMT) and Endothelial to Mesenchymal Transition (EndMT): Role and Implications in Kidney Fibrosis. Results Probl Cell Differ 2017;60:345-72.

66. Gonzalez DM, Medici D. Signaling mechanisms of the epithelial-mesenchymal transition. Sci Signal 2014;7:re8.

67. Choi SH, Hong ZY, Nam JK, Lee HJ, Jang J, Yoo RJ, et al. A Hypoxia-Induced Vascular Endothelial-to-Mesenchymal Transition in Development of Radiation-Induced Pulmonary Fibrosis. Clin Cancer Res 2015;21:3716-26.

68. Hu H, Huang J, Zhang S, Zhang B, Li W, Sun K. Tumor necrosis factor-alpha stimulation endothelial-to-mesenchymal transition during cardiac fibrosis via endothelin-1 signaling. J Biochem Mol Toxicol 2023;37:e23411.

69. Strippoli R, Loureiro J, Moreno V, Benedicto I, Perez Lozano ML,

Barreiro O, et al. Caveolin-1 deficiency induces a MEK-ERK1/2-Snail-1-dependent epithelial-mesenchymal transition and fibrosis during peritoneal dialysis. EMBO Mol Med 2015;7:102-23.

70. Lu X, Gong J, Dennery PA, Yao H. Endothelial-to-mesenchymal transition: Pathogenesis and therapeutic targets for chronic pulmonary and vascular diseases. Biochem Pharmacol 2019;168:100-7.

71. Dupont C, Armant DR, Brenner CA. Epigenetics: definition, mechanisms and clinical perspective. Semin Reprod Med 2009;27:351-7.

72. Surace AEA, Hedrich CM. The Role of Epigenetics in Autoimmune/Inflammatory Disease. Front Immunol 2019;10:1525.

73. Hillyar C, Rallis KS, Varghese J. Advances in Epigenetic Cancer Therapeutics. Cureus 2020;12:e11725.

74. Sarkar S, Horn G, Moulton K, Oza A, Byler S, Kokolus S, et al. Cancer development, progression, and therapy: an epigenetic overview. Int J Mol Sci 2013;14:21087-113.

75. Zhang L, Lu Q, Chang C. Epigenetics in Health and Disease. Adv Exp Med Biol 2020;1253:3-55.

76. Xue T, Qiu X, Liu H, Gan C, Tan Z, Xie Y, et al. Epigenetic regulation in fibrosis progress. Pharmacol Res 2021;173:105910.

77. Chen Y, Hong T, Wang S, Mo J, Tian T, Zhou X. Epigenetic modification of nucleic acids: from basic studies to medical applications. Chem Soc Rev 2017;46:2844-72.

78. Page A, Mann DA. Epigenetic regulation of liver fibrosis. Clin Res Hepatol Gastroenterol 2015;39 Suppl 1:S64-8.

79. Wang XC, Song K, Tu B, Sun H, Zhou Y, Xu SS, et al. New aspects of the epigenetic regulation of EMT related to pulmonary fibrosis. Eur J Pharmacol 2023;956:175959.

80. Ding H, Zhang L, Yang Q, Zhang X, Li X. Epigenetics in kidney diseases. Adv Clin Chem 2021;104:233-97.

81. Timmermann S, Lehrmann H, Polesskaya A, Harel-Bellan A. Histone acetylation and disease. Cell Mol Life Sci 2001;58:728-36.

82. Yoon S, Eom GH. HDAC and HDAC Inhibitor: From Cancer to Cardiovascular Diseases. Chonnam Med J 2016;52:1-11.

83. Ghosh AK. FAT-free p300 is good for scar-free tissue repair. J Cell Biochem 2014;115:1486-9.

84. Giles RH, Peters DJ, Breuning MH. Conjunction dysfunction: CBP/p300 in human disease. Trends Genet 1998;14:178-83.

85. Dekker FJ, Haisma HJ. Histone acetyl transferases as emerging drug targets. Drug Discov Today 2009;14:942-8.

86. Dou C, Liu Z, Tu K, Zhang H, Chen C, Yaqoob U, et al. P300 Acetyltransferase Mediates Stiffness-Induced Activation of Hepatic Stellate Cells Into Tumor-Promoting Myofibroblasts. Gastroenterology 2018;154:2209-21 e14.

87. Iyer NG, Ozdag H, Caldas C. p300/CBP and cancer. Oncogene 2004;23:4225-31.

88. Ghosh AK, Varga J. The transcriptional coactivator and acetyltransferase p300 in fibroblast biology and fibrosis. J Cell Physiol 2007;213:663-71.

89. Ghosh AK, Vaughan DE. Fibrosis: is it a coactivator disease? Front Biosci (Elite Ed) 2012;4:1556-70.

90. Rubio K, Molina-Herrera A, Perez-Gonzalez A, Hernandez-Galdamez HV, Pina-Vazquez C, Araujo-Ramos T, et al. EP300 as a Molecular Integrator of Fibrotic Transcriptional Programs. Int J Mol Sci 2023;24.

91. Kim TH, Yoo JY, Choi KC, Shin JH, Leach RE, Fazleabas AT, et al. Loss of HDAC3 results in nonreceptive endometrium and female infertility. Sci Transl Med 2019;11.

92. Lee SY, Park SY, Lee SH, Kim H, Kwon JH, Yoo JY, et al. The deubiquitinase UCHL3 mediates p300-dependent chemokine signaling in alveolar type II cells to promote pulmonary fibrosis. Exp Mol Med 2023;55:1795-805.

93. Gao J, Wei B, Liu M, Hirsova P, Sehrawat TS, Cao S, et al. Endothelial p300 Promotes Portal Hypertension and Hepatic Fibrosis Through C-C Motif Chemokine Ligand 2-Mediated Angiocrine Signaling. Hepatology 2021;73:2468-83.

94. Rai R, Sun T, Ramirez V, Lux E, Eren M, Vaughan DE, et al. Acetyltransferase p300 inhibitor reverses hypertension-induced cardiac fibrosis. J Cell Mol Med 2019;23:3026-31.

95. Ghosh AK, Bhattacharyya S, Lafyatis R, Farina G, Yu J, Thimmapaya B, et al. p300 is elevated in systemic sclerosis and its expression is positively regulated by TGF-beta: epigenetic feed-forward amplification of fibrosis. J Invest Dermatol 2013;133:1302-10.

96. Sanchez-Molina S, Oliva JL, Garcia-Vargas S, Valls E, Rojas JM, Martinez-Balbas MA. The histone acetyltransferases CBP/p300 are degraded in NIH 3T3 cells by activation of Ras signalling pathway. Biochem J 2006;398:215-24.

97. Huang WC, Chen CC. Akt phosphorylation of p300 at Ser-1834 is essential for its histone acetyltransferase and transcriptional activity. Mol Cell Biol 2005;25:6592-602.

98. Thomas PD, Ebert D, Muruganujan A, Mushayahama T, Albou LP, Mi H. PANTHER: Making genome-scale phylogenetics accessible to all. Protein Sci 2022;31:8-22.

99. Tang D, Chen M, Huang X, Zhang G, Zeng L, Zhang G, et al. SRplot: A free online platform for data visualization and graphing. PLoS One 2023;18:e0294236.

100. Fan M, Yang K, Wang X, Chen L, Gill PS, Ha T, et al. Lactate promotes endothelial-to-mesenchymal transition via Snail1 lactylation after myocardial infarction. Sci Adv 2023;9:eadc9465.

101. Cao Y, Hu J, Sui J, Jiang L, Cong Y, Ren G. Quercetin is able to alleviate TGF-beta-induced fibrosis in renal tubular epithelial cells by

suppressing miR-21. Exp Ther Med 2018;16:2442-8.

102. Zhao J, Wang L, Cao AL, Jiang MQ, Chen X, Wang Y, et al. HuangQi Decoction Ameliorates Renal Fibrosis via TGF-beta/Smad Signaling Pathway In Vivo and In Vitro. Cell Physiol Biochem 2016;38:1761-74.

103. Lovisa S, Fletcher-Sananikone E, Sugimoto H, Hensel J, Lahiri S, Hertig A, et al. Endothelial-to-mesenchymal transition compromises vascular integrity to induce Myc-mediated metabolic reprogramming in kidney fibrosis. Sci Signal 2020;13.

104. Naas S, Schiffer M, Schodel J. Hypoxia and renal fibrosis. Am J Physiol Cell Physiol 2023;325:C999-C1016.

105. Li ZL, Liu BC. Hypoxia and Renal Tubulointerstitial Fibrosis. Adv Exp Med Biol 2019;1165:467-85.

ABSTRACT IN KOREAN

신장 섬유화 진행 과정에서의 히스톤 아세틸화 효소 p300의 생리학적 기능 규명

만성 신장 질환은 전 세계적으로 높은 유병률을 보이며 일반적으로 조직 내 심한 섬유화가 동반된다. 그러나 현재까지 정확한 발병 기전 규명 및 효과적인 치료법 개발을 위한 연구는 아직 부족하기 때문에 이에 대한 심도 깊은 추가적 연구가 필요하다. 본 연구에서는 히스톤 아세틸 전이 효소인 E1A-associated protein p300 (p300)이 국소 분절 사구체 경화증 및 면역 글로불린 A 신장병과 같은 만성 신장 질환 환자에서 증가한다는 것을 확인하였고, 사람 신장 섬유화를 모방한 각기 다른 세 가지의 쥐 섬유화 유도 모델에서도 p300 단백질의 상승을 확인 하였다. 특히, 신장 섬유증 진행 중 신장 근위 세뇨관 세포에서 p300 단백질이 특이적으로 상승함을 확인했으며, 쥐 신장 섬유화 모델에서 근위세뇨관에서 p300을 특이적으로 결손 시켰을 때, 신장 섬유화 발생이 완화 되는 것을 검증 하였다. 추가적으로 p300 단백질의 안정성은 AKT 신호를 통한 p300의 세린 1834번째 아미노산의 인산화에 의해 조절된다는 것을 확인하였으며 p300을 탈 인산화 하는 결합 파트너인 PPM 계열 단백질, Protein Phosphatase, Mg2+/Mn2+ Dependent 1K (PPM1K)를 선별한 후 PPM1K 단백질이 AKT 매개 p300 단백질의 안정화를 억제 함을 확인하였다. 그리고 신장 섬유화 진행 중의 p300 단백질의 하위 전사 조절 유전자 선별 및 p300 단백질에 의해 조절되는 생리학적 분자 조절 경로 확인을 위해 RNA-Sequencing 및 CUT&TAG-Sequencing을 사용하여 신장 섬유화를 유도한 신장 근위 세뇨관 세포 특이적 p300 결손 마우스의 유전자 발현 조절을 확인 하였을 때, 신장 섬유증 진행 과정에서 간질 세포 전환 및 혈관 신생이 조절되는 것을 확인하였다. 그리고 신장 섬유화 발달에 의해 증가한 신장 근위 세뇨관 세포의 p300이 간질 세포 전환 관련 분비 단백질 POSTN, FSTL1 및 FSCN1 발현을 조절하여 혈관 내피세포의 간질 세포 전환 (EndoMT) 및 상피세포의 간질 세포 전환 (EMT)를 증가시켜 신장 섬유증 발생을 촉진한다는

것을 검증했다. 마지막으로, p300 특이적 저해제인 C646과 A6 처리 시 p300 매개 EndoMT 저해와 섬유화 유발이 감소함을 쥐 섬유화 유도 모델을 이용하여 확인하였다. 종합하자면, 본 연구는 신장 섬유증 발생 과정에서 신장 근위 세뇨관 세포의 p300의 역할을 입증하였으며, p300을 신장 섬유증 표지자 또는 치료표적으로 제안 하고자 한다.

핵심되는 말 : p300, 만성 신장 질환, 신장 섬유화, EndoMT, PPM1K

PUBLICATION LIST

1. **Kim H**, Park SY, Lee SY, Kwon JH, Byun S, Kim MJ, et al. Therapeutic effects of selective p300 histone acetyl-transferase inhibitor on liver fibrosis. BMB Rep 2023;56:114-9.
2. **Kim H**, Jang S, Lee SY, Kwon JH, Byun S, Yoo JY, et al. JMJD4 promotes tumor progression via inhibition of the PDCD5–TP53 pathway. BMB Rep (Accepted)
3. Lee SY, Park SY, Lee SH, **Kim H**, Kwon JH, Yoo JY, et al. The deubiquitinase UCHL3 mediates p300-dependent chemokine signaling in alveolar type II cells to promote pulmonary fibrosis. Exp Mol Med 2023;55:1795-805.
4. Lee SY, Park SY, Lee GE, **Kim H**, Kwon JH, Kim MJ, et al. Aucuparin Suppresses Bleomycin-Induced Pulmonary Fibrosis Via Anti-Inflammatory Activity. J Med Food 2021;24:151-60.